Sofie Olsen Hauge

# Study of organic and inorganic pollutants in former industry areas in Ny-Ålesund, Svalbard, and potential effects on drinking water reservoir Tvillingvatnet

**NTNU**
Norwegian University of
Science and Technology

Sofie Olsen Hauge

# Study of organic and inorganic pollutants in former industry areas in Ny-Ålesund, Svalbard, and potential effects on drinking water reservoir Tvillingvatnet

**NTNU**
Norwegian University of
Science and Technology

# Abstract

This master's thesis is a study of selected elements and per- and polyfluoroalkyl substances (PFAS) in sediment, soil, and water samples collected in Ny-Ålesund at Svalbard in August 2022. The thesis is a continuation of the specialization project written as a part of the course TKJ4540 at NTNU in 2022. Parts of this project is therefore reproduced in this work, including some theoretical background, experimental methods and results.

The purpose of this project was to assess element concentrations, including heavy metals, and PFAS in the relatively isolated research center of Ny-Ålesund, and possibly relate these results to local sources, especially former mining activity in the area. This study is a part of important research on the chemical situation in the Arctic, and on Svalbard specifically.

36 sediment and soil samples and 13 water samples were collected in the area around Ny-Ålesund. Concentrations of 54 elements were determined, with a special focus on heavy metals and elements related to mining activity, in a total of 34 sediment and soil samples and 15 water samples. Element analysis was performed by ICP-MS analysis. In addition to the element analysis, a total of 36 sediment and soil samples, and two water samples, were analyzed for 35 types of PFAS. PFAS analysis was performed using LC-MS/MS instrument. Total organic carbon (TOC) and total inorganic carbon (TIC) were also determined in two water samples and all 36 sediment/soil samples. In addition to this, pH and conductivity were measured directly at 6 locations in Tvillingvatnet. Principal component analysis (PCA) was performed for dimension reduction and for further evaluation of the results, and possibly identification of patterns and relationships.

In sediment and soil samples, the TOC results ranged from 0.2% to 26%, and the TIC results ranged from 0.05% to 2.79%. In Tvillingvatnet, the pH had an average of 8.14 and conductivity had an average of 315 µS/cm. PFAS detected in the samples include PFOS, PFOA, PFNA, PFHxA, PFDA, FOSAA, PFUnA, PFHxDA, PFHpA and 6:2 FTS. The highest concentrations were found for PFOS and PFUnA with concentrations as high as 12.8 ng/g of soil (dry weight). The elemental analysis showed higher concentrations of several elements in the hill area east of Tvillingvatnet, which is located close to the former mining industry area. Especially high levels of Ni, Cd, Cu and Zn were found in a puddle in the hill. The same results were not found for samples collected on the other side of the mining area, close to Smithelva.

The study showed higher levels of both PFAS and some heavy metals in the hill area closer to former mining area than at Tvillingvatnet. The levels were not as high as could be expected at Smithelva, which is also close to the mining area. Therefore, the results do not directly indicate pollution contribution from the mining area.

# Sammendrag

Denne masteroppgaven er en studie av utvalgte grunnstoffer og per- og polyfluoralkylstoffer (PFAS) i sediment-, jord- og vannprøver tatt i Ny-Ålesund på Svalbard i august 2022. Oppgaven er en videreføring av fordypningsprosjektet skrevet som en del av emnet TKJ4540 ved NTNU i 2022. Deler av dette prosjektet er derfor gjengitt i dette arbeidet, inkludert noe teoretisk bakgrunn, eksperimentelle metoder og resultater.

Hensikten med dette prosjektet var å vurdere grunnstoffkonsentrasjoner, inkludert tungmetaller, og PFAS i det relativt isolerte forskningssenteret i Ny-Ålesund, og eventuelt relatere disse resultatene til lokale kilder, spesielt tidligere gruvevirksomhet i området. Denne studien er en del av viktig forskning på den kjemiske situasjonen i Arktis, og spesielt på Svalbard.

Det ble samlet inn 36 sediment- og jordprøver og 13 vannprøver i området rundt Ny-Ålesund. 54 grunnstoffer ble kvantifisert, med spesielt fokus på tungmetaller og grunnstoffer knyttet til gruveaktivitet, i totalt 34 sediment- og jordprøver og 15 vannprøver. Elementanalyse ble utført ved ICP-MS-analyse. I tillegg til elementanalysen ble totalt 36 sediment- og jordprøver, og to vannprøver, analysert for 35 typer PFAS. PFAS-analyse ble utført ved bruk av LC-MS/MS-instrument. Totalt organisk karbon (TOC) og totalt uorganisk karbon (TIC) ble også bestemt i to vannprøver og alle 36 sediment/jordprøver. I tillegg til dette ble pH og ledningsevne målt direkte på 6 steder i Tvillingvatnet. Prinsipalkomponentanalyse (PCA) ble utført for dimensjonsreduksjon og for videre evaluering av resultatene, og eventuelt identifisering av mønstre og sammenhenger.

I sediment- og jordprøver varierte TOC-resultatene fra 0,2% til 26%, og TIC-resultatene varierte fra 0,05% til 2,79%. I Tvillingvatnet hadde pH et gjennomsnitt på 8,14 og konduktivitet hadde et gjennomsnitt på 315 µS/cm. PFAS påvist i prøvene inkluderer PFOS, PFOA, PFNA, PFHxA, PFDA, FOSAA, PFUnA, PFHxDA, PFHpA og 6:2 FTS. De høyeste konsentrasjonene ble funnet for PFOS og PFUnA med konsentrasjoner så høye som 12,8 ng/g jord (tørrvekt). Grunnstoffanalysen viste høyere konsentrasjoner av flere elementer i bakkeområdet øst for Tvillingvatnet, som ligger like ved det tidligere gruveindustriområdet. Spesielt høye nivåer av Ni, Cd, Cu og Zn ble funnet i en sølepytt i bakken. De samme resultatene ble ikke funnet for prøver tatt på den andre siden av gruveområdet, like ved Smithelva.

Studien viste høyere nivåer av både PFAS og enkelte tungmetaller i bakkeområdet nærmere tidligere gruveområde enn ved Tvillingvatnet. Nivåene var ikke så høye som man kunne forvente ved Smithelva, som også ligger like ved gruveområdet, og det er altså ingen direkte indikasjon på forurensningsbidrag fra gruveområdet.

# Acknowledgement

This thesis is the final product of my Master's degree in Analytical Chemistry, and is a part of the study program Chemical Engineering and Biotechnology (MTKJ). It was written at the Department of Chemistry at Norwegian University of Science and Technology (NTNU).

First of all, I would like to thank my supervisor Øyvind Mikkelsen for his guidance and encouragement through every part of the project. All the way from sampling at Svalbard, to the chemical analyses and throughout the writing process. I am grateful for letting me take part in the field trip to Svalbard and Ny-Ålesund, and for the opportunity to write my thesis on the Arctic. I also want to thank him for providing waffles and social gatherings on Fridays.

I want to thank my co-supervisor Alexandros Asimakopoulos for guidance regarding the PFAS analysis and data management. Furthermore, I want to thank Hanne Vistnes for providing the extraction procedure of PFAS, and also practical help in my laboratory work. I also thank Gabriela Castro Varela for help with LC-MS/MS analysis, and Kyyas Seyitmuhammedov for guidance on the microwave digestion procedure and ICP-MS analysis.

The field trip to Svalbard and Ny-Ålesund provided several new acquaintances and fellow students. I am grateful for these new friendships, and the academic support these have provided through the last year. I want to thank Joséphine specifically for great guidance in the lab, and Pauline for academic collaboration and support.

I also thank my fantastic fellow students for friendship, support, and encouragements throughout my studies, and for countless much needed lunch and coffee breaks. A special thanks to Nadia, who has been my closest classmate since the beginning of our time at NTNU, and Amalie, for all help, support, and friendship, as the only fellow analytical chemist in our class. I also want to thank my previous and current basketball teammates at NTNUI Basket, who have provided breaks from the studies, lots of laughs and also life long friendships. Finally, I want to thank the rest of my friends, my family, and Per, for your support, pushing me when needed, and listening to my rants on pollution. I am forever grateful for you.

# Abbreviations

| | |
|---|---|
| AFFF | Aqueous film forming foam |
| AMAP | Arctic Monitoring & Assessment Programme |
| AMD | Acid Mine Drainage |
| BCR | The Bureau of Certified Reference Materials |
| CRM | Certified reference material |
| ESI | Electrospray ionization |
| FFTS | Firefighting training sites |
| HPLC | High-Performance Liquid Chromatography |
| IS | Internal standard |
| ICP-MS | Inductively coupled plasma mass spectrometry |
| LOD | Lower limit of detection |
| LOQ | Lower limit of quantification |
| LSE | Liquid-solid extraction |
| LRAT | Long Range Atmospheric Transport |
| MS | Mass Spectrometry |
| m/z | Mass-to-charge ratio |
| NIST | National Institute of Standards and Testing |
| NP | Normal phase |
| PFAS | Per- and polyfluoroalkyl substances |
| PFCA | Perfluoroalkyl carboxylic acids |
| PFSA | Perfluoroalkyl sulfonic acids |
| POPs | Persistant Organic Pollutants |
| QC | Quality control |
| QA | Quality assurance |
| ROC | Residual oxidizable carbon |
| RP | Reverse phase |
| SD | Standard deviation |
| SPE | Solid Phase Extraction |
| TC | Total Carbon |
| TIC | Total Inorganic Carbon |
| TOC | Total Organic Carbon |

# Table of Contents

# List of Figures

# List of Tables

# 1 Introduction

The Arctic environment is, due to its location far away from larger pollution sites, expected to have low levels of toxic compounds. However, the monitoring of pollutants is important as it provides important information on long-range transport mechanisms, and contributes to more information on possible local sources. It is also important to assess the development and effects these local and remote sources of pollution have on relatively isolated ecosystems. This is increasingly important as global warming is happening faster in polar regions, affecting the release of pollutants trapped in ice and the mechanisms of transportation in the atmosphere and ocean [1] [2].

PFAS, per- and polyfluoroalkyl substances, is a group consisting of more than a thousand different synthetic fluorinated chemicals [3]. They are particularly known for being fat, water, and stain repellent, as well as to be stable, and are widely used in a multitude of products and industries such as electronics, aviation, clothing, food packaging, and firefighting equipment [4]. Although they have widespread use, concerns related to PFAS have increased recently due to their increased presence in nature, persistence, and possible toxic and bioaccumulating effects [3]. Therefore, it is important to regulate the use of PFAS and monitor its release to nature, including remote areas such as the Arctic.

90 elements may be found naturally in the crust of the Earth, and some of these have high densities and are commonly known as heavy metals [5] [6]. Although these are a natural part of the environment, they are known to be toxic, and pollution of these may increase the levels above natural concentrations in the ecosystems and have adverse effects. Some of the most common are lead (Pb), arsenic (As), cadmium (Cd), chromium (Cr), and mercury (Hg) [6]. Among the most concerning anthropogenic sources of heavy metals are waste incineration, metal smelters, combustion of fossil fuel and mining. Mines have been shown to be sources of Hg, Cd, Pb, As, and copper (Cu), among others [7].

While mining activity on Svalbard is decreasing, the research activity is increasing. One of the previous mining centers, Ny-Ålesund, has become a research infrastructure after the closure of all mines, and scientists come here from all over the world to conduct research in the area within several scientific fields. Tvillingvatnet is a lake located about 1.5 kilometers from the center of Ny-Ålesund. Even though this lake is the drinking water reservoir for Ny-Ålesund, limited research has been conducted on the water chemical status, and possible contamination by local or remote sources of the drinking water [2].

The purpose of this study is to produce additional data related to the chemical condition of Tvillingvatnet, as well as the area in proximity to this lake, and to further review possible sources of PFAS and inorganic contamination in the area. Both water and sediment samples were collected from the lake and surroundings [2]. The results of this study include the determination of elements, PFAS, TOC, and TIC, as well as pH and conductivity measurements from Tvillingvatnet. Soil and sediment samples were digested by UltraClave before ICP-MS analysis for elemental determination. Solid phase extraction was performed on sediment, soil and water samples, before analysis by LC-MS/MS for determination of PFAS.

The analysis of sediments related to Tvillingvatnet is considered important to assess the possibility of contamination of the drinking water reservoir from accumulated compounds in the sediment. Runoff from closed-off mines in the area is a possible source of contamination of drinking water.

It is also important with regular monitoring, as changes in physicochemical properties due to the changing climate[1] could shift the equilibrium and increase the flux of contaminants into the water[2].

This thesis will present some theory about the Arctic, Svalbard, and Ny-Ålesund, as well as an introduction to PFAS, trace elements and heavy metals, and theory on the sample preparation techniques and analytical tools used. It also includes methods for sampling of water, sediment, and soil samples and sample preparations, as well as analytical techniques. The results of PFAS and element quantification are included, as well as the results from the analysis of total organic and total inorganic carbon and the pH and conductivity measurements. Principal component analysis (PCA) was also performed and these results are also included and discussed.

# 2   Theoretical background

This theoretical part includes an introduction to the Arctic environment, geography and history, as well as Svalbard and Ny-Ålesund specifically, and gives some theoretical background on the pollutants relevant for this study. Some theory on the specific analytical methods and sample preparations performed, in addition to some statistical tools and terminologies, are also included in this part. Several parts, including whole or parts of Sections 2.1, 2.2, 2.4, and 2.5, are reproduced from the specialization project.

## 2.1   The Arctic and pollutants

The Arctic is defined as the geographic area within the Arctic Circle, i.e., north of 66°32' N [8]. The position of the arctic makes the environment here unlike any other, with limited vegetation, tundra and low air temperatures being some of the characteristics [8]. Despite its remote location, the Arctic is subject to pollutants, both by local sources and by long-range transportation. Several contaminants accumulate in the Arctic and have a bioaccumulation potential and adverse effects on the marine and terrestrial biota. This has been a cause of concern and led to the formation of international collaborations in order to protect the environment, such as the Arctic Monitoring & Assessment Programme (AMAP) [9] [10]. Both organic and inorganic pollutants are transported towards the Arctic by global distillation. This is a process by which chemicals evaporate or travel by aerosols, and as the chemicals reach colder temperatures in the Arctic, cold condensation occurs and pollutants are deposited in the Arctic. The effect is related to the "grasshopper effect", as chemicals can be deposited and remobilized one or several times during their migration [11] [2].

### 2.1.1   Svalbard

Svalbard is the collection of islands placed between 74° and 81° north, and 10° and 35° east, and is under Norwegian jurisdiction. The population of Svalbard is around 3000, and the majority lives in the administrative center of Longyearbyen. Historically, mining, fishing and whale hunting have been the most important activities on Svalbard. Today, tourism and research activity have passed mining as the most predominant activities [12]. The increase in tourism activity is mainly dominated by cruise tourism. This, combined with the challenges introduced by climate change, poses a threat to the environment on Svalbard due to the impact on marine and terrestrial ecosystems, and therefore protection of Svalbard and the Arctic in general is considered important for future environmental maintenance [13] [2].

### 2.1.2   Mining and cultural heritage

During four centuries of human presence on Svalbard, mining has been a major part of the anthropogenic activity. The preservation of this cultural heritage is important for the conservation of Svalbard's history. At the same time, because all cultural monuments from before 1946 are protected by law, there are many visible remains from the 20th century. These remains have an impact on the natural environment in the form of objects left behind that litter the landscape. In addition, old mine fillings are possible sources of both inorganic and organic pollutants, and may also cause harm to local wildlife. Figure 2.1 shows how such residuals affect the landscape in the

mining area in Ny-Ålesund. The cleanup is therefore multifaceted, as the cultural heritage must be preserved while keeping the environment and wildlife protected [14].



Figure 2.1: Remains after mining activity in Ny-Ålesund.

### 2.1.3 Ny-Ålesund

North of Longyearbyen, the research center of Ny-Ålesund located, where several nations are conducting research in many fields of science. Ny-Ålesund, and the attached airport, is owned and operated by Kings Bay AS, officially known as Kings Bay Kull Company A/S [15]. Historically, extensive mining has been carried out in the area around Ny-Ålesund, in multiple periods from 1916 to 1963 [16] [2]. Following a series of fatal accidents, an explosion in the Ester I mine in 1962 cost 21 lives, resulting in the closure of all mining activity in Ny-Ålesund [17]. As illustrated in Figure 2.1, many remains of the mining activity are still scattered throughout the area, including residuals of coal, mining equipment, and remains of the railroad. This contributes to the possible local sources of pollution in the area.

Tvillingvatnet is located approximately 1.5 km south-west of the research station Ny-Ålesund, and serves as the water supply for the settlement. It is surrounded by mountains and glaciers (Vestre Brøggerbreen, Austre Brøggerbreen and Zeppelin mountain), as well as the small airport and Kolhaugen. Kolhaugen is a pile where waste has been dumped, containing remains from mining activity, and may also contain electronics, building materials, and other unknown materials [2].

## 2.2   Per- and polyfluoroalkyl substances (PFAS)

### 2.2.1   Chemical structure and physio-chemical properties

Per- and polyfluoroalkyl substances (PFAS) is a collective term for chemical substances that contain one or more carbon atoms where one or more hydrogen atoms have been substituted with fluorine atoms. PFAS have the general formula $C_nF_{2n+1}-$. In perfluoroalkyl substances, all hydrogen atoms have been replaced by fluorine. The term PFAS includes thousands of chemical compounds that have a wide variety of carbon chain lengths, fluorine presence and functional groups, which also give them different chemical properties and an extensive range of possible uses [18]. One of the most important assets of many PFAS is their combined hydrophobic and lipophobic properties, which make them able to repel water, as well as oil-based substances. This is a very useful capability, and therefore PFAS can be found in products such as textile impregnation and coatings on cooking ware and in a variety of other industries. They are also widely used as a surfactant in products such as fire-fighting foam. PFAS have been used since the 1940s, and the strong bonds between carbon and fluoride make the chemicals extremely stable and resistant to break down [19] [2].

Properties such as melting and boiling point, vapor pressure, and partition coefficients have a significant influence on the behavior and fate of PFAS in the environment and biota. The melting and boiling point will influence the phase the component has, given the temperature in the environment. The boiling point is also highly related to the vapor pressure, $P_v$, and compounds with a high vapor pressure will be more easily partitioned into the gas phase, i.e., they are more volatile. Several partition coefficients are utilized to predict the partitioning of compounds between different solutions and phases, such as air, soil, water, vegetation, and aerosol particles at equilibrium. Examples of such coefficients are the partition coefficients between octanol and water, $K_{OW}$, water and air, $K_{AW}$, and octanol and air, $K_{OA}$ [20] [21]. Some logarithmic values of the vapor pressure, $K_{OW}$, $K_{AW}$ and $K_{OA}$ of some selected PFAS are presented in Table 2.1 [2].

Table 2.1: Physical properties of selected PFAS[22].

| CAS | Acronym | $\log P_v$ [Pa] | $\log K_{OW}$ | $\log K_{AW}$ | $\log K_{OA}$ |
|-----|---------|-----------------|---------------|---------------|---------------|
| 375-73-5 | PFBS | 2.12 | 0.14 | 1.02 | 4.58 |
| 355-46-4 | PFHxS | 1.68 | 1.35 | 2.15 | 5.29 |
| 1763-23-1 | PFOS | 1.23 | 2.56 | 3.29 | 5.99 |
| 375-22-4 | PFBA | 2.40 | -0.62 | 0.30 | 4.13 |
| 2706-90-3 | PFPA | 2.18 | -0.02 | 0.86 | 4.48 |
| 307-24-4 | PFHxA | 1.96 | 0.59 | 1.43 | 4.84 |
| 375-85-9 | PFHpA | 1.74 | 1.19 | 2.00 | 5.19 |
| 335-67-1 | PFOA | 1.51 | 1.79 | 2.57 | 5.55 |
| 375-95-1 | PFNA | 1.29 | 2.40 | 3.14 | 5.90 |
| 335-76-2 | PFDA | 1.07 | 3.00 | 3.70 | 6.25 |
| 2058-94-8 | PFUnA | 0.88 | 3.51 | 4.18 | 6.55 |
| 307-55-1 | PFDoA | 0.62 | 4.21 | 4.84 | 6.96 |
| 376-06-7 | PFTA | 0.22 | 5.30 | 5.87 | 7.60 |
| 754-91-6 | FOSA | 1.18 | 2.70 | 3.42 | 6.07 |
| 31506-32-8 | MeFOSA | 1.01 | 3.17 | 3.86 | 6.35 |
| 4151-50-2 | EtFOSA | 0.87 | 3.53 | 4.21 | 6.57 |
| 1691-99-2 | EtFOSE | 0.64 | 4.17 | 4.81 | 6.94 |
| 24448-09-7 | MeFOSE | 0.77 | 3.81 | 4.46 | 6.73 |
| 25268-77-3 | MeFOSEA | 0.36 | 4.92 | 5.51 | 7.38 |
| 2043-47-2 | 4:2 FTOH | 2.02 | 0.41 | 1.26 | 4.73 |
| 647-42-7 | 6:2 FTOH | 1.58 | 1.62 | 2.40 | 5.44 |
| 678-39-7 | 8:2 FTOH | 1.13 | 2.82 | 3.54 | 6.15 |
| 865-86-1 | 10:2 FTOH | 0.69 | 4.03 | 4.67 | 6.86 |

PFAS are separated into classes based on their chemical structure. Examples of some of the most widely known classes are perfluoroalkyl carboxylic acids (PFCA), perfluoroalkyl sulfonic acids (PFSA), and fluorotelomer sulfonic acids (FTSA). PFCA have the general formula $C_nF_{15}COOH$ and the substance most discussed in the group is perfluorooctanic acid (PFOA). PFSA have the general formula $C_nF_{2n+1}SO_3H$, and here the most discussed substance is perfluorooctane sulfonic acid (PFOS). Both PFOA and PFOS have attracted a great deal of attention because of their toxicological effect on the environment and human health, and several companies have phased out or reduced their use. However, they are still considered to pose a threat due to their persistence in the environment. FTSA have the general formula $C_nF_{2n+1}CH_2CH_2SO_3H$, and includes 6:2 fluorotelomer sulfonic acid (6:2 FTS). These have been found in FFTS, among others[18]. The chemical structures of PFOS, PFOA, and 6:2 FTS are included in Figure 2.2[2].
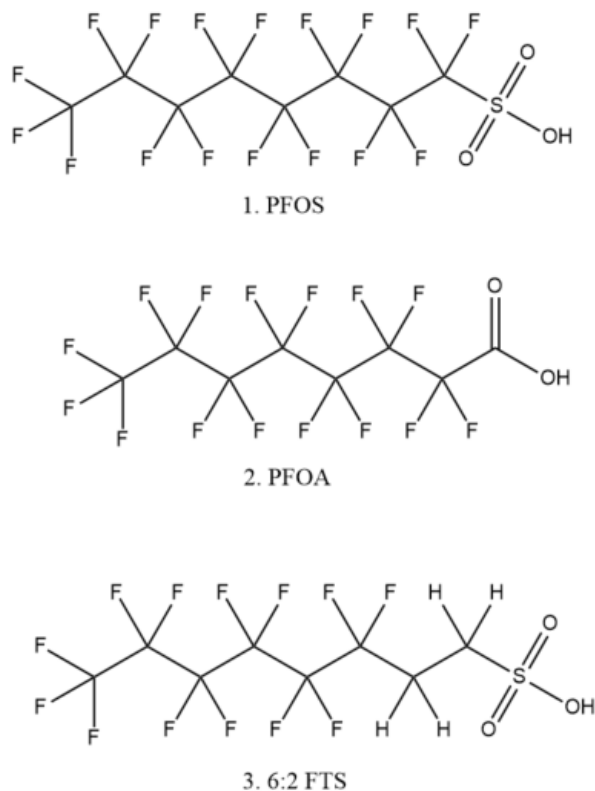
Figure 2.2: Chemical structures of PFOS, PFOA and 6:2 FTS.

### 2.2.2 Distribution in the environment

As mentioned in Section 2.2.1, the distribution of PFAS in the environment is highly dependent on their physical and chemical properties, including partition coefficients. In the environment, PFAS are constantly shifting between environmental media such as air, aerosols, water, and soil, and the partitioning plays an important role in the transportation of PFAS, both locally and globally. PFAS have been found in all parts of the environment, including water, air, soil, and organisms like fish. PFAS are likely to bioaccumulate due to their chemical properties and persistence, so higher concentrations may be found in plants and organisms. However, despite their persistence, some degradation of PFAS occur. For example, long-chained PFAS could be degraded to short-chained PFAS, which will change their properties and partitioning [23] [24].

Due to their distribution in several media, PFAS have the ability to be transported over long distances and can now be found all over the world. They may be transported by water in aerosols or ocean currents, and some may evaporate and be transported by the atmosphere. All of these effects contribute to the transport of PFAS and other POPs from remote sources to the Arctic [25] [26]. The partition coefficients $K_{OW}$ and $K_{OA}$ could be used to estimate the long-range transportation potential of PFAS, especially through long-range atmospheric transportation (LRAT). For example, components with high vapor pressures will be more easily evaporated and can be transported in the atmosphere. The partition coefficients between air and other substances, such as water and octanol, will also affect the probability of LRAT. As an example, a low value $K_{OA}$ indicates a higher flux of the component into the air from the soil. However, since many PFAS have mainly hydrophobic

properties, these may adsorb to organic carbon in soil and sediments, and therefore have higher $K_{OA}$ and $K_{OW}$ and will be more easily partitioned into solid phases. However, other PFAS have both a hydrophobic tail and a hydrophilic head, which makes them work as surfactants. These tend to partition themselves on the air-water interface and orient themselves with the hydrophobic tail in the air phase and the hydrophilic head in the water phase. This effect could lead to accumulation on the water surface, increasing the possibility of LRAT of PFAS in aerosols [27]. In addition, increasing temperature as a result of global warming changes both physical and biological processes and hence the trends in long-range transportation of POPs. These effects are especially prominent in Arctic areas, and changes in long-range transport here are observed and expected in the future [28] [2].

As PFAS were introduced in the 1940s, it is possible that they were used in the mining industry. PFAS contamination in the area around Ny-Ålesund, and on Svalbard in general, could therefore be a product of the mining industry and the lack of extensive clean-up. However, more probable local sources are related to recent anthropogenic activity in Ny-Ålesund. A study has already established that the use of aqueous film-forming foam (AFFF) used at firefighting training sites (FFTS) contributes to the PFAS pollution in Ny-Ålesund. Although tourism is low and limited to the center of Ny-Ålesund, researchers are hiking and sampling in the area around the station. Modern hiking gear popularly uses water repellent chemicals containing PFAS, and this could also contribute to local PFAS pollution [29] [2].

As previously mentioned, some PFAS tend to accumulate in soils and sediments. Fluxes from sediments to water reservoirs and to air are regulated by the partition coefficients between the solid material, water and air. However, partitioning mechanisms are also highly affected by properties of the soil or sediment and water in question, such as organic carbon content and charges of components in the soil and in the water. Therefore, several factors must be taken into account when assessing the partitioning and fluxes of PFAS, and contaminants in general [27] [2].

### 2.2.3 Toxic effects

Measurable levels of PFAS can now be found in most of the population of the developed world, and scientists are concerned about the toxic effect PFAS have on the human body. Many PFAS, such as PFOS, have the ability to bioaccumulate, and this, together with their persistence and toxicity, led to their inclusion in the Stockholm Convention. The toxicity of PFAS has also been found to increase with increasing chain length [18]. The Stockholm Convention is an international environmental agreement signed in 2001. It addresses the issue of persistent organic pollutants (POPs) and their increasingly problematic role in the environment. The role of the convention is to regulate the use of these chemicals of concern [30]. Several animal and human studies have related exposure to PFAS to increased liver weight, reduced response to vaccines and resistance to infection, decreased thyroid hormones, and complications related to pregnancies [31] [2].

## 2.3 Trace elements and heavy metals

90 different elements are naturally occurring on Earth, with a large variety of abundance in different materials and locations. At the crust of the Earth, the most abundant elements are oxygen (O), silicon (Si), aluminum (Al), iron (Fe), calcium (Ca), sodium (Na), potassium (K), and magnesium (Mg). Many other elements occur at lower concentrations. The elements may be separated into three groups based on their abundance in biological systems. The first class includes the major elements, which are carbon (C), hydrogen (H), nitrogen (N), and O. Next, the minor elements include Ca, chloride (Cl), Mg, phosphorus (P), and K. Finally, the least abundant elements are called trace elements and include the remaining elements [32].

Although they occur in low concentrations, some of these trace elements play an important role in biological processes and are known as essential. Other trace elements do not have such an importance and are known as non-essential. Some elements are also known to be toxic, including mercury (Hg), lead (Pb), and cadmium (Cd), which have adverse effects even at low concentrations [32]. These elements are typically known as heavy metals, which may be defined as metallic elements with high densities (five times higher than that of water) [6]. Within this definition, some metalloids such as As are also included in the term "heavy metals" as a result of their toxicity at low levels. It should be noted that all of the other trace elements also have possible toxic effect at concentrations above the safe limit of exposure, and that this limit varies considerably between the elements [32].

### 2.3.1 Contamination sources, fate and pathways

Most elements are not present as free elements; they are often present as salts in aluminosilicates, carbonites, sulfates, oxides, or sulfides. They are also often present as colloids or adsorbed to organic or mineral material in waters. Many trace elements are not soluble in water and will accumulate in bottom sediments. The chemical form in which the elements are present depends on the nature of the surroundings like pH, other species present, as well as the nature of the ions and bonded functional groups. As the solubility in water is usually low, trace elements naturally accumulate in soils. Especially soils with small diameter particles, like clay, will adsorb many trace elements on the large surface area. Clay can hence contain high levels of trace elements, despite low levels as part of the actual particle structure. High levels of organic matter in soils will also contribute to water regulation capacity, ion exchange capacity, and metal ion sorption [32].

Trace elements occur naturally in the environment, but increased levels may occur due to anthropogenic pollution from a multitude of sources. Some of the main global sources contributing to trace element and heavy metal contamination are coal and fuel combustion, waste incineration, metal smelters, agricultural activity, nuclear activity and mining activity [32]. Locally on Svalbard, sources of importance are the mines and acid mine drainage (AMD), fuel combustion, and seabird feces [33]. Studies have been conducted on AMD from the mines on Svalbard. Water and oxygen in the mines react with sulphide minerals, leading to acidic water. The water will dissolve metal ions, and hence be a source to metal pollution. As the pH increases by dilution and alkaline contribution, the metal ions may form hydroxides and precipitate. Therefore, metals can be transported from the bedrock to waters, sediments, and the tundra by AMD and could possibly cause damage to tundra vegetation [34].

Some typical elemental contamination related to mining activity are Pb, Cd, Cr, Cu, and Hg[7], but also beryllium (Be), fluoride (F), Al, vanadium (V), iron (Fe), cobalt (Co), Ni, zinc (Zn), As, selenium (Se), Sn, thorium (Th), and uranium (U)[32]. For coal mines specifically, elevated levels of Fe, Cr, Ni, Cu, Zn, Cd and Pb have been found near mining areas, compared to background levels[35][36][37]. On Svalbard, higher levels of Fe, Al, As, Cu, Ni, and Zn were found in coal and rock sampled in proximity to the coal samples taken from mining areas in Longyearbyen and Svea[38]. Study of the AMD from mine tailings in Bjørndalen on Svalbard also shows increased levels of Fe, Zn and sulfate with increased proximity to the tailings. Concentrations levels of several elements like Cu, Zn, Cd, and Ni were elevated compared to natural background levels[34].

Although contamination levels tend to be higher near major emission sources, smaller particulate and aerosol pollutants can be transported over large distances. An example is the increasing levels of Pb both in the Arctic and Antarctic since the 1920s[32]. The contaminants reaching the Arctic are mainly originating from Europe, Siberia, and North America. The aerosol measurements in Ny-Ålesund show low levels of Ni, indicating little to no impact of long-range transportation of such heavy metals to this area[33].

### 2.3.2 Toxic effects

Heavy metals have a variety of known toxic effects in humans if exposure exceeds safety limits. Some are known to cause cancer, such as As, Cd, Cr, and Ni. Others, such as Pb, Hg, and Mn, may affect the nervous system, causing memory loss and reduced learning, concentration, and reaction capacity. Some metals also have adverse effects on the heart, kidneys, and immune system[39]. Table 2.2 presents sources and toxic effects of As, Pb, Cd, Ni, and Zn.

Table 2.2: Some sources and toxic effects of selected heavy metals.

| Element | Sources | Toxic effect on the human body |
|---------|---------|-------------------------------|
| As | Volcanic eruption, wood impregnation, burning of fossil fuel and metal smelters[6][39] | Impacts the nervous system, most organs, reproduction, the endocrine and immune system, and can cause cancer[6][39]. |
| Cr | Volcanic eruption and earth erosion, industry and car catalysts[39]. | Cause lung cancer, irritation and reduced lung function[39]. |
| Cd | Plating industry, Cd-Ni batteries, fertilizers and coal combustion[6][39]. | "Itai-Itai" disease, deactivating enzymes, effect Ca, Zn and Fe balance, kidney defect, bone softening, and lung cancer[6][39]. |
| Pb | Lead-containing fuel, steel industry, electronic waste, ammunition and paint[6][39]. | Impacts blood formation, nervous system, reproduction ability, endocrine function and kidneys[39]. |
| Ni | Industrial production, fossil fuel combustion and tobacco[39]. | Carcinogenic, cause weight and hair loss, bronchitis, and reduced lung function[6]. |
| Zn | Mining, steel production, coal combustion and waste incineration[39]. | Cause cardiovascular disease and elevated blood pressure, nausea and stomach damage and neurotoxic effect[6]. |

## 2.4 Sample preparations and analytical methods

### 2.4.1 Carbon detection

Analysis of total organic carbon (TOC) gives information about the amount of organic carbon in solid or water samples by means of oxidation, combustion, acid treatment, or ashing. The results can for instance be used in the determination of carbon content in soil, the degree of humification of waste, and assessing fluxes of carbon in water systems. Residues from plants, animals, and microorganisms, as well as elemental carbon, contribute to the amount of organic carbon in sediment and soil samples[40]. The content of organic carbon is also related to the sorption of organic contaminants such as PFAS in sediments. Higher concentrations of organic material, which can be measured by TOC analysis, could also be an indication of increased concentrations of PFAS[41]. Therefore, TOC analysis is considered important, also in relation to the analysis of organic environmental pollutants. Furthermore, TOC determination often also involves quantification of total inorganic carbon (TIC), which indicates the amount of carbon contained in minerals[2].

The method used to measure TOC can be direct or indirect. In the direct method, TOC is quantified directly. Here, either inorganic carbon is removed by acid treatment before measuring the TOC, or TOC is determined directly by oxidation. Organic carbon can be oxidized by combustion, also known as ashing. As organic carbon combusts at a lower temperature than inorganic carbon, around 400 °C, combustion of exclusively organic carbon is achieved by controlling the temperature. When oxidized, the organic carbon will form $CO_2$, which can be detected and quantified, most commonly by IR spectrometry. Residual oxidicable carbon (ROC) and TIC can then be quantified by increasing the temperature, as ROC will combust at around 600 °C, and TIC will combust at around 900 °C. In the indirect approach, TIC and the total amount of carbon (TC) are measured, and the TOC is calculated by subtracting TIC from TC. TC is quantified by oxidation, while TIC is measured using the purging gas from the acid treatment or by decomposition after removal of the organic carbon[40] [2].

### 2.4.2 Solid Phase Extraction (SPE)

Solid Phase Extraction (SPE) is a commonly used sample preparation technique that is used to extract target compounds from a sample matrix. The method is based on the principle of passing a liquid with the matrix through a solid phase, or sorbent, where the target analytes have an affinity towards the solid phase and are retained[42]. SPE usually consists of five steps: conditioning the solid phase, rinsing/equilibration, loading of the sample, washing, and elution of the analytes. The conditioning and equilibration steps are used to activate and clean the sorbent, and ensures the correct chemical conditions for optimal analyte-sorbent interactions. Then, the solvent can be applied to the cartridge in a careful manner. After the sample passes through the sorbent, the column is washed to remove any contamination residue. The target analyte will be retained by the sorbent and can be eluted with a suitable eluent[43] [2].

The selection of solvents depends on the type of target analytes, the sample matrix, and the solid phase. For target analytes containing polar groups, normal phase (NP) extraction can be used, where the solid phase is polar while the sample solvent, the conditioning, equilibration, and wash solvents are nonpolar. The solvent used for the elution is polar. For nonpolar compounds, reverse phase (RP) extraction is used to extract the analytes, where the solid phase is nonpolar, the sample

solvent, the conditioning and washing solvents are polar, and the solution used for the elution is a mixture of aqueous buffer and a polar organic solvent [44] [2].

### 2.4.3 LC-MS/MS

Chromatography is the general principle of separating components on the basis of their distribution in two phases, one stationary phase and one mobile phase. Because of differences in the affinity the compounds have towards the two phases, quantified by the distribution constants, the compounds will be eluted at different times. Components with high affinity for the stationary phase will be eluted later than components that have a higher affinity for the mobile phase, as these will have a higher retention. All components spend the same amount of time in the mobile phase, but the time spent on the stationary phase, where they are retained, varies and increases the time before elution [45]. The time spent in the chromatography column by a solution that is not retained by the stationary phase is called the migration time, $t_M$. Retention time is the time passed from injection of the component to elution, and can be written as $t_R = t_M + t_M k$. k is the retention factor and is defined as the ratio of the distribution between the two phases, $k = n_s/n_m$. $n_s$ and $n_m$ are the amount of molecules in the stationary and mobile phase, respectively [44] [2].

Chromatography can be performed using an NP or an RP column. In NP chromatography, the stationary phase generally has polar properties, while the mobile phase has a nonpolar nature. In this type of chromatography, the more polar components will be retained more and will be eluted last. In RP chromatography, the stationary phase is more nonpolar, while the mobile phase is polar, and the more polar components will elute first. The choice of column type will depend on the analytes that one wants to separate [44] [2].

It is possible to perform chromatography in several ways, and one of the most common ones is liquid chromatography, where the mobile phase is a liquid. The use of smaller particles in the packed stationary phase has changed classical chromatography into high-performance liquid chromatography (HPLC), as the use of smaller particles increases the separation efficiency [44] [2].

Each chromatography method must be coupled with a detection method. Often chromatography methods are coupled with mass spectrometry (MS) detection, as this method is very sensitive and selective. This detection method requires that the analytes may be ionized and transferred to the gas phase. The device between the column and the mass spectrometer is called the interface, and this is where the ionization and evaporation of the compounds occur [44]. The ions in MS are separated on the basis of their mass-to-charge ratio (m/z), and presents a mass spectrum with the detection of these ratios [5] [2].

Although MS is highly sensitive and precise, which provides accurate results even at low concentrations, some issues and possible errors exist, especially related to interference. One problem that may occur is the overlap of masses, also called spectroscopic interference. This may happen if there are ions with the same m/z ratio as a target analyte ion. Increasing the resolution of the spectrometer may solve these issues [5]. Another possible error is matrix interference, where the matrix affects the detected signal of the target analyte, either suppressing or enhancing the signal. This may happen because of interference by molecules from the matrix with the ionization process. To solve this, the sample could be diluted, the interfering species removed or the introduction procedure changed [5] [46].

One of the most used ionizing methods in MS is electrospray ionization (ESI). Here, the compounds in the solution is subject to high voltage, the compounds are hence ionized and form charged droplets. The droplets are mixed with a stream of nebulizing gas, and a stream of dry gas is sent in the opposite direction, breaking down and decreasing the size of the droplets. The detection is then performed either in positive or negative mode [44] [2].

Several types of mass analyzers may be used for detection. One of the more common methods is to use a quadrupole mass analyzer. In this method, four cylindrical rods are used and act as mass filters. The rods are subjected to adjusted voltages, creating an oscillating electric field that allows only fragments with a certain m/z ratio to pass. Adjusting voltages allows for the selection and analyzing of specific m/z values [44] [2].

In tandem MS, mass spectrometry occurs in two steps. After the initial fragmentation and mass analysis, a precursor ion is selected and goes through fragmentation once more. Thus, product ions are formed, making it possible to obtain ion spectra with large amounts of detailed information. This detection method also works well with chromatographic methods because the mass spectrometer is then only exposed to one compound at the same time, so it is well suited for use when chromatographic methods are used [5] [2].

### 2.4.4   ICP-MS

Inductively coupled plasma mass spectrometry (ICP-MS) is a type of atomic mass spectrometry, commonly used for elemental analysis. It uses an inductively coupled plasma (ICP) ion source and a mass analyzer, and allows for simultaneous determination of many elements within a short time frame. The possibility of multi-element analysis and determination of isotope ratios, combined with a wide dynamic range and high sensitivity (detection limits are often below 1 ppb), makes ICP-MS analysis highly attractive [5].

To be able to analyze samples by atomic spectroscopic techniques, the sample must be converted to free atoms and ions in the gas phase. The most common way of introducing the sample to the ICP is by direct nebulization, where a nebulizer converts the sample to an aerosol before it is introduced into a plasma and forms a continuous stream of ions, atoms, and molecules. In ICP, an argon plasma is used and flows through quartz tubes at a flow rate between 11 and 17 L/min. The argon ions and cations in the sample are the conducting species in the plasma. Ion sources in atomic mass spectrometry generally need to be very energetic to be able to convert the sample into atoms and ions. The ICP is a radio-frequency power source, and the cations in the plasma absorb the energy. As a result, the plasma reaches temperatures up to 10,000 K, which dries and decomposes the aerosol particles, forming ions [5].

The ions can then be analyzed by a mass analyzer, which normally consists of a quadrupole. Here, the ions are sorted based on their mass-to-charge ratio and detected, as previously described in Section 2.4.3. Because the ICP is run at atmospheric pressure, while the MS needs high vacuum, a sampler and a skimmer are placed at the interface. These are two metal cones with apertures around 1 mm, which allow the ions to pass through, and are guided into the mass analyzer. The result of the detection is a mass spectra with isotope peaks from which the elements can be identified and quantified [5]. As with the MS detector in LC-MS/MS, errors with ICP-MS are related to spectroscopic and matrix interferences.

## 2.5 Quality Control (QC) and Quality Assurance (QA)

### 2.5.1 Calibration curve and Internal standard method

In many analytical techniques, a calibration curve is needed for quantitative analysis. This curve could be made by plotting the instrument response versus some known analyte concentrations. The response-to-concentration relationship should preferably be linear, at least in the concentration range relevant for the unknown sample. In that case, a linear regression could be used through the plot to make the calibration curve. The response-concentration plot could be made using different methods, and using internal standards (IS) is one of the most common methods [44] [2].

In the internal standard method, a compound similar to the target analytes, IS, is added at a known concentration to all samples and to all calibration samples. Calibration samples also contain the target analytes in known concentrations. The calibration is then performed by plotting the response (peak area) of the analyte peak divided by the response of the IS. The equation used to calculate this ratio is presented in Equation 1 [44]. An example of the resulting calibration curve is presented in Figure 2.3 [2].

$$\text{Ratio} = \frac{\text{Area of target analyte peak}}{\text{Area of IS peak}} \tag{1}$$
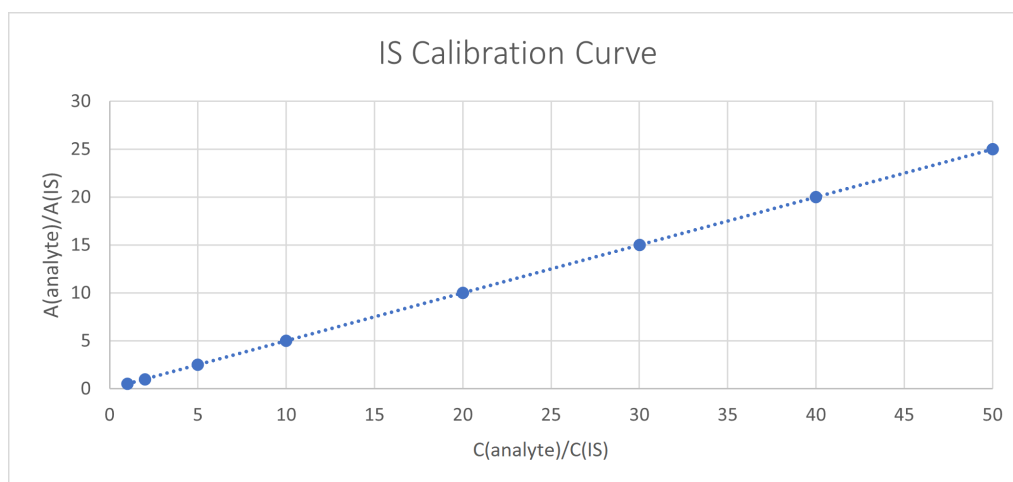


Figure 2.3: Example of a calibration curve made with IS method. A(analyte) stands for the area of the target analyte peak, A(IS) stands for the area of the IS peak, C(analyte) stands for concentration of analyte, and C(IS) stands for the concentration of IS.

Although the IS should be similar to the analytes, for it to behave similarly in the sample matrix and chromatographic column, it must be possible to detect the IS separately from the target analytes. Furthermore, no amount of IS can be present in the sample matrix prior to addition [44]. This is often achieved by using $^{13}C$ labeled molecules. These molecules contain isotope carbon atoms that have an extra neutron. In practice, these molecules will behave exactly like analyte compounds but can be detected separately by MS due to the difference in mass [47]. The use of the internal standard method provides a higher degree of precision, as it compensates for errors or variations in sample loading or sample preparation because these errors will affect the amount of IS and the analyte equally [5] [2].

### 2.5.2   Limit of Detection (LOD) and Limit of Quantification (LOQ)

Limit of detection (LOD) and limit of quantification (LOQ) describe the lowest concentrations of an analyte that may be measured with a certain reliability, and are essential characters for method validation[48]. LOD defines the lowest concentration needed for detection, while LOQ is the lowest concentration needed for quantification of the signal[44][48]. LOD and LOQ may be defined and calculated in several ways. Typical definitions are that LOD has a signal-to-noise (S/N) ratio of 3, while LOQ concentration has a S/N ratio of 10[44]. Another common way to calculate LOD and LOQ is by using the linear regression analysis. Here, the standard deviation of the y-interception and the slope of the calibration curve is used, and LOD and LOQ are calculated as

$$LOD = 3.3 \frac{SD}{S} \tag{2}$$

and

$$LOQ = 10 \frac{SD}{S}, \tag{3}$$

where $SD$ is the standard deviation in the interception and $S$ is the slope of the calibration curve.

### 2.5.3   Certified reference material (CRM)

An additional important part of quality assurance and quality control in analytical chemistry is the use of certified reference material (CRM), which is a type of reference material that includes documentation of the property values of the materials and related uncertainties from an authoritative body like the National Institute of Standards and Testing (NIST) and The Bureau of Certified Reference Materials (BCR). These materials could, for instance, be pure chemical solutions, standard solutions, or matrix reference materials, and are used for calculating recovery, calibration, evaluating method validation and measurement uncertainty, and QC of the analysis[49][32][2].

## 2.6   Statistical tools

### 2.6.1   Box plot

A practical way to represent a data set is using box plots. Box plots present the data visually by showing the first and third quartiles, median, the minimum, and maximum values in the first and third quartile, and outliers in the data set. In this way, the box plot illustrates well the variability and symmetry of the data set. The box plot consists of a square between the first and third quartiles of the data, which represents 50% of the data points. A horizontal line inside the box shows the median value. Vertical lines called whiskers above and below the square show the relative extremes outside the first and third quartiles, excluding possible outliers. Any outliers are marked as individual data points outside the whiskers[50]. Figure 2.4 shows a box plot with an outlier above the upper whisker.
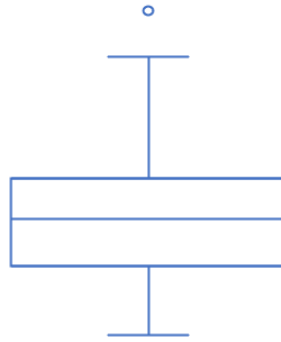
Figure 2.4: Example of a box plot.

### 2.6.2 Principal Component Analysis

Principal component analysis (PCA) is a method to visualize higher-dimensional spaces, and does this by projecting the higher dimensional data down onto a lower dimensional space. By doing this, the number and type of coordinates are changed, and one can plot the data and assess it visually. PCA uses latent variables for the representation of the data, which are linear combinations of the original variables. These latent variables are in PCA the principal components (PC). With these, the data can be presented in a score plot[51].

The scores are the coordinates of the data points with the new PC axes. The score plot can be used to identify possible outliers and patterns within the data set. A typical score plot is shown in Figure 2.5a. To assess how much influence a specific variable has on the direction of a PC, a loading plot is helpful. The loadings explain how the variables are mixed in the linear combination that forms the latent variables. The loading plot belonging to the score plot is shown in Figure 2.5b. From the loading plot one can assess the impact of the variables on the PCs, find correlations and negative correlations between the variables, and detect negligible variables that have little to no effect on the PCs.

PCA is hence a useful tool for visual presentation of complex data sets, finding correlations between variables, and making predictions. Large amounts of data can be presented in a simplified way, while not so obvious patterns can be detected.



(a) Score plot
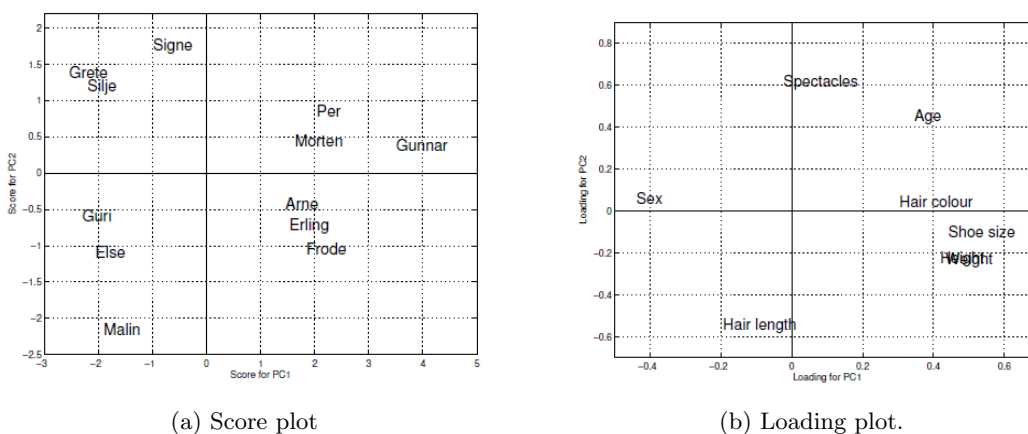


(b) Loading plot.

Figure 2.5: Examples of score and loading plots for a people data set[51].

# 3 Experimental

This section presents experimental methods. First, details on the sampling are presented, followed by sampling preparation methods including extraction and microwave digestion procedures, and details on the analytical methods and instruments used. As with Section 2, several parts are reproduced from the specialization project, including whole or parts of Sections 3.1, 3.2.1, 3.2.2, 3.2.3 and 2.2.

## 3.1 Sampling

All samples were collected on 23.08.22 and 24.08.22, in proximity to Ny-Ålesund, Svalbard. Figure 3.1 shows the location of Ny-Ålesund marked with a red dot, on the west coast of Svalbard.



Figure 3.1: Map showing Svalbard, and the location of Ny-Ålesund is marked with a red label [52]

18 sediment and soil samples were collected in sample cups, and 18 sediment and soil samples were collected in 50 mL polypropylene tubes. 15 water samples were filtered and collected in 15 mL tubes, and 50 mL of unfiltered water was collected at two locations in Tvillingvatnet. Details on the sampling equipment are presented in Table 3.1. Sampling locations are illustrated on maps in Figure 3.2, Figure 3.3 and Figure 3.4, and coordinates are presented in Table 3.2. A map with the locations of all the mines that have been active in Ny-Ålesund is included in Figure A.1 in Appendix A [2].

Table 3.1: Sampling equipment details.

| Equipment | Details |
| --- | --- |
| 15 mL tube | VWR, centrifuge tubes PP with PE-lid, metal free 525-1121 |
| 50 mL tube | VWR, centrifuge tubes PP with PE-lid, metal free 525-1125 |
| Beaker | Coulter, 20ml analysis beaker in PS with PE-lid |
| Syringe | HENKE-JECT, Luer-spiss 20mL 613-2046 |
| Filter | VWR, Syringe filter, 0.45um, PES 514-1261 |
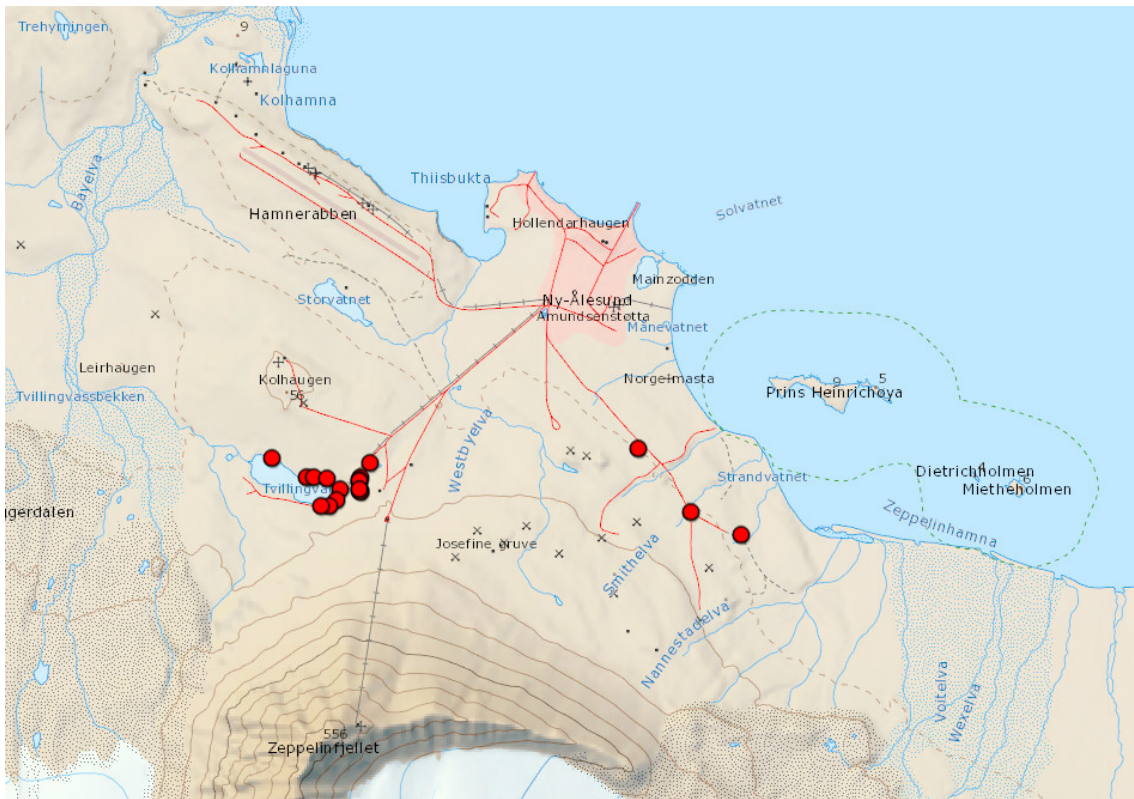


Figure 3.2: Map showing the sampling locations around Tvillingvatnet and Smithelva[52].
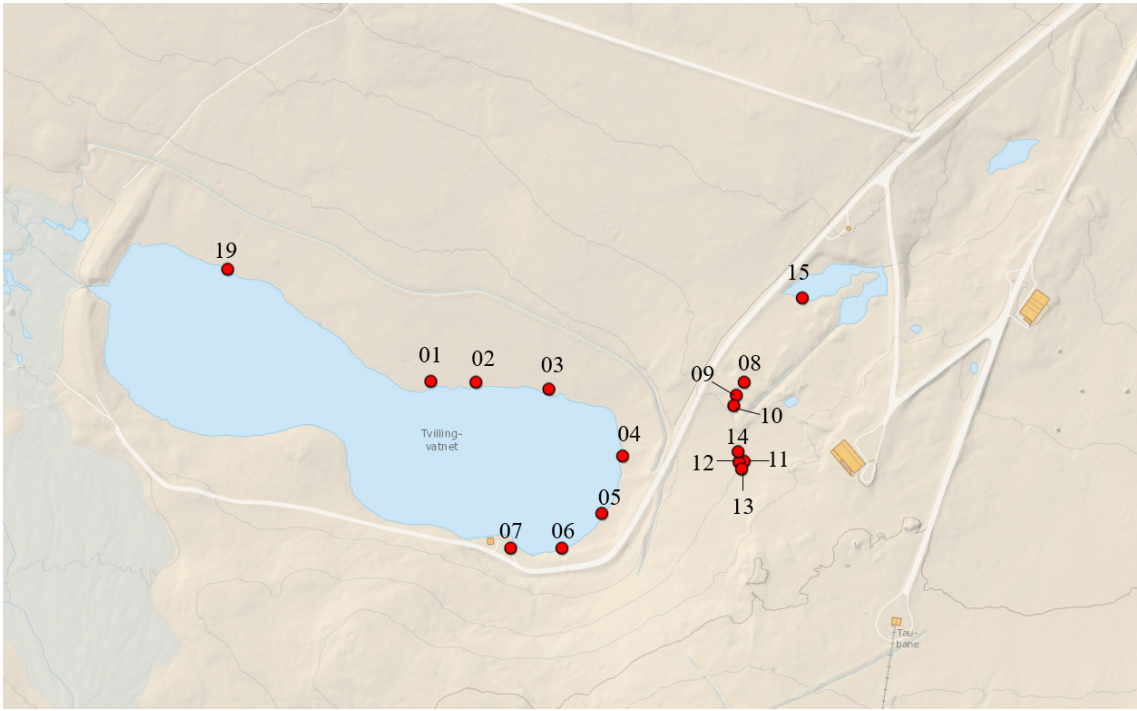
Figure 3.3: Map showing the sampling locations in and around Tvillingvatnet in more detail[52].
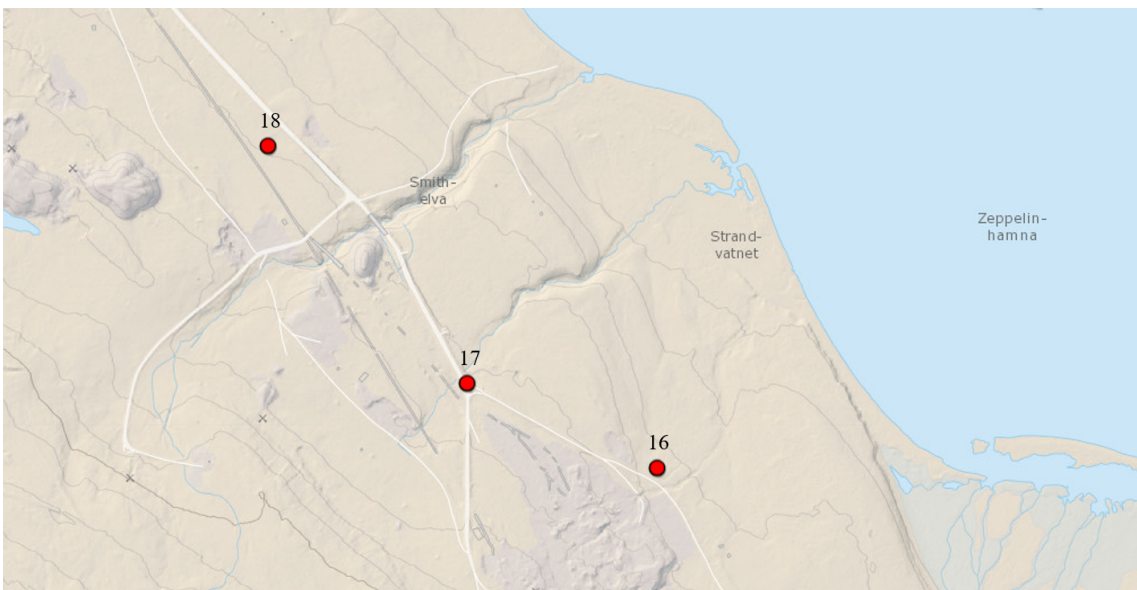


Figure 3.4: Map showing sampling locations 16, 17 and 18 by the Smithelva[52].

Table 3.2: Sampling location number and sampling location.

| Sampling location number | Coordinates (Longitude, Latitude) |
| --- | --- |
| 01 | 78.91686°N, 11.87296°E |
| 02 | 78.91687°N, 11.87450°E |
| 03 | 78.91685°N, 11.87716°E |
| 04 | 78.91642°N, 11.87987°E |
| 05 | 78.91602°N, 11.87923°E |
| 06 | 78.91577°N, 11.87789°E |
| 07 | 78.91576°N, 11.87609°E |
| 08 | 78.91697°N, 11.88404°E |
| 09 | 78.91688°N, 11.88381°E |
| 10 | 78.91680°N, 11.88372°E |
| 11 | 78.91643°N, 11.88421°E |
| 12 | 78.91642°N, 11.88402°E |
| 13 | 78.91638°N, 11.88411°E |
| 14 | 78.91649°N, 11.88395°E |
| 15 | 78.91756°N, 11.88597°E |
| 16 | 78.91866°N, 11.94077°E |
| 17 | 78.91628°N, 11.95226°E |
| 18 | 78.91550°N, 11.96291°E |
| 19 | 78.91755°N, 11.86549°E |

The samples collected at locations 8, 9, 10, 11, 12, and 13 are top soil samples, not sediment samples, and the samples from location 14 are from a small puddle. Figure 3.5 shows a photo of the puddle where sediment samples 14a and 14b and water sample W14 were collected. The water samples W1, W2, W3, W4, W5, W6, and W7 were sampled directly from Tvillingvatnet with a syringe and filtered. Samples W5a and W6a were sampled from drain pipes at locations 05 and 06, respectively, and filtered. The drain pipes are illustrated in Figure 3.6. Water samples WA and WB were not filtered. Tables 3.3 and 3.4 include more details of every sample. More photos of the sampling are included in Appendix B [2].
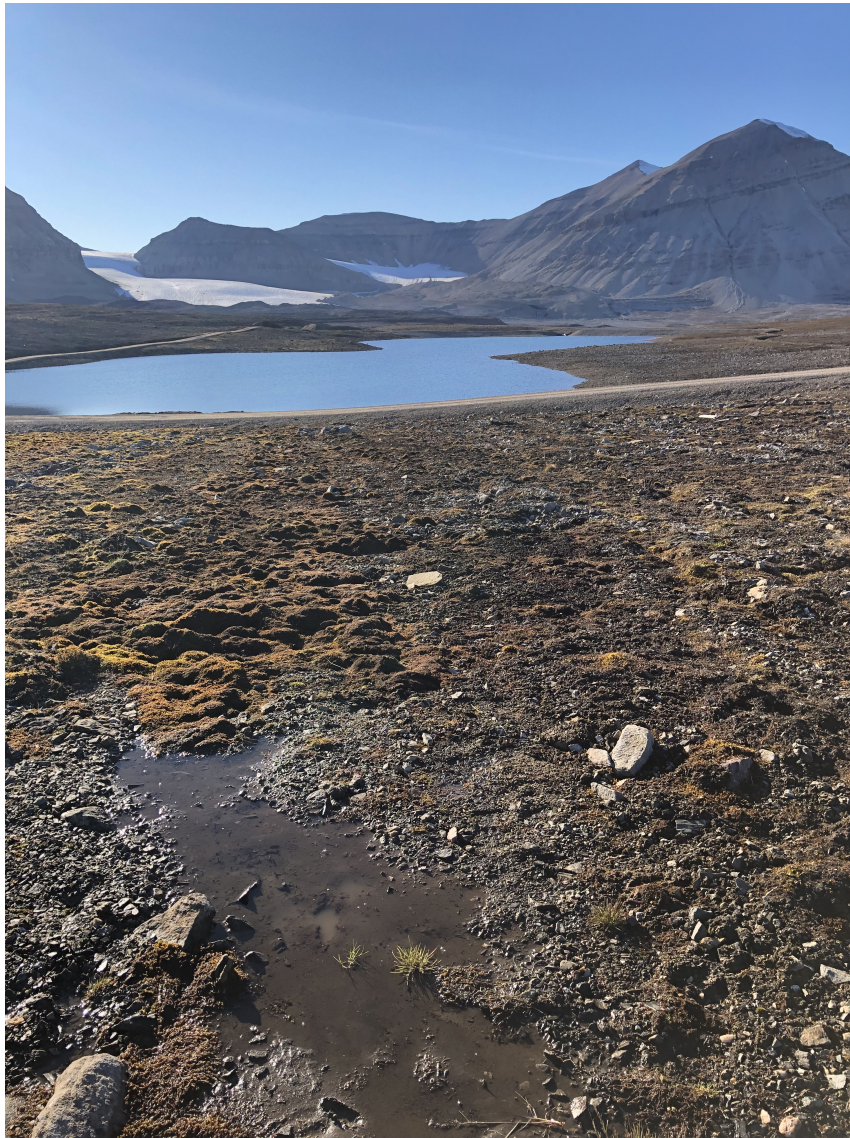
Figure 3.5: Photo of puddle on location number 14, where sediment samples 14a and 14b and water sample W14 were sampled. The lake in the background is Tvillingvatnet.

Figure 3.6: Drain pipes on location 05 and 06.

Table 3.3: Water sample names and descriptions.

| Sample name | Type of sample | Sampling location |
|---|---|---|
| W1 | 10 mL filtered water sample from Tvillingvatnet | 01 |
| W2 | 10 mL filtered water sample from Tvillingvatnet | 02 |
| W3 | 10 mL filtered water sample from Tvillingvatnet | 03 |
| W4 | 10 mL filtered water sample from Tvillingvatnet | 04 |
| W5 | 10 mL filtered water sample from Tvillingvatnet | 05 |
| W5a | 10 mL filtered water sample from drainage system | 05 |
| W6 | 10 mL filtered water sample from Tvillingvatnet | 06 |
| W6a | 10 mL filtered water sample from drainage system | 06 |
| W7 | 10 mL filtered water sample | 07 |
| W14 | 10 mL filtered water sample from small puddle | 14 |
| W15 | 10 mL filtered water sample | 15 |
| WA | 50 mL unfiltered water sample | 07 |
| WB | 50 mL unfiltered water sample | 19 |

Table 3.4: Sediment and soil sample names and descriptions.

| Sample name | Type of sample | Sampling location |
|---|---|---|
| 1a | Above water sediment sample | 01 |
| 2a | Above water sediment sample | 02 |
| 3a | Above water sediment sample | 03 |
| 4a | Above water sediment sample | 04 |
| 5a | Above water sediment sample | 05 |
| 6a | Above water sediment sample | 06 |
| 7a | Above water sediment sample | 07 |
| 8a | Soil sample | 08 |
| 9a | Soil sample | 09 |
| 10a | Soil sample | 10 |
| 11a | Soil sample | 11 |
| 12a | Soil sample | 12 |
| 13a | Soil sample | 13 |
| 14a | Above water sediment sample | 14 |
| 15a | Above water sediment sample from water close to Tvillingvatnet | 15 |
| 16a | Above water sediment sample from water close to Smithelva | 16 |
| 17a | Above water sediment sample from water close to Smithelva | 17 |
| 18a | Above water sediment sample from water close to Smithelva | 18 |
| 1b | Under water sediment sample | 01 |
| 2b | Under water sediment sample | 02 |
| 3b | Under water sediment sample | 03 |
| 4b | Under water sediment sample | 04 |
| 5b | Under water sediment sample | 05 |
| 6b | Under water sediment sample | 06 |
| 7b | Under water sediment sample | 07 |
| 8b | Soil sample | 08 |
| 9b | Soil sample | 09 |
| 10b | Soil sample | 10 |
| 11b | Soil sample | 11 |
| 12b | Soil sample | 12 |
| 13b | Soil sample | 13 |
| 14b | Under water sediment in small puddle | 14 |
| 15b | Under water sediment sample from water close to Tvillingvatnet | 15 |
| 16b | Under water sediment sample from water close to Smithelva | 16 |
| 17b | Under water sediment sample from water close to Smithelva | 17 |
| 18b | Under water sediment sample from water close to Smithelva | 18 |

## 3.2 Sample preparations and Analytical methods

Several preparation techniques were used to prepare samples for various analyses. This section includes details of the preparation techniques and analytical instruments and parameters. All sediment and soil samples were freeze dried completely for 48 hours before any further sample preparation[2]. Details on purity and brands of chemicals used for solid phase extraction (SPE) and microwave digestion (UltraClave) are included in Table 3.5.

Table 3.5: Chemicals used for SPE and microwave digestion (UltraClave).

| Procedure | Chemical | Purity | Brand |
|---|---|---|---|
| SPE | Methanol ($CH_3OH$) | HiPerSolv CHROMANORM | VWR Chemicals |
| | Acetonitrile ($C_2H_2N$) | HiPerSolv CHROMANORM | VWR Chemicals |
| | Hydrochloric acid ($HCl$) | AnalaR NORMAPUR | VWR Chemicals |
| | | | |
| | Nitric acid ($HNO_3$) | AnalaR NORMAPUR | VWR Chemicals |
| UltraClave | Hydrogen peroxide ($H_2O_2$) | AnalaR NORMAPUR | VWR Chemicals |
| | Sulphuric acid ($H_2SO_4$) | Suprapur | Merck KGaA |

### 3.2.1 pH and Conductivity measurements

pH and conductivity were measured directly at sampling locations 1, 3, 4, 5, 6 and 7 in Tvillingvatnet, as well as in the smaller water close to Tvillingvatnet at location number 15. A WTW 340 multi meter instrument with a SenTix 940 pH electrode was used to measure the pH, and a Multi 3500i Handheld Multimeter, WTW with a ConOx electrode was used to measure conductivity.

### 3.2.2 Carbon determination

For TOC and TIC analysis of the water samples WA and WB, the instrument Shimadzu Total Organic Carbon Analyzer TOC-L was used. This instrument uses a combustion catalytic oxidation method to quantify the organic and inorganic carbon content of the water sample. This means that organic carbon is oxidized by combustion and can be quantified as $CO_2$ gas by an infrared gas analyzer. The instrument possesses an autosampler. A TC standard stock solution was prepared as described in the manual provided[53]. 2.125 g of potassium hydrogen phthalate was dissolved in 1 L of Milli-Q water, resulting in a carbon concentration of 1000 ppm. 1 mL of this stock solution was then further diluted with 500 mL of Milli-Q water, until a concentration of 2 ppm was reached. The IC standard stock solution was prepared by solving 3.497 g sodium hydrogen carbonate and 4.412 g sodium carbonate in 1 L Milli-Q water. This resulted in a carbon concentration of 1000 ppm, and was diluted in the same way as the TC standard until a final concentration of 2 ppm[2].

The TOC and TIC of the sediment and soil samples were analyzed using Skalar PRIMACS$^{SNC-100}$ ANALYZER instrument for the measurement of TN / TC / IC, with an autosampler. Ceramic crucibles were cleaned in a dishwasher and burned at 900°C before application of samples. The calibration standard used contained 2.37 g of ammonium oxalate monohydrate with a carbon content of 16.90%. 0.40 g of carbon black, 3.33 g of calcium carbonate with a carbon content of 12.00% and aluminum oxide until a final mass of 20.0 grams. Seven standards were prepared with

masses 10.0, 25.2, 50.3, 74.8, 100.3, 125.1 and 150.6 mg. All 36 sediment and soil samples were analyzed, and the results are presented in Figure 4.3 and 4.4[2].

### 3.2.3 SPE of PFAS

SPE was used to extract PFAS from the sediment and soil samples, as well as two water samples. The extraction was performed according to procedure provided by Hanne Vistnes. The two un-filtered water samples (WA and WB) taken from Tvillingvatnet were filtered and the filters were freeze dried. A blank filter was prepared by filtering 50 mL distilled water. After freeze-drying, the filters were inserted into 15 mL Eppendorf tubes and 20 μL internal standards of 1 ppm of the three standards were added. 5 mL of Milli-Q water, acidified to a pH below 3 with hydrochloric acid (HCl), was added and liquid-solid extraction (LSE) was performed by vortexing the tubes for one minute. The mixtures were then ultrasonicated for 45 minutes at 35 °C. The samples were centrifuged at 3000 rmp for 5 minutes and the supernatant was collected and diluted with acidified Milli-Q water with a pH below 3, until a final volume of 50 mL. Vortex mixing was performed on all samples for one minute, and then SPE was performed[2].

STRATA X-RP cartridges were used for the SPE. Initially, the cartridges were conditioned with 10 ml of methanol and then equilibrated with 10 mL of acidified Milli-Q water, with a pH below 3. The samples were then loaded onto the cartridges and then washed with acidified Milli-Q water. The cartridges were then dried under vacuum for about 30 minutes, until completely dry. The analytes were eluted with 10 mL of a mixture of 1:1 methanol and acetonitrile and collected in 15 ml Eppendorf tubes. The SPE procedure is illustrated in Figure 3.7. The eluents were evaporated to a final volume of about 250 μL, using TurboVAP at 40°C and a gentle stream of nitrogen gas. Finally, they were diluted to 1 mL with a mixture of 1:1:2 of methanol, acetonitrile, and Milli-Q water. The final samples were analyzed for various PFAS using LC-MS/MS analysis[2].
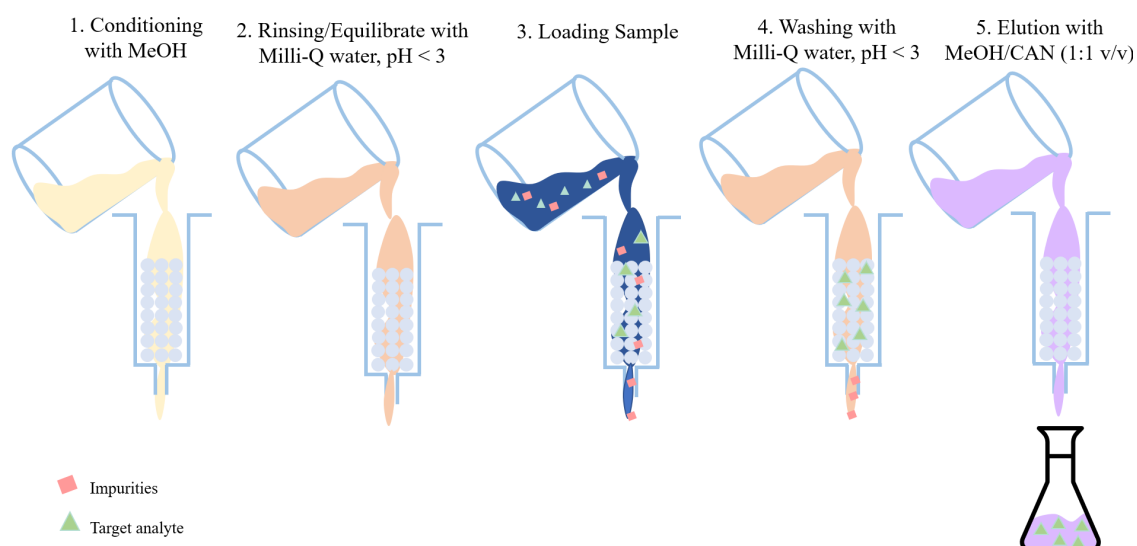


Figure 3.7: Illustration showing the SPE procedure used.

### 3.2.4  PFAS analysis by LC-MS/MS

Before SPE was performed, all samples were spiked with 20 µ$L$ internal standard solution containing $^{13}C$ isotope-labeled PFOS, PFOA and 6:2 FTS, all present in concentrations of 1 ppm. The samples were analyzed using an UPLC-Xevo TQS instrument and the method was optimized by Kristine Vike-Jonas. The column was a Kinetex column (30 x 2.1 mm, 1.3 µm, 100Å Phenomenex), serially connected to a Phenomenex (C18, 2.1 mm) guard column. The mobile phase consisted of a mixture of a water phase with 2 mM ammonium acetate and an organic phase with methanol. The column temperature was 30 °C, and flow rate was 0.25 mL/min. An injection volume of 4 µL was used, and wash solvent consisted of MeOH : ultrapure water (1:1), with 0.1% formic acid. 8 second injection was used pre-injection, and 10 second post-injection. The ionizer was an ESI ionizer, operating in negative mode. Tune parameters and gradient used are described in Table 3.6 and 3.7[2].

Table 3.6: Ionization tuning parameters.

| | |
|---|---|
| Capillary | 2 kV |
| Cone | 25 V |
| Source Offset | 40 V |
| Desolvation temperature | 450 °C |
| Desolvation Gas flow | 650 L/h |
| Cone | 150 L/h |
| Neblulizer | 6 Bar |
| Source Temperature | 150 °C |

Table 3.7: Gradient used in UPLC system.

| Time | % Water phase | % Organic phase |
|---|---|---|
| Initial | 80 | 20 |
| 0.1 | 80 | 20 |
| 0.2 | 50 | 50 |
| 0.8 | 30 | 70 |
| 1.5 | 20 | 80 |
| 2.8 | 15 | 85 |
| 4.5 | 0 | 100 |
| 5.5 | 0 | 100 |
| 5.6 | 80 | 20 |
| 6 | 80 | 20 |

### 3.2.5 Microwave digestion and ICP-MS analysis

All water samples that were sent to ICP-MS analysis were filtered at the sampling site. Three drops of concentrated HNO₃ were added to all the water samples the day after sampling. Sediment and soil samples were digested by microwave digestion instrument (UltraClave, Milestone, GmbH, Leutkirch, Germany) prior to analysis by ICP-MS. In this procedure, the vials were rinsed three times with Milli-Q grade water, before 250-350 g of sediment or soil sample were added to the vials. 9 mL 50% (v/v) nitric acid ($HNO_3$) was added to each of the vials before placement in the UltraClave instrument. The water bath in the instrument consisted of 300 mL distilled water, 30 mL 30% hydrogen peroxide ($H_2O_2$) and 2 mL concentrated sulphuric acid ($H_2SO_4$). After completed digestion, the samples were diluted with ultrapure water until a final HNO₃ concentration of 0.6 M and transferred to 15 mL polypropylene tubes.

The samples were analyzed using 8800 Triple Quadrupole ICP-MS system (Agilent, USA). System parameters used when the analyses were performed 02.02.2023 and 03.03.2023 are listed in Table 3.8 and 3.9.

Table 3.8: ICP-MS parameters (02.02.2023).

| General Parameters | |
| --- | --- |
| RF Power | 1550 W |
| Nebulizer Gas | 0.80 L/min |
| Makeup Gas | 0.38 L/min |
| Sample depth | 8.0 mm |
| Ion lenses | x-lens |
| $H_2$ mode | |
| $H_2$ gas flow | 4.5 mL/min |
| He gas flow | 1.0 mL/min |
| $O_2$ mode | |
| $O_2$ gas flow | 0.45 mL/min |
| He gas flow | 1.0 mL/min |

Table 3.9: ICP-MS parameters (03.03.2023).

| General Parameters | |
| --- | --- |
| RF Power | 1600 W |
| Nebulizer Gas | 0.78 L/min |
| Makeup Gas | 0.38 L/min |
| Sample depth | 8.0 mm |
| Ion lenses | s-lens |
| $H_2$ mode | |
| $H_2$ gas flow | 7.5 mL/min |
| He gas flow | 3.5 mL/min |
| $O_2$ mode | |
| $O_2$ gas flow | 0.6 mL/min |
| He gas flow | 2.0 mL/min |

# 4  Results and Discussion

In this section, the results of all analyzes are presented and discussed. First, the results from pH and conductivity measurements are presented, then TOC and TIC quantification, before the element quantification from ICP-MS analysis and PFAS results are presented. Finally, PCA results are included. Results from pH, conductivity, TOC, and TIC are reproduced from the specialization project.

## 4.1  pH and Conductivity

### 4.1.1  pH

pH measurements are presented in the bar chart in Figure 4.1. The average pH value in Tvillingvatnet (including only pH values from locations 1, 3, 4, 5, 6, and 7) was 8.14, resulting in a slightly alkaline pH value. The highest pH was measured at sample location 15, in the water above Tvillingvatnet, with a pH value of 8.36. The highest pH values measured in Tvillingvatnet were at locations 6 and 7, which were close to where the drain water entered the lake. The lowest pH value, 7.87, was measured at sample location 4 [2].
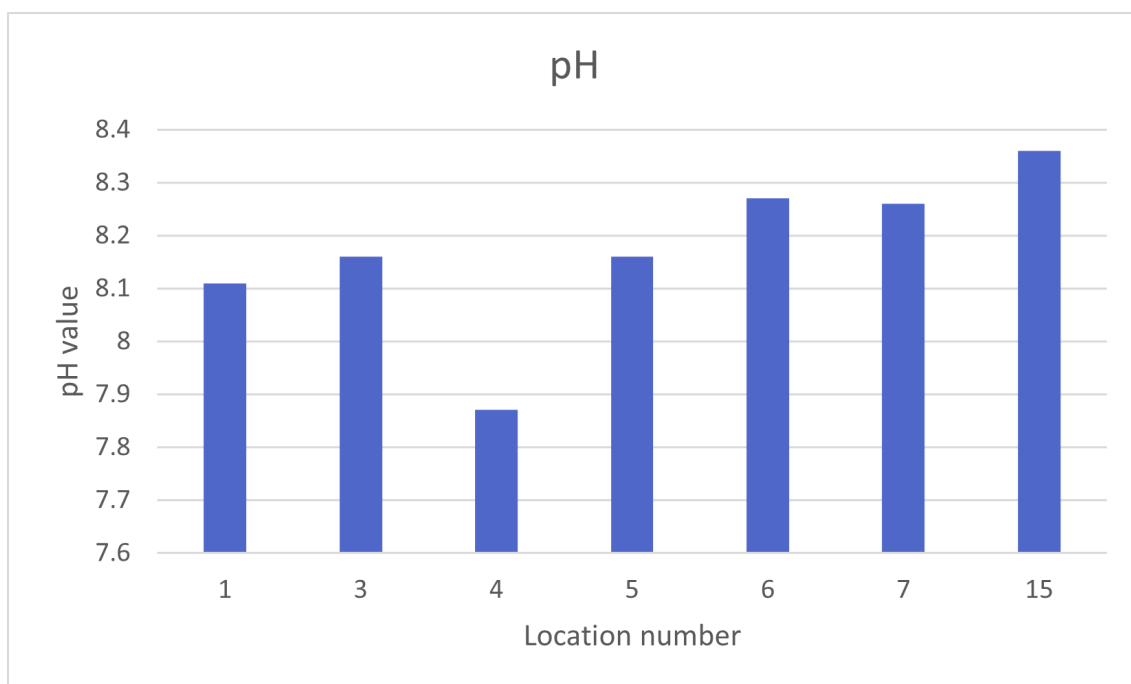


Figure 4.1: Results of pH measurements.

### 4.1.2  Conductivity

Conductivity measurements are presented in the bar chart in Figure 4.2. Tvillingvatnet had an average conductivity of 315 µS/cm. The highest measurements were made at locations 5 and 15, with a conductivity of 455 µS/cm at location 5, and 397 µS/cm at location 15. As the water at location 15 is smaller, a higher conductivity could be expected as a result of less dilution of the conductive elements [2].
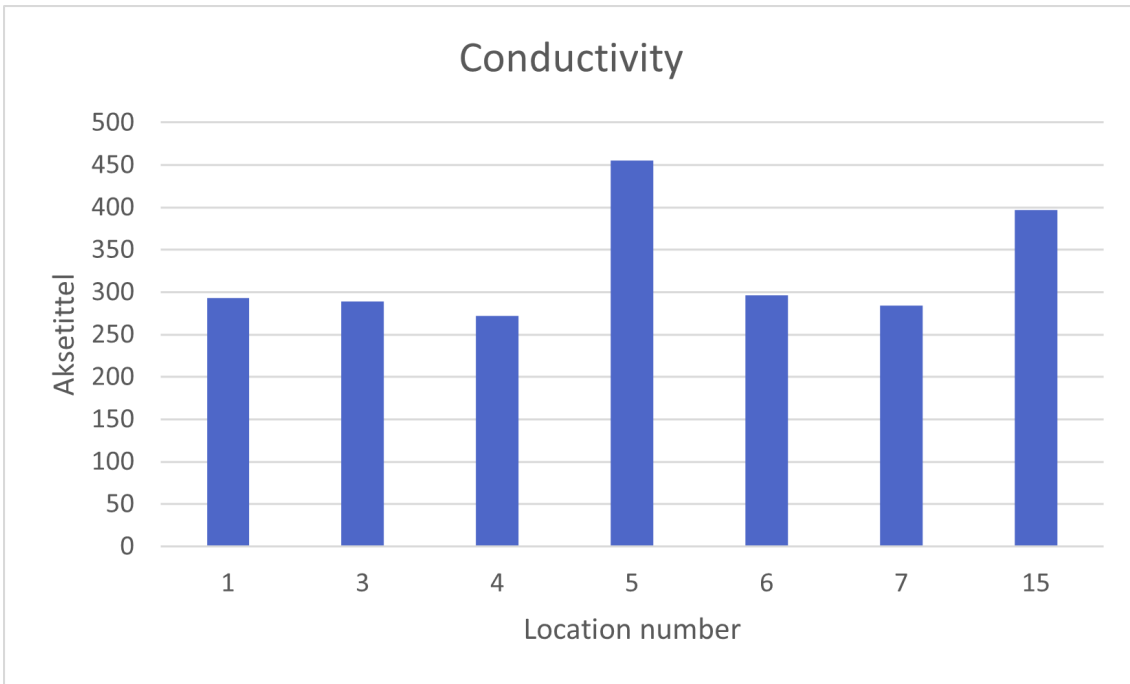
Figure 4.2: Results of conductivity measurements.

## 4.2 TOC and TIC

The results of the TOC and TIC analysis of water samples WA and WB, and soil and sediment samples are presented in Table 4.1, Figure 4.3 and Figure 4.4[2].

### 4.2.1 TIC and TOC in water samples

Table 4.1: TOC and TIC results in water samples WA and WB.

| Sample location | TOC | TIC |
|---|---|---|
| A | 1.276 mg/L | 15.65 mg/L |
| B | 1.419 mg/L | 17.92 mg/L |

### 4.2.2 TIC and TOC in sediment/soil samples

As mentioned in Section 3.1, the samples collected at locations 8, 9, 10, 11, 12, and 13 are top soil samples. Some of the higher values of organic carbon can be assumed to be due to organic matter such as plants and microorganisms, as these samples contain some moss and other vegetation. However, the highest concentration of organic carbon is found in the sediment sample taken below the water surface at location 18. The TOC concentration in the overbank sediment sample collected only centimeters from the water edge is much lower. This might raise concern about contamination of this specific sample[2].
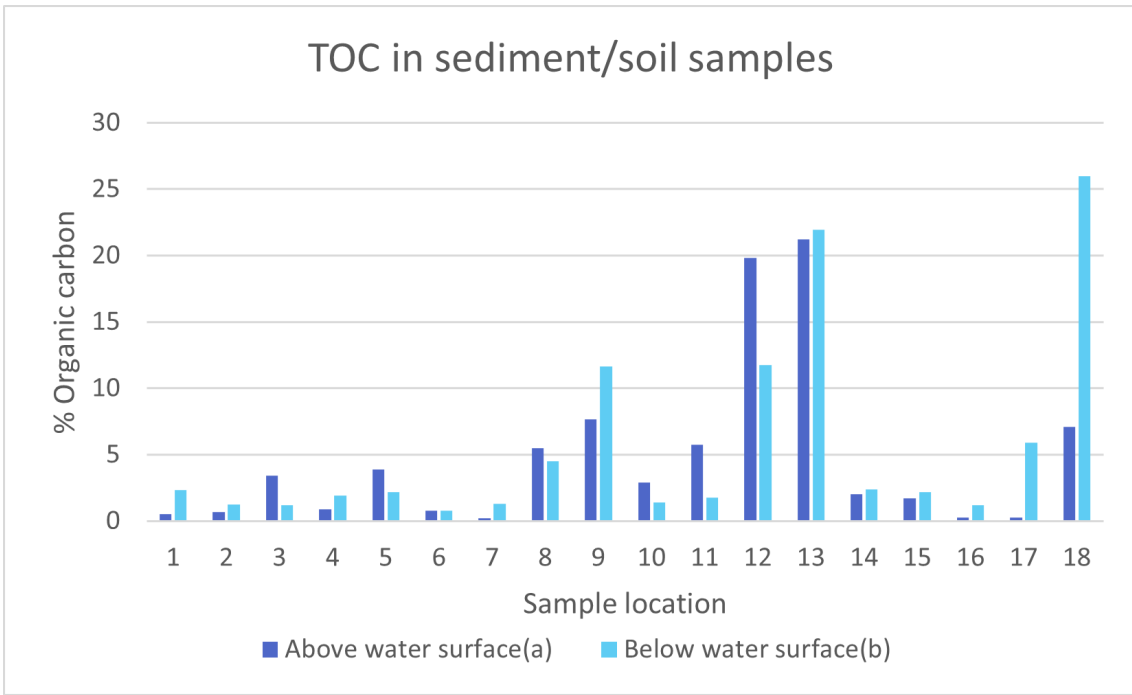
Figure 4.3: Results from TOC analysis of sediment and soil samples. Note that all samples at locations 8 to 13 are top soil samples.

In the analysis of TIC, there is a large concentration difference between the two soil samples collected at location 10. The samples were collected close to each other (within one meter), but may have a wide variety of vegetation and mineral content, since the soil surface had a high degree of heterogeneity. However, the possibility of contamination should not be neglected[2].
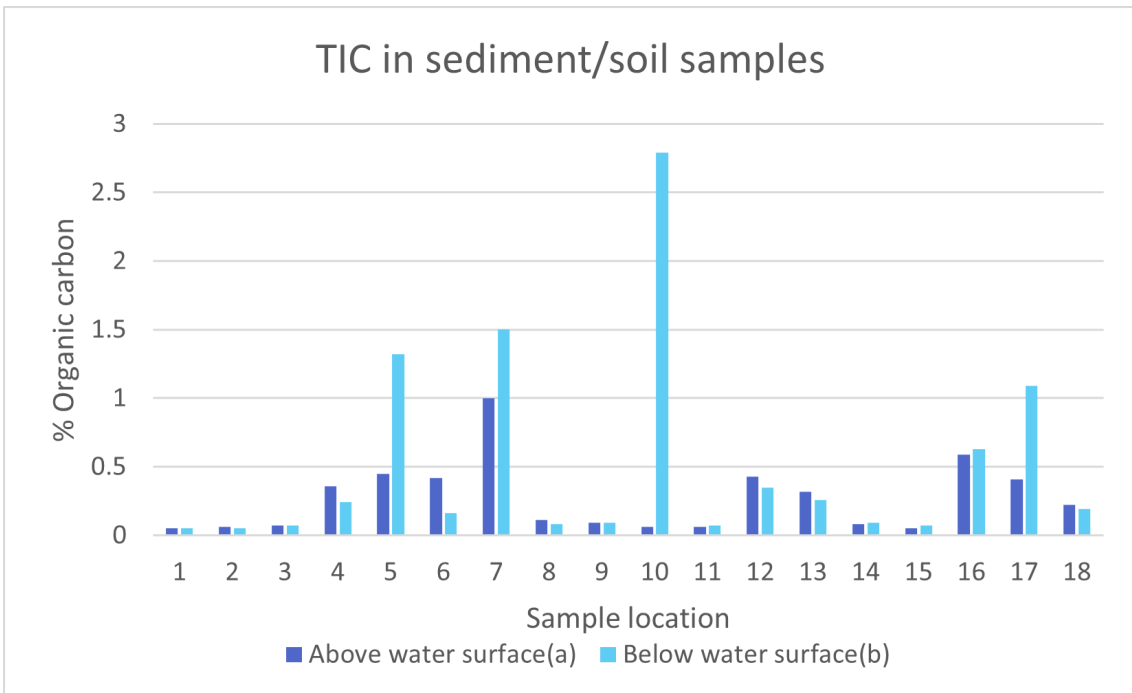


Figure 4.4: Results from TIC analysis of sediment and soil samples. Note that all samples at locations 8 to 13 are top soil samples.

## 4.3 PFAS

### 4.3.1 Calibration curve

Eventual signals in blanks (0 ng/mL) were subtracted from the analyte signal. Quantification was then performed using the internal standard calibration method (see Equation 1), using the IS with the retention time closest to the target analyte in question. However, PFOA-13C8 was only applied for PFOA detection, as this IS is known to cause calibration curves with reduced quality. Calibration curves were made using concentrations ranging from 0.1 ng/mL to 10 ng/mL as all concentrations found were well below 10 ng/mL. However, for PFOS, the highest concentration in the calibration curve is 5 ng/mL, as this significantly improved LOD and LOQ and all analyte concentrations were well within this range. The calibration curves for PFOS and PFOA are presented in Figure 4.5 and Figure 4.6, respectively. The remaining calibration curves are presented in Appendix C.
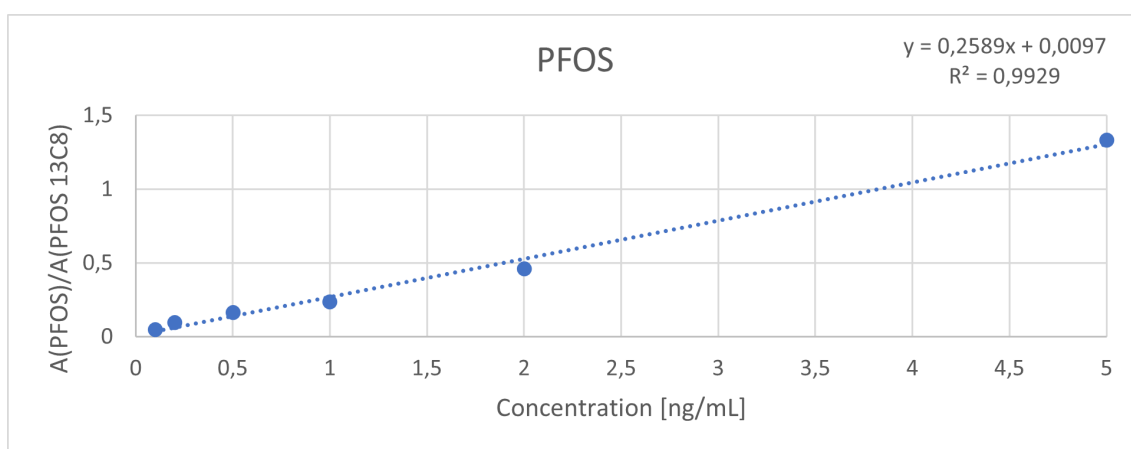


Figure 4.5: Calibration curve for PFOS.
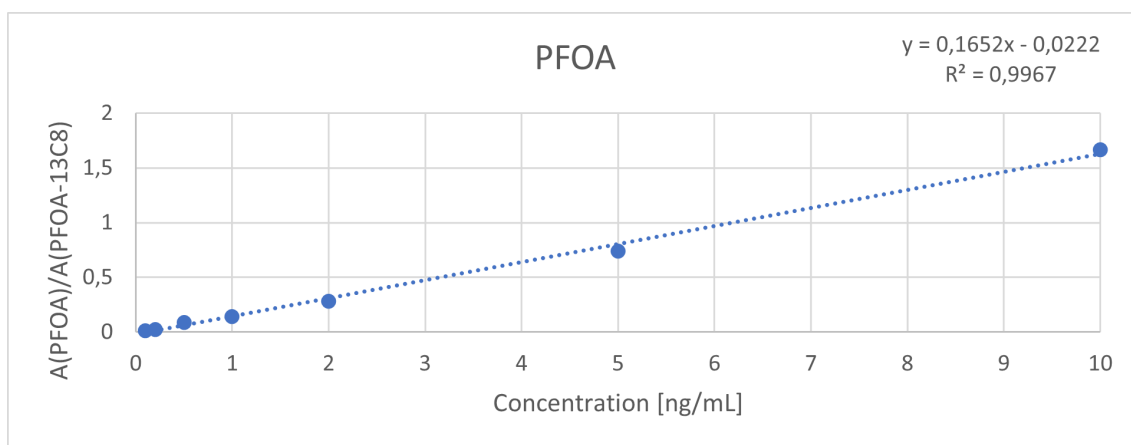


Figure 4.6: Calibration curve for PFOA.

### 4.3.2 LOD and LOQ

LOD and LOQ levels were calculated using linear regression, and using Equation 2 and Equation 3, respectively. The data analysis tool in Excel was utilized to calculate the SD in the intercept and find the slope of the calibration curve. LOD and LOQ values for the PFAS analyzed are presented in Table 4.2. The highest LOD and LOQ values are found for PFPeA and DiSAMPAP with LOD values of 1.508 ng/mL and 2.200 ng/mL respectively, and LOQ values of 4.570 ng/mL and 6.663 ng/mL respectively. Such high LOD and LOQ values indicate a poor sensitivity of the analytical method for these compounds. The remaining compounds generally have LOD values below 0.5 ng/mL, except EtFOSE, PFDoDA, MeFOSE, PFBS, PFHpA and PFDS, which have values <0.7 ng/mL. As LOD and LOQ are related, PFPeA and DiSAMPAP also have the highest LOQ values.

Table 4.2: Limit of detection (LOD) and Limit of quantification (LOQ) calculated for the analysis of PFAS by LC-MS/MS.

| PFAS | LOD [ng/mL] | LOQ [ng/mL] |
|---|---|---|
| PFNA | 0.144 | 0.439 |
| PFPeA | 1.51 | 4.57 |
| PFHxA | 0.312 | 0.945 |
| 4:2 FTS | 0.425 | 1.29 |
| 7H-PFHpA | 0.177 | 0.537 |
| NaDONA | 0.297 | 0.901 |
| PFOA | 0.368 | 1.11 |
| PFHpS | 0.352 | 1.07 |
| P37DMOA | 0.205 | 0.621 |
| PFOSA | 0.278 | 0.843 |
| PFOS | 0.314 | 0.952 |
| MeFOSA | 0.159 | 1.48 |
| PFDA | 0.178 | 0.541 |
| EtFOSA | 0.223 | 0.685 |
| EtFOSAA | 0.173 | 0.525 |
| 6:2 FTS | 0.431 | 1.305 |
| 8:2 FTS | 0.437 | 1.324 |
| 9Cl-PF3ONS | 0.160 | 0.486 |
| FOSAA | 0.142 | 0.430 |
| PFUnA | 0.294 | 0.890 |
| MeFOSAA | 0.294 | 0.584 |
| EtFOSE | 0.612 | 1.85 |
| PFDoDA | 0.521 | 1.58 |
| MeFOSE | 0.644 | 1.95 |
| 10:2 FTS | 0.452 | 1.37 |
| PFTriDa | 0.419 | 1.27 |
| DiSAMPAP | 2.20 | 6.66 |
| PFTDA | 0.507 | 1.54 |
| PFHxDA | 0.280 | 0.849 |
| PFBS | 0.609 | 1.84 |
| PFHeS | 0.201 | 0.610 |
| PFHpA | 0.589 | 1.79 |
| PFHxS | 0.179 | 0.541 |
| PFECHS | 0.252 | 0.762 |
| PFNS | 0.421 | 1.28 |
| PFDS | 0.542 | 1.64 |
| PFOcDA | 0.330 | 1.00 |

### 4.3.3 Presence of PFAS in samples

No PFAS was detected in the two water samples. Concentrations above LOQ were found for PFOS, PFNA, and PFUnA. Concentrations below LOQ but above LOD were found of PFHxA, PFOA, PFDA, FOSAA, PFHxDA, PFHpA and 6:2 FTS. PFAS concentrations were calculated as ng/g of soil or sediment, and detected concentrations are presented in Table 4.3.

Table 4.3: Concentrations of PFAS in samples [ng/g soil or sediment]. Bold font indicates concentrations >LOQ.

| Sample | PFOS | PFOA | PFNA | PFHxA | PFDA | FOSAA | PFUnA | PFHxDA | PFHpA | 6:2 FTS |
|---|---|---|---|---|---|---|---|---|---|---|
| 5a | | | | 5.80 | 1.90 | | | | | |
| 6a | | | | 6.40 | | | | | | |
| 7a | 3.25 | | **6.94** | 5.76 | | | | | | |
| 8a | 4.56 | | | | | | | | 5.95 | |
| 9a | 6.54 | | | | | | **8.88** | | | |
| 10a | **12.2** | | | | | | **11.5** | | | |
| 11a | | | | | | | | 2.80 | | |
| 15a | | | | | 2.37 | | | | | |
| 4b | | | | | | 1.45 | | | | |
| 5b | | | | | | 1.24 | | | | |
| 8b | **12.8** | | | | | | | | | |
| 9b | **12.7** | | | | | | **8.49** | | | |
| 10b | 7.93 | 7.34 | | | | | 6.84 | | | |
| 16b | | | | | | | | | | 4.91 |
| 18b | | 5.77 | | | | 4.26 | | | | |

The highest concentrations were found for PFOS, with concentrations as high as 12.8 ng/g. PFOS was also detected in the most samples, with concentrations in samples 7a, 8a, 8b, 9a, 9b, 10a, and 10b. This is also expected as PFOS is among the most used PFAS, historically. PFOA was detected in two samples, 10b and 18b, but with concentrations lower than LOQ. PFNA concentrations were only found in sample 7a, with a concentration of 6.49 ng/g. Levels of PFUnA were also found above the LOQ in three of the samples, and also below the LOQ in one sample. PFUnA was detected in all samples from location 9 and 10, while it was not detected at any other location.

More PFAS concentrations were found at locations 7, 8, 9 and 10 than at the other locations. This may be related to their proximity to the road and the airport and previous FFTS close to the airport. This may also be due to possibly higher content of vegetation these samples, and bioaccumulation of PFAS in plants.

A previous study of the presence of PFAS in relation to the FFTS in Ny-Ålesund found a sum of PFAS of 1140 ng/g at the site[29], with PFOS as a major contributor. The study also found that only 200 m from the site, the concentration was only 312 ng/g, one third of that at the site. The samples collected in this study are located at least 1.2 km from the FFTS described in the study. Such a large distance could indicate a low influence of the training site at these locations. However, PFAS could be transported by wind, birds, and vehicles along the road to these locations, and the detected concentrations could originate from the training site and possibly also from the airport.

## 4.4 Elemental analysis

### 4.4.1 LOD

LOD values were provided with the ICP-MS results and are presented in Table 4.4. All LODs are well bellow the detected concentrations in the samples.

Table 4.4: Detection limits for water samples and soil/sediment samples by ICP-MS analysis.

| Element | Water [µg/L] | Soil/sed. [µg/L] | Element | Water [µg/L] | Soil/sed. [µg/L] |
|---------|--------------|------------------|---------|--------------|------------------|
| Li | 0.00166 | 0.00152 | Sr | 0.000373 | 0.000137 |
| Be | 0.000240 | 0.000518 | Y | 0.000116 | 0.00000 |
| B | 0.0573 | 0.0571 | Nb | - | 0.0000477 |
| Na | 0.110 | 0.0378 | Zr | 0.000314 | - |
| Mg | 0.0189 | 0.000778 | Mo | 0.000784 | 0.00160 |
| Al | 0.00571 | 0.00136 | Ru | - | 0.00248 |
| Si | 0.546 | 0.528 | Cd | 0.000394 | 0.00000 |
| P | 0.0345 | 0.0453 | In | 0.0000799 | 0.0000473 |
| S | 0.166 | 0.200 | Sn | 0.000878 | 0.000388 |
| Cl | 102 | - | Sb | 0.000275 | 0.000340 |
| K | 0.0551 | 0.0717 | Cs | 0.000407 | 0.000272 |
| Ca | 0.0125 | 0.0113 | Ba | 0.00130 | 0.00106 |
| Sc | 0.000162 | 0.000159 | La | 0.000104 | 0.0000283 |
| Ti | 0.00862 | 0.00114 | Ce | 0.0000930 | 0.0000327 |
| V | 0.000626 | 0.000186 | Pr | - | 0.00000 |
| Cr | 0.00759 | 0.00203 | Nd | - | 0.00000 |
| Mn | 0.00280 | 0.00136 | Eu | 0.000181 | 0.00000 |
| Fe | 0.00601 | 0.00514 | Lu | - | 0.00000 |
| Co | 0.00112 | 0.000780 | Tl | 0.000587 | 0.000578 |
| Ni | 0.00757 | 0.00315 | Yb | 0.000113 | - |
| Cu | 0.0227 | 0.00410 | Hf | 0.00000 | 0.00000 |
| Zn | 0.00818 | 0.00178 | Hg | 0.00858 | 0.00186 |
| Ga | 0.00015 | 0.000146 | Th | 0.0000312 | 0.00000 |
| As | 0.00127 | 0.000830 | Pb | 0.00108 | 0.000534 |
| Se | 0.0202 | 0.00454 | Bi | 0.000182 | 0.000671 |
| Br | 0.175 | - | U | 0.0000187 | 0.00000 |
| Rb | 0.00156 | 0.000478 | | | |

### 4.4.2 Selected elements

Some selected results from elemental analysis by ICP-MS are included in this section. The elements included were chosen due to previous studies that have related these elements to mining activity, as explained in Section 2.3.1. Table 4.5 presents the mean, median and standard deviations of the selected elements.

Table 4.5: Mean, median, and standard deviation (SD) values for selected elements in soil/sediment and water samples.

| Element | Sediment/soil [µg/g] | | | Water [µg/L] | | |
|---------|------|--------|------|------|--------|------|
| | Mean | Median | SD | Mean | Median | SD |
| Fe | 18400 | 17400 | 5000 | 2.56 | 3.27 | 1.48 |
| As | 4.63 | 4.50 | 1.66 | 0.0622 | 0.0665 | 0.0188 |
| Cd | 0.364 | 0.241 | 0.491 | 0.0314 | 0.00282 | 0.0816 |
| Cr | 35.3 | 36.4 | 10.5 | - | - | - |
| Cu | 14.8 | 13.3 | 6.30 | 0.132 | 0.0993 | 0.110 |
| Ni | 28.9 | 20.5 | 34.4 | 1.69 | 0.359 | 4.03 |
| Al | 27500 | 26200 | 10200 | 2.43 | 1.82 | 1.25 |
| Pb | 11.1 | 11.5 | 3.14 | - | - | - |
| Zn | 77.8 | 54.2 | 111 | 2.30 | 0.299 | 6.35 |
| V | 42.6 | 42.6 | 13.8 | 0.0299 | 0.0292 | 0.0136 |
| S | 2050 | 1260 | 2320 | 36200 | 21500 | 28500 |

The following results are presented in bar charts, where every bar presents concentrations found by one ICP-MS analysis from one sample, sampled at one location. In the bar charts showing concentrations in sediment and soil samples, the bars are marked in purple, blue, and green colors. Purple indicates sediment samples from above water surface, blue indicated sediment samples from below water surface, and green indicates surface soil samples. Note that samples *8b* and *9b* are missing. These samples were not analyzed with ICP-MS due to lack of space in the instrument and due to the fact that these samples are of the same material as samples *8a* and *9a*, respectively. Box plots are also included. The remaining results can be found in Appendix D. The elemental results will be further discussed in Section 4.5.

**Iron**

Iron concentrations were detected in all sediment, soil, and water samples. Figure 4.7 presents box plots, and Figures 4.8 and 4.9 present iron concentrations in soil/sediment samples and water samples, respectively. The highest concentration of iron in the sediment/soil samples were found in sample 14b, with a concentration greater than 30 000 µg/g (3%). The highest concentration among the water samples were found at location 3, with a concentration of 4.44 µg/L.

(a) Sediment and soil.                                    (b) Water.
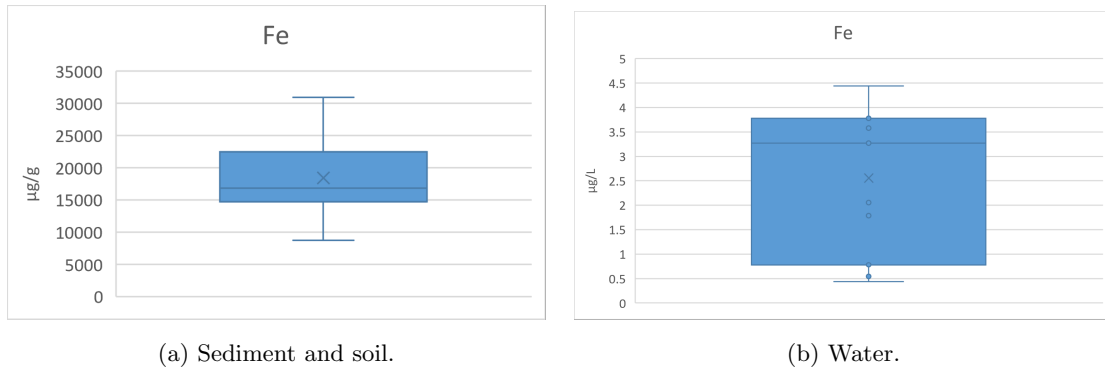
Figure 4.7: Box plots for Fe.
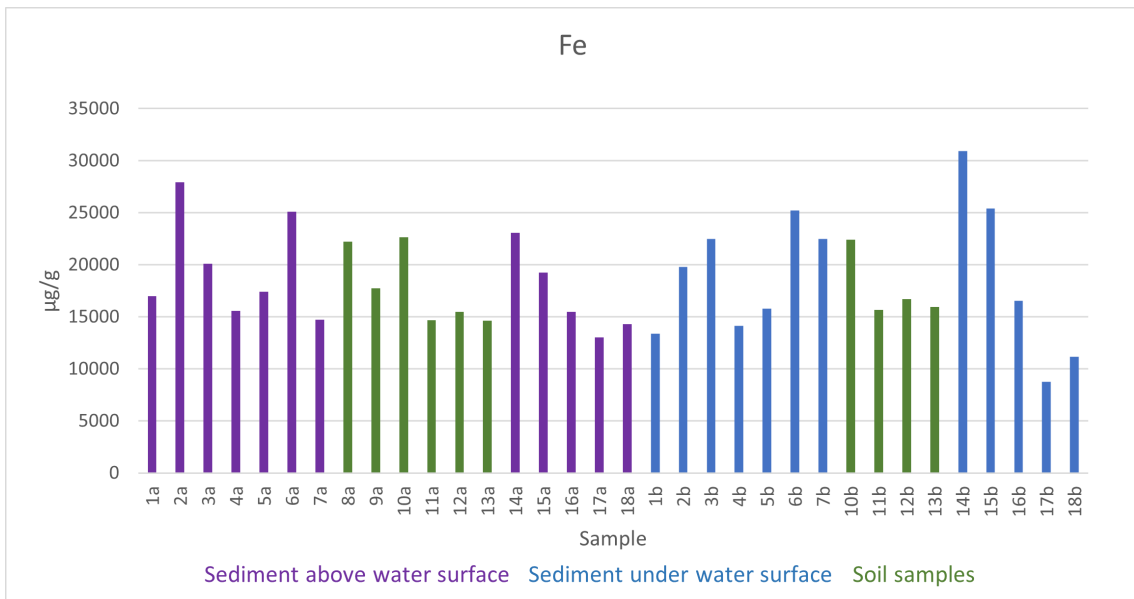


Figure 4.8: Bar chart presenting Fe concentrations in soil and sediment samples.
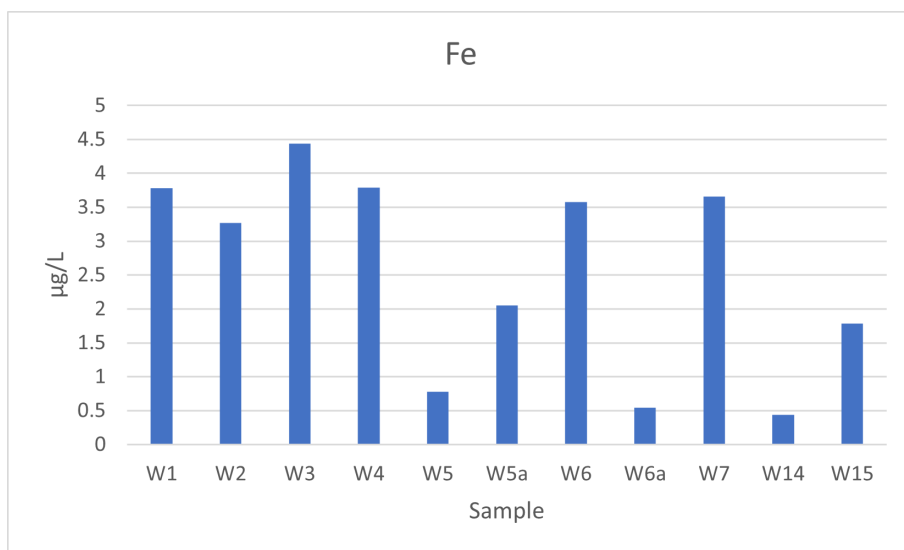


Figure 4.9: Bar chart presenting Fe concentrations in water samples.

**Arsenic**

Detectable levels of arsenic were found in all soil, sediment, and water samples. Figure 4.10 presents box plots, and Figures 4.11 and 4.12 present the concentrations of arsenic in soil/sediment samples and water samples, respectively. The highest concentrations were found at locations 6 and 13 in soil and sediment samples. The concentrations were highest at sites 4 and 7 in the water samples and lowest in the drain water samples (W5a and W6a).



(a) Sediment and soil.
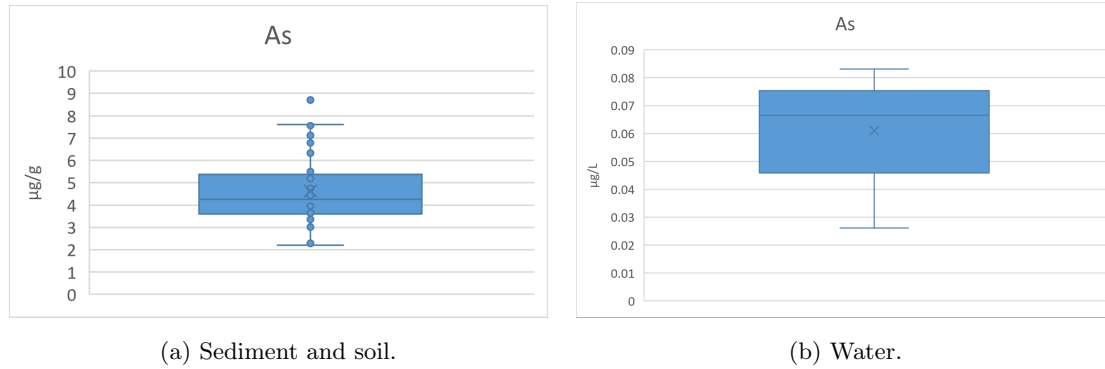


(b) Water.

Figure 4.10: Box plots for As.
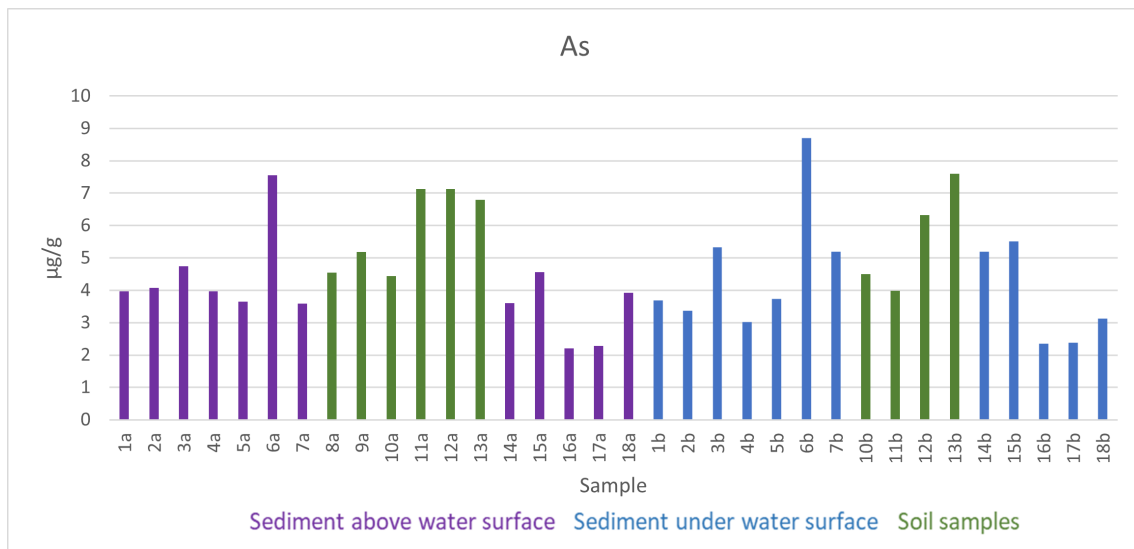


Figure 4.11: Bar chart presenting As concentrations in soil and sediment samples.
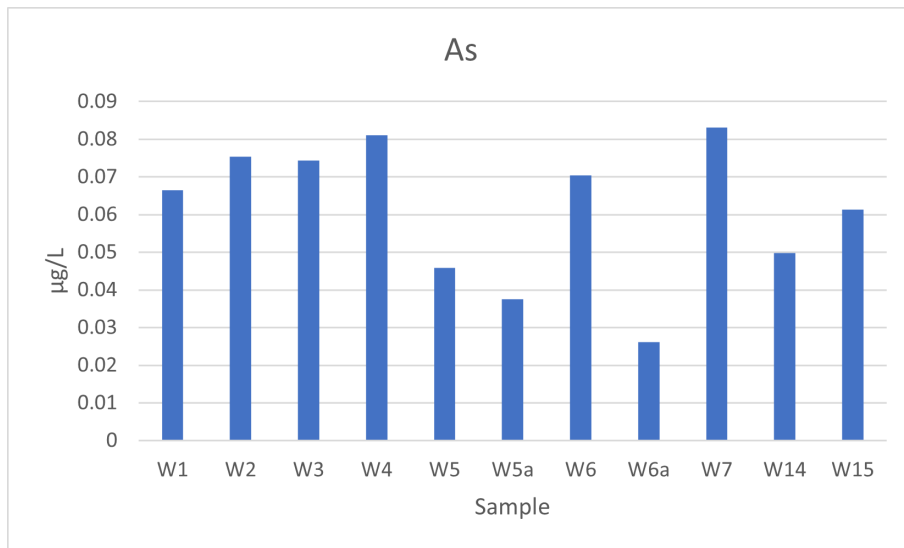
Figure 4.12: Bar chart presenting As concentrations in water samples.

**Cadmium**

Cadmium concentrations were found in soil, sediment and water samples. Figure 4.13 presents box plots, and Figures 4.14 and 4.15 presents the concentrations of cadmium in soil/sediment samples and water samples, respectively. The concentrations in both sediment and water samples were a great deal higher in/around the puddle at location 14 than at the remaining sampling locations. The concentration in sample 14b (2.66 µg/g) is almost ten times higher than the average concentration in soil and sediment samples, excluding samples 14a and 14b (0.28 µg/g). The concentration in water sample W14 (0.28 µg/L) is more than ten times higher than the second highest concentration which is found in sample W5a (0.03 µg/L). Sample W5a is drain water coming from the same area that sample W14 was collected. This is also visible in the box plots, where these samples are marked as outliers.



(a) Sediment and soil.
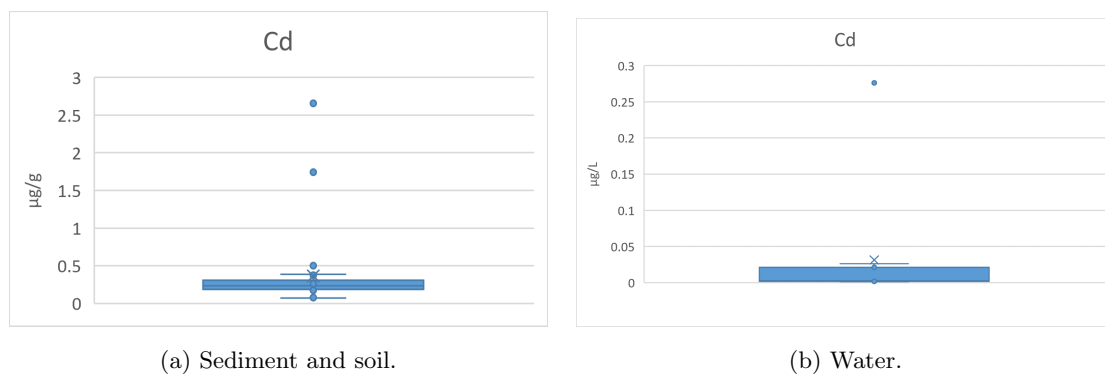


(b) Water.

Figure 4.13: Box plots for Cd.
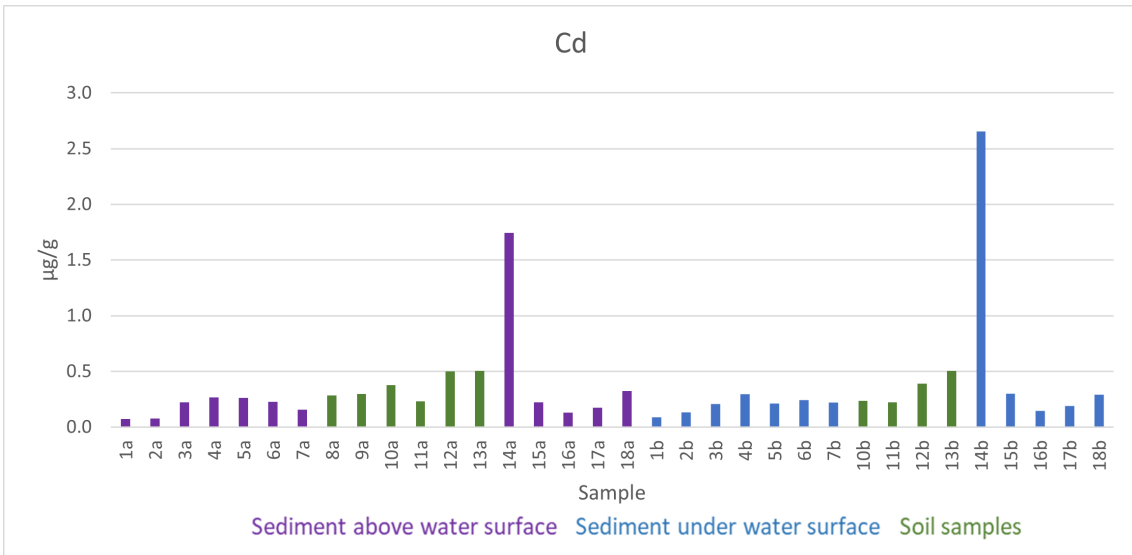
Figure 4.14: Bar chart presenting Cd concentrations in soil and sediment samples.
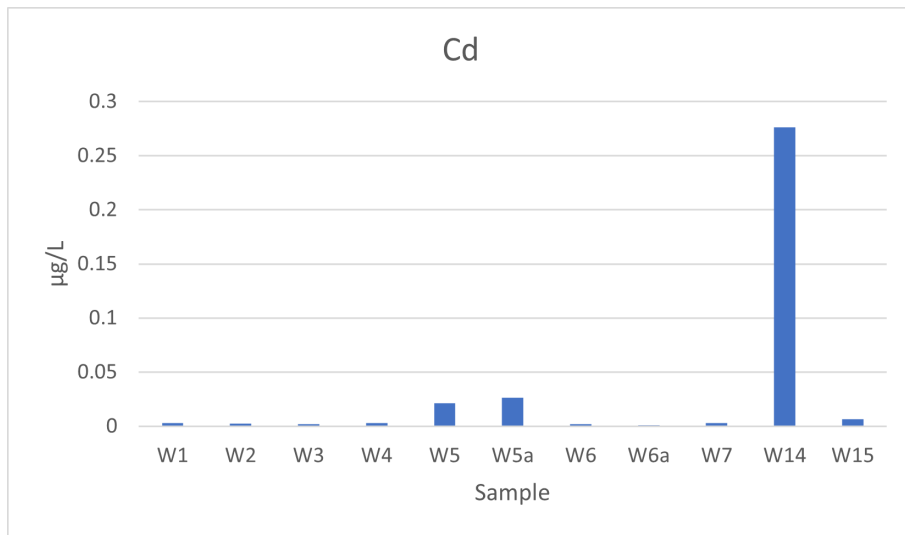


Figure 4.15: Bar chart presenting Cd concentrations in water samples.

**Chromium**

Chromium levels were detected in all soil and sediment samples, but not in the water samples. Figure 4.16 presents the box plot, and Figure 4.17 presents the concentrations of chromium in the soil and sediment samples. The highest concentrations were found around locations 12 and 13.
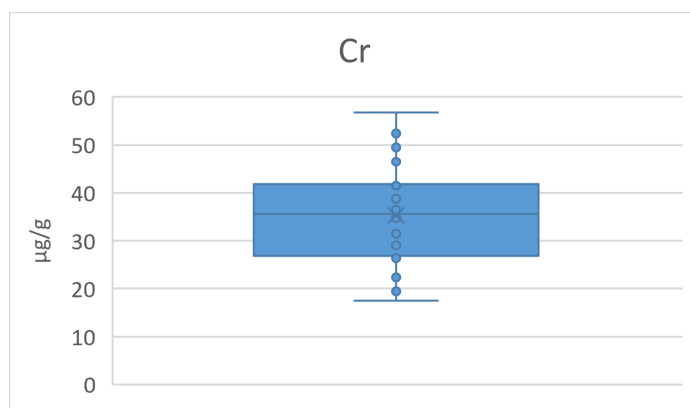
Figure 4.16: Box plot of Cr results for sediment and soil samples.
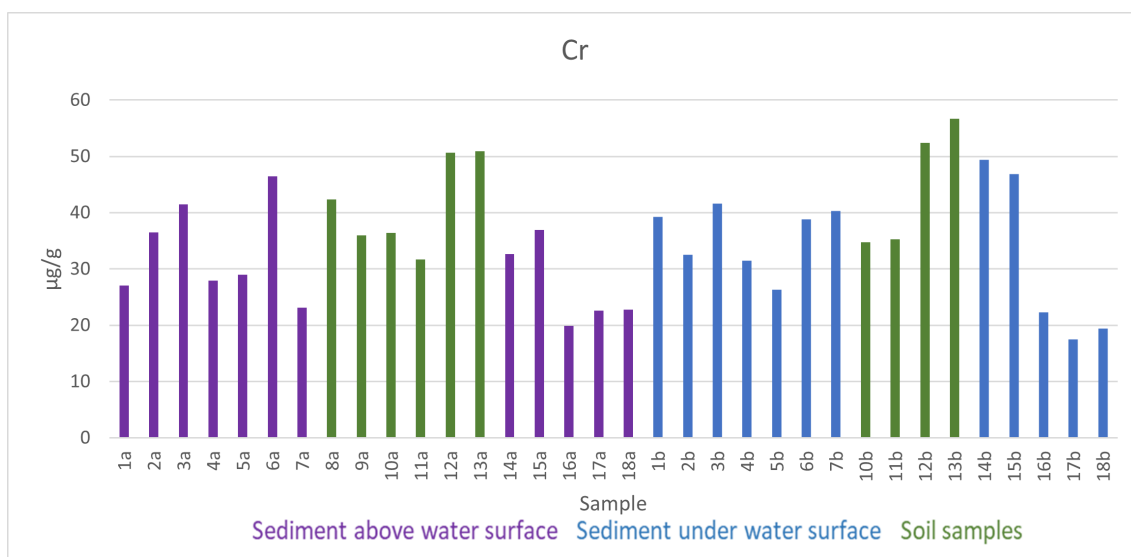


Figure 4.17: Bar chart presenting Cr concentrations in soil and sediment samples.

**Copper**

Measurable concentrations of copper were found in all sediment, soil and water samples, except for water sample W6a. Figure 4.18 presents box plots, and Figures 4.19 and 4.20 presents copper concentrations in soil/sediment samples and water samples respectively. The highest concentrations were found at location 12, 13, and 14, with the highest concentration in sediment sample 14b (36.68 µg/g), and in water sample W14 (0.14 µg/L). Especially in the water samples, concentrations were much higher at location 14, and this sample is clearly marked as an outlier in the box plot.

(a) Sediment and soil.                    (b) Water.
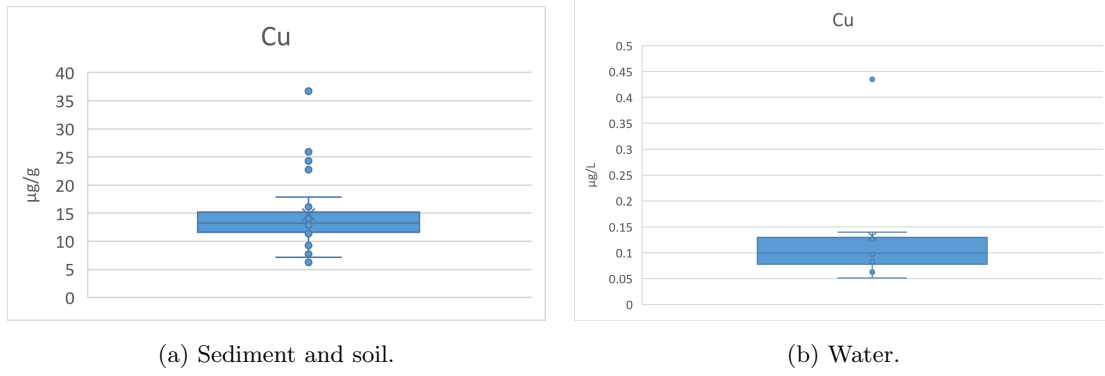
Figure 4.18: Box plots for Cu.
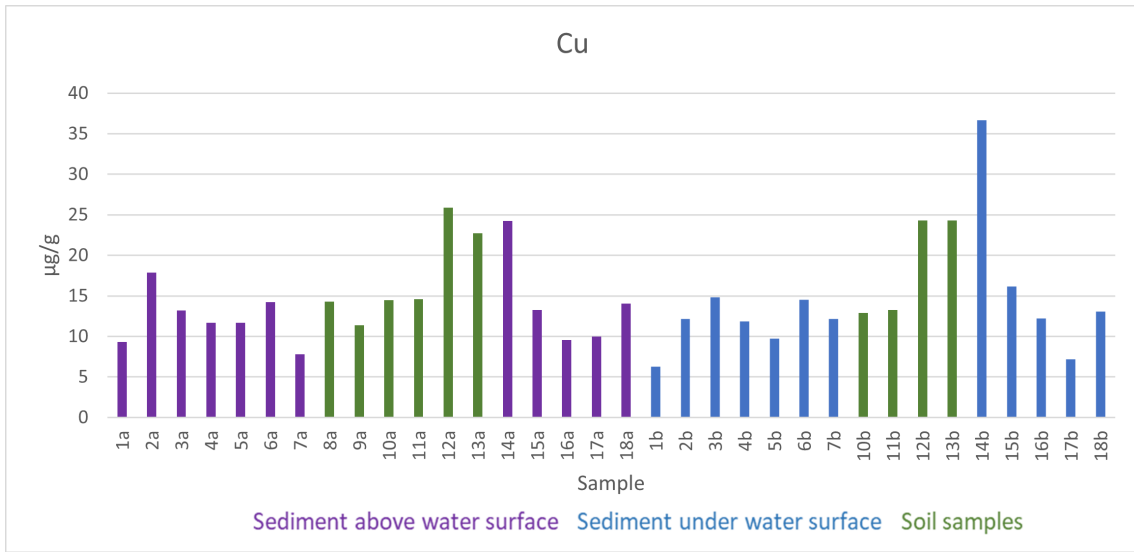


Figure 4.19: Bar chart presenting Cu concentrations in soil and sediment samples.
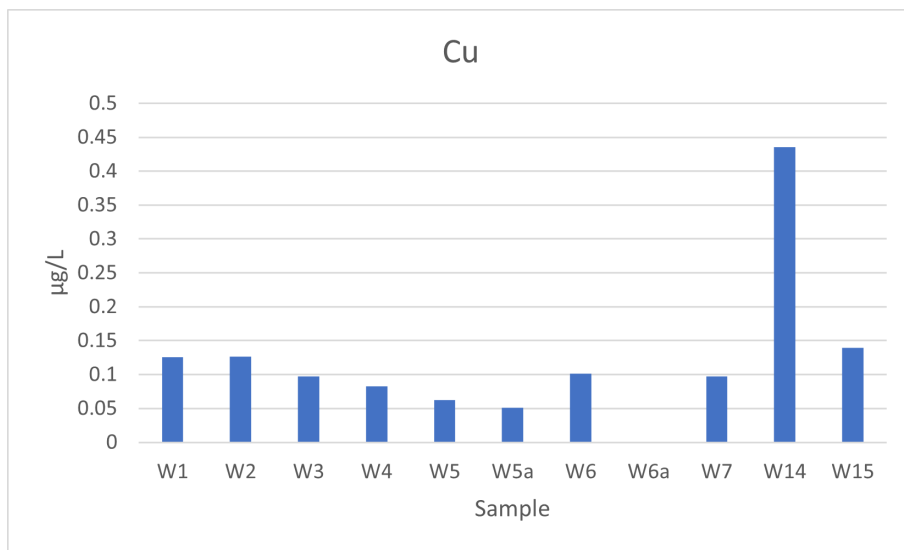


Figure 4.20: Bar chart presenting Cu concentrations in water samples.

**Nickel**

Nickel concentrations were found in all soil and sediment samples. As with Cd, concentrations were considerably higher at location 14, both in sediment and water samples. Figure 4.21 presents box plots, and Figures 4.22 and 4.23 presents concentrations of nickel in soil/sediment and water samples respectively.



(a) Sediment and soil.
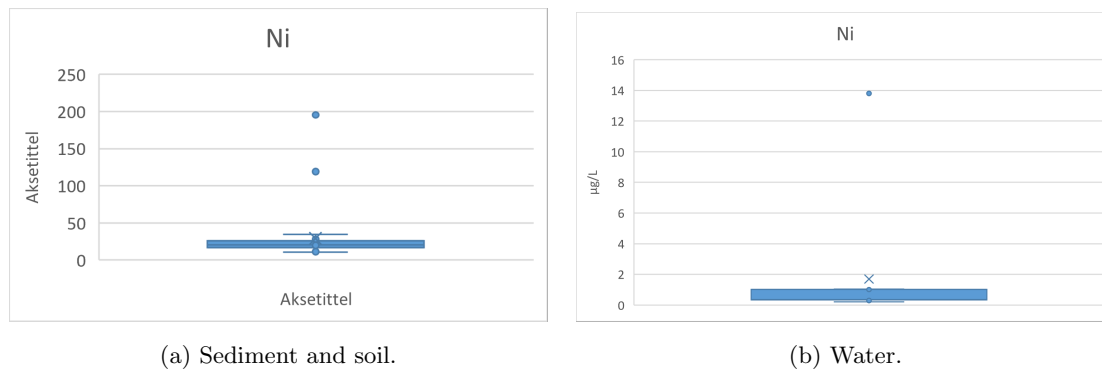


(b) Water.

Figure 4.21: Box plots for Ni.
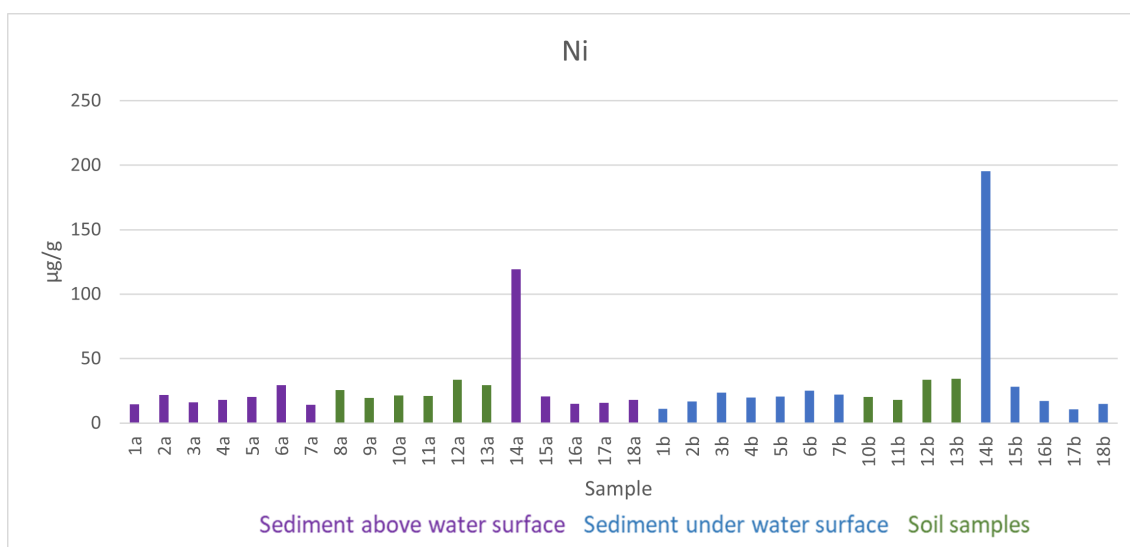


Figure 4.22: Bar chart presenting Ni concentrations in soil and sediment samples.
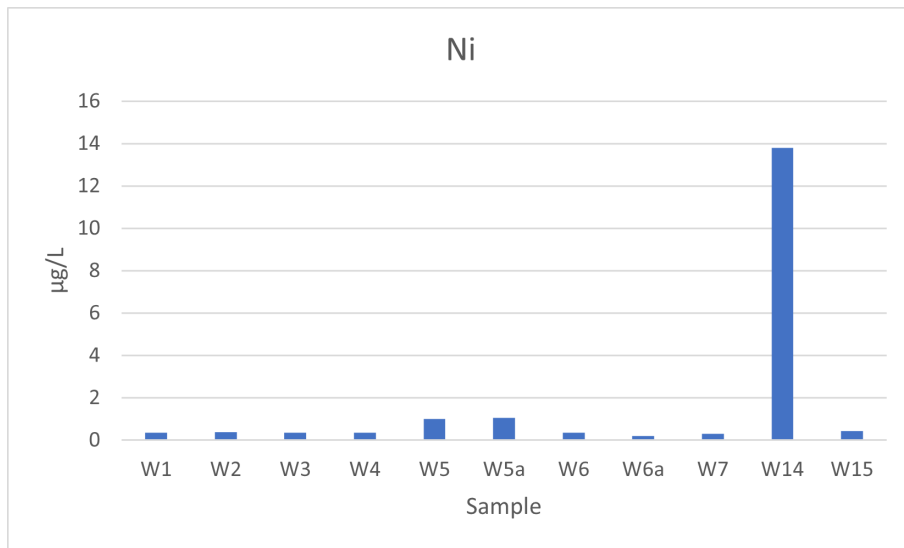
Figure 4.23: Bar chart presenting Ni concentrations in water samples.

**Aluminum**

Aluminum concentrations were detected in all soil, sediment and water samples. Figure 4.24 presents box plots, and Figures 4.25 and 4.26 present aluminum concentrations in soil/sediment and water samples respectively. The highest concentrations in the soil/sediments were found at location 12 and 13, and at location 5 in the water samples.



(a) Sediment and soil.
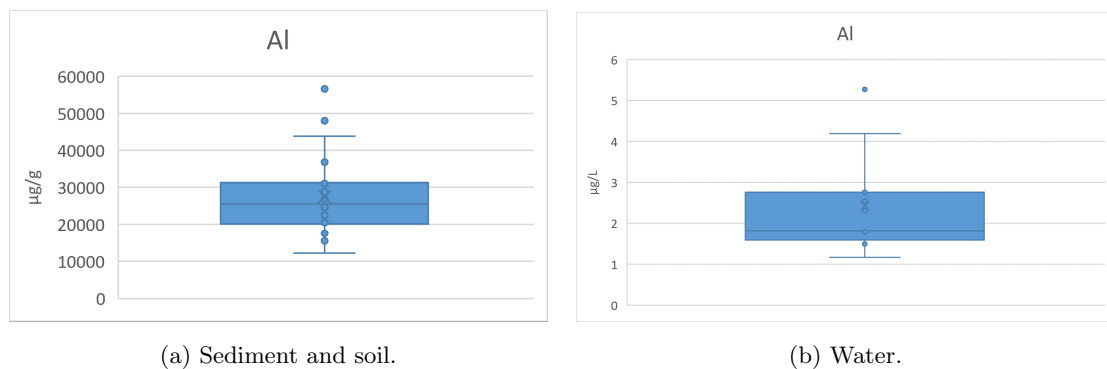


(b) Water.

Figure 4.24: Box plots for Al.
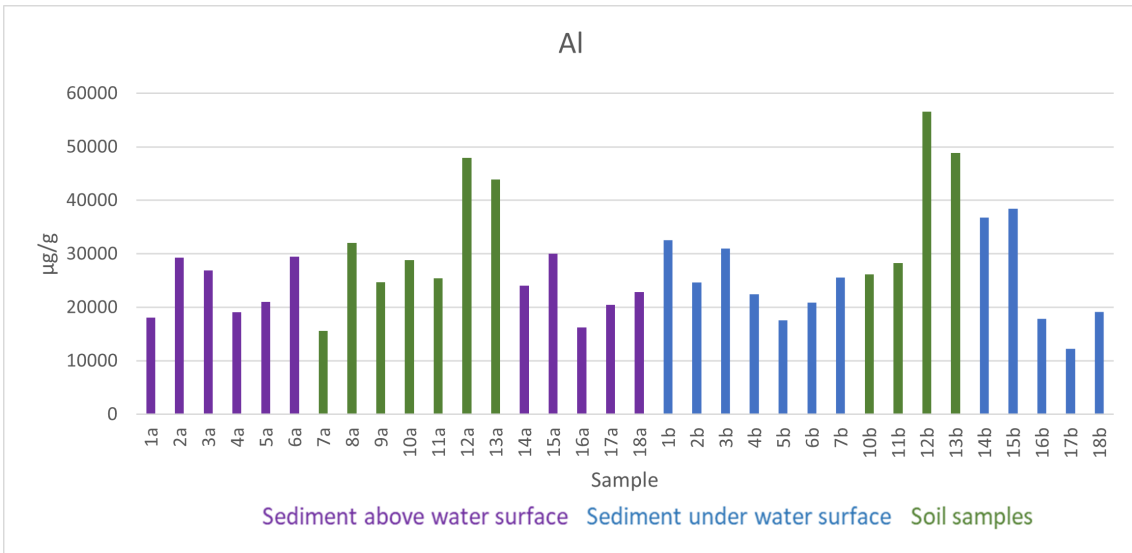
Figure 4.25: Bar chart presenting Al concentrations in soil and sediment samples.
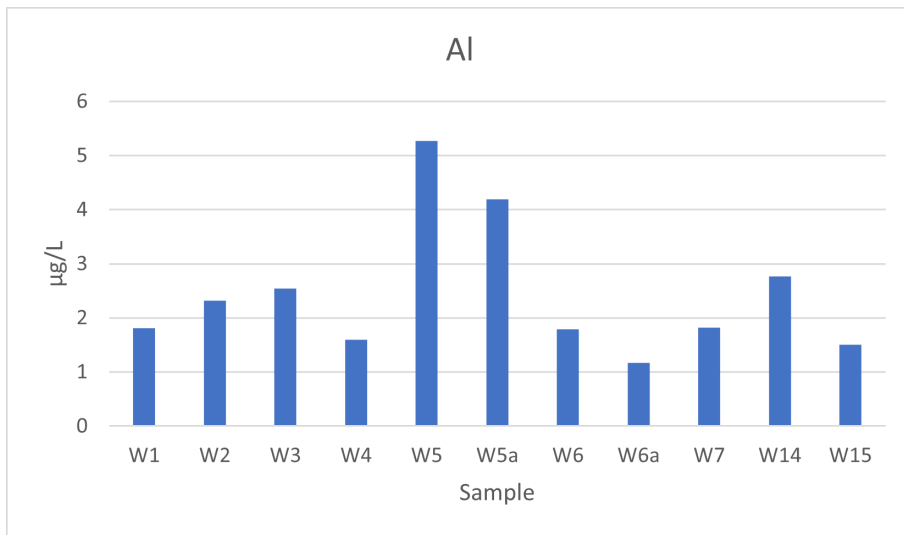


Figure 4.26: Bar chart presenting Al concentrations in water samples.

**Lead**

Detectable concentrations of lead were found in all soil and sediment samples, but none of the water samples. Figure 4.27 presents the box plot, and Figure 4.28 presents lead concentrations in soil and sediment samples. The highest concentrations were found in samples 13a, 13b and 14b.
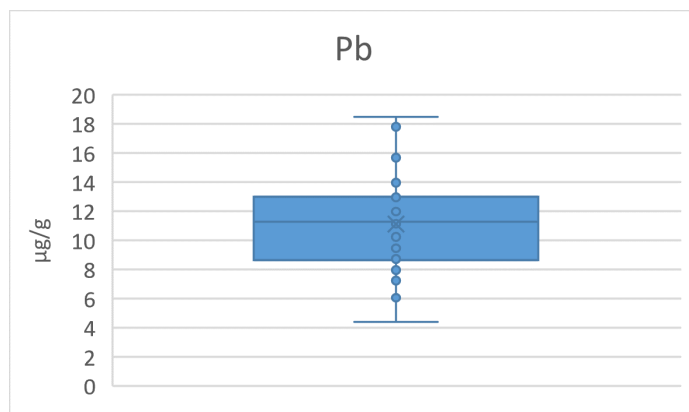
Figure 4.27: Box plot of Pb results for sediment and soil samples.
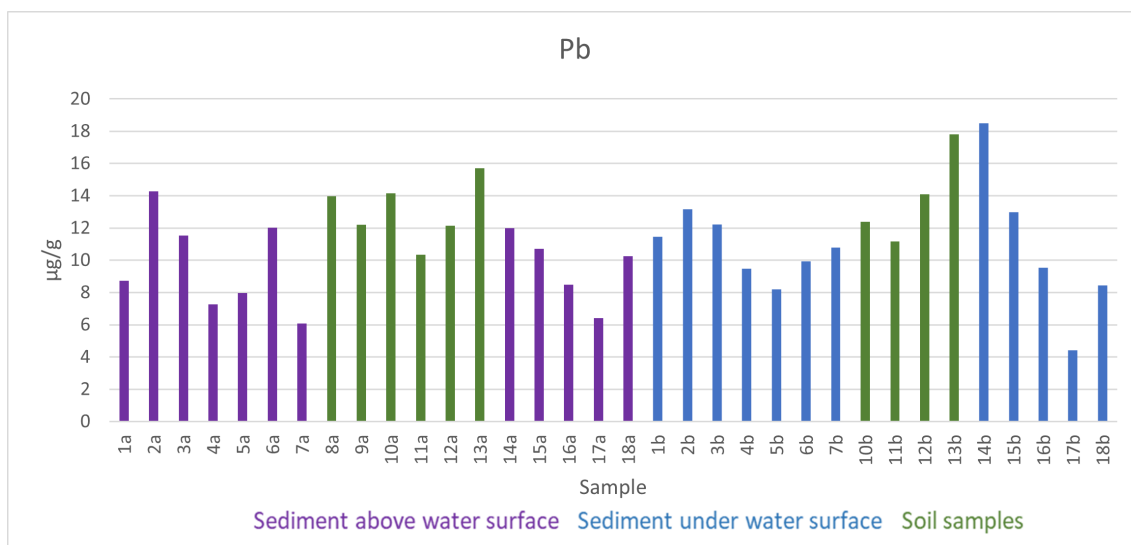


Figure 4.28: Bar chart presenting Pb concentrations in soil and sediment samples.

**Zinc**

Zinc concentrations were found in all soil and sediment samples. Figure 4.29 presents box plots, and Figures 4.30 and 4.31 present zinc concentrations in soil/sediment and water samples, respectively. As with Cd and Ni, concentrations were considerably higher at location 14. The remaining Zn concentrations are below 100 µg/g.

(a) Sediment and soil.
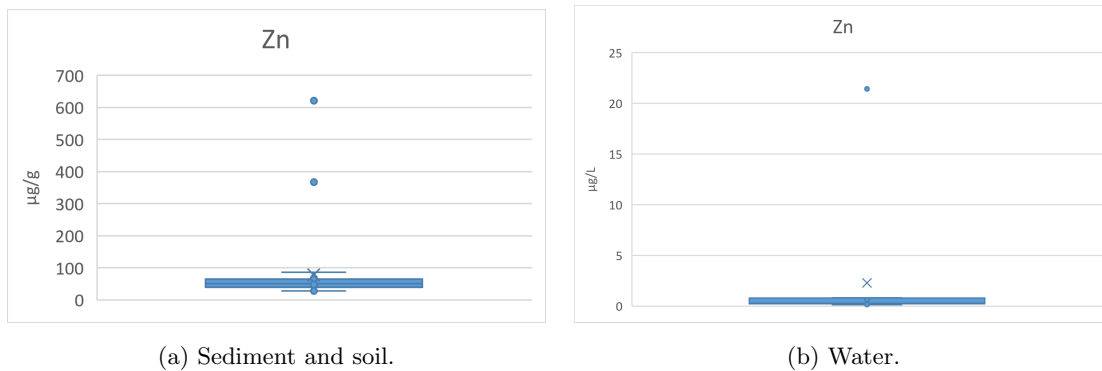
(b) Water.

Figure 4.29: Box plots for Zn.
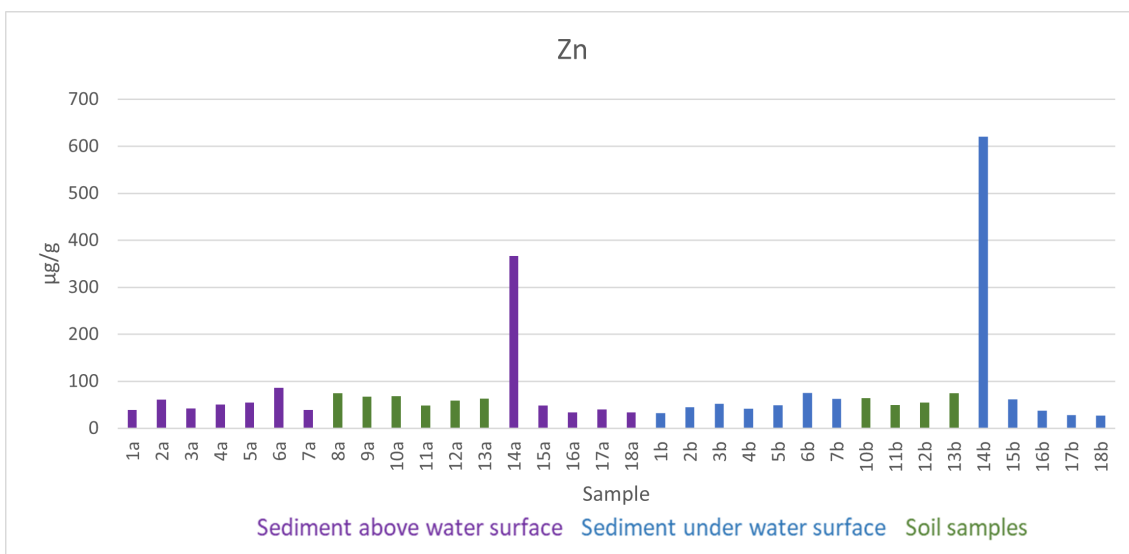


Figure 4.30: Bar chart presenting Zn concentrations in soil and sediment samples.
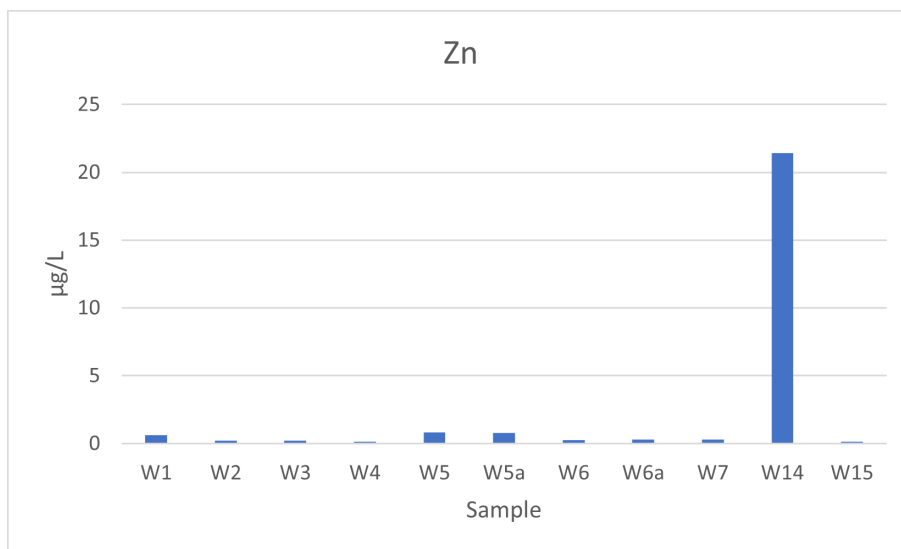


Figure 4.31: Bar chart presenting Zn concentrations in water samples.

**Vanadium**

Vanadium concentrations were found in all sediment/soil samples and water samples. Figure 4.32 presents box plots, and Figures 4.33 and 4.34 presents the vanadium concentrations found in sediment, soil and water samples. The highest concentrations are found in soil samples at locations 12 and 13, with concentrations of around 70 µg/g soil. In the water samples however, low concentrations below 0.07 µg/L are found.



(a) Sediment and soil.    (b) Water.
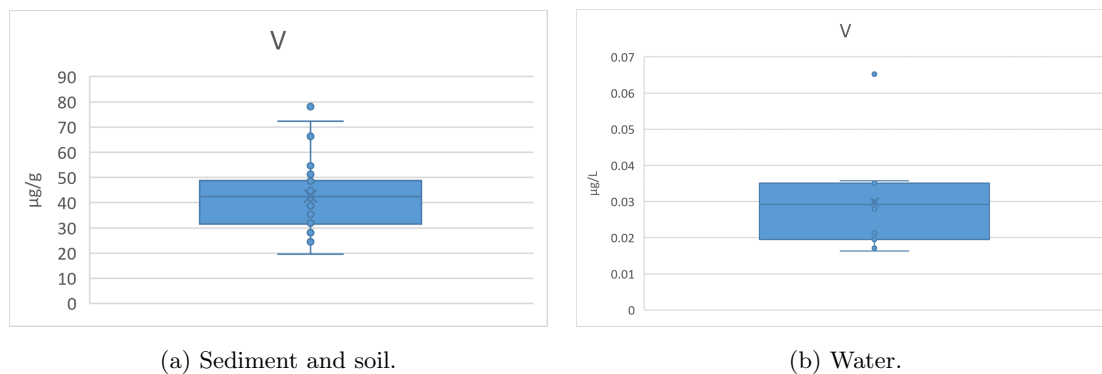
Figure 4.32: Box plots for V.
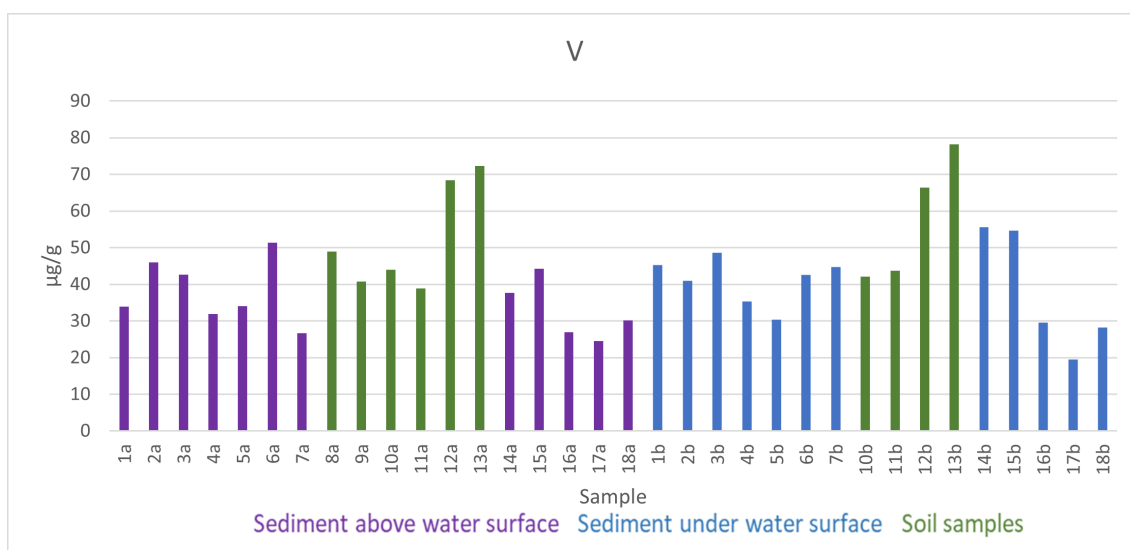


Figure 4.33: Bar chart presenting concentrations of V in soil and sediment samples.
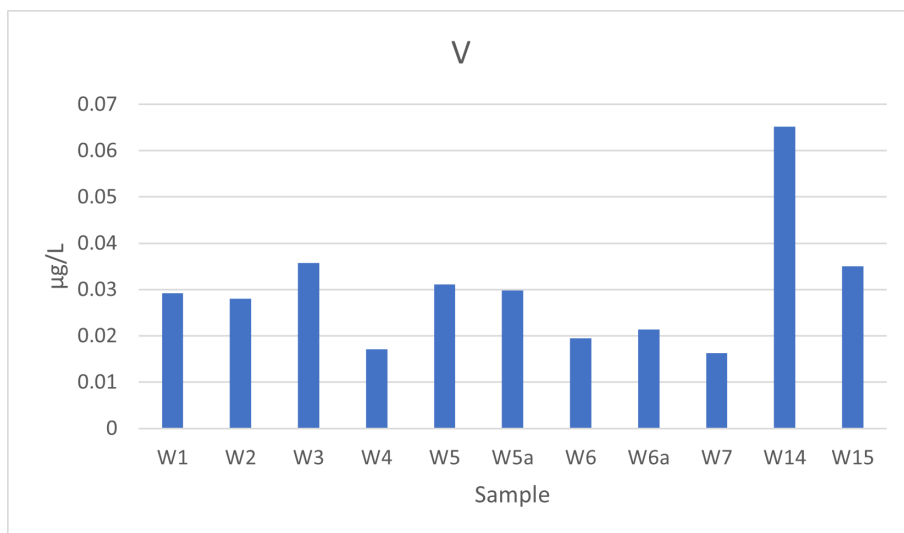
Figure 4.34: Bar chart presenting concentrations of V in water samples.

**Sulphur**

Concentrations of sulphur were found in all sediment, soil, and water samples. Figure 4.35 presents box plots, and Figures 4.36 and 4.37 present the concentrations in soil/sediment and water samples. The highest concentrations were found at locations 12, 13, and 18 in the soil and sediment samples, and in water samples W5, W5a and W14. Sample locations 12, 13 and 14 are in the hill area east of Tvillingvatnet, and sample W5a is runoff water from this area.



(a) Sediment and soil.
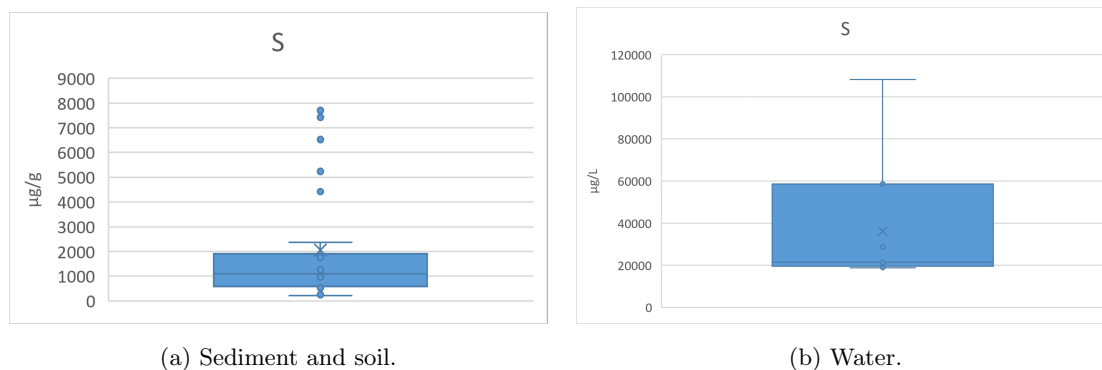


(b) Water.

Figure 4.35: Box plots for S.
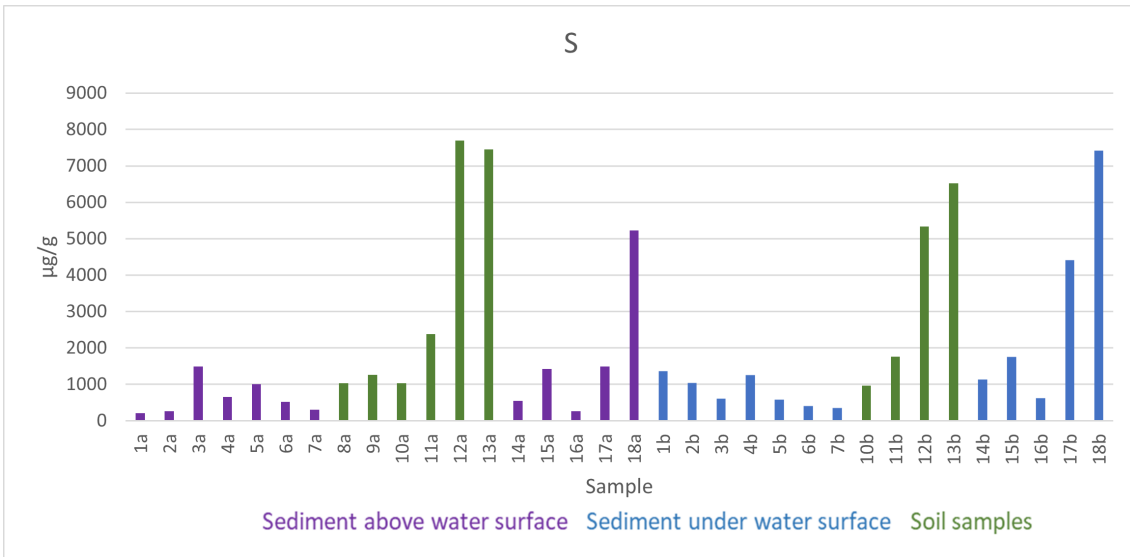
Figure 4.36: Bar chart presenting concentrations of S in soil and sediment samples.
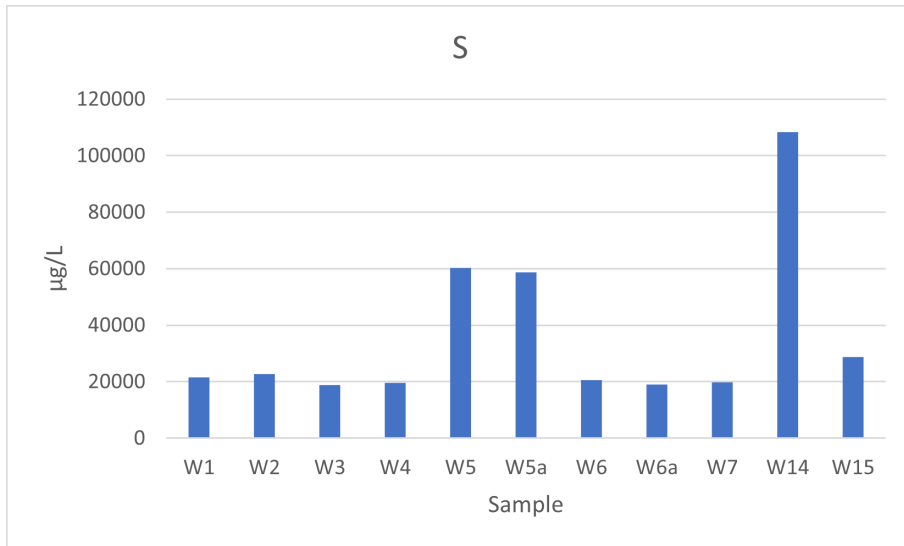


Figure 4.37: Bar chart presenting concentrations of S in water samples.

### 4.4.3 Summary of elemental analysis

The elemental analyzes generally showed the highest concentrations of several elements in sediment and soil samples from locations 12, 13 and 14, and water samples W5, W5a, and W14. Locations 12, 13, and 14 are located in the hill area, east of Tvillingvatnet. This area is close to some of the former mining areas, as shown in Figure A.1 in Appendix A. Water sample 5a is drainage water from this area, and this water affects the concentrations on location 5 in Tvillingvatnet as well.

Although high concentrations were also found at other locations, the samples collected at location 14 (sediment samples 14a and 14b, and water sample W14) had significantly higher concentrations of Cd, Ni, Zn, and Co and somewhat higher concentrations of Cr, Cu, and Pb. Higher concentrations in these samples is expected, since sampling location 14 is a small puddle, which is different from all other sample locations. It seems some elements accumulate in this puddle.

## 4.5 PCA

PCA was performed using soil/sediment samples alone, water samples alone, and all samples combined. Analyzes and interpretations will be presented and discussed in this section.

### 4.5.1 PCA of sediments and soil

Figure 4.38 presents the loading plot, and Figure 4.39 presents the score plot for PCA of sediment and soil samples, created with the results of elemental, PFAS, TOC, and TIC analyses. PC-1 and PC-2 describe 44 % and 15 % of the variance, respectively. Samples from location 14 were excluded from the PCA analysis, as these samples vary considerably from the other samples and had an excessive influence on the PCA plot.
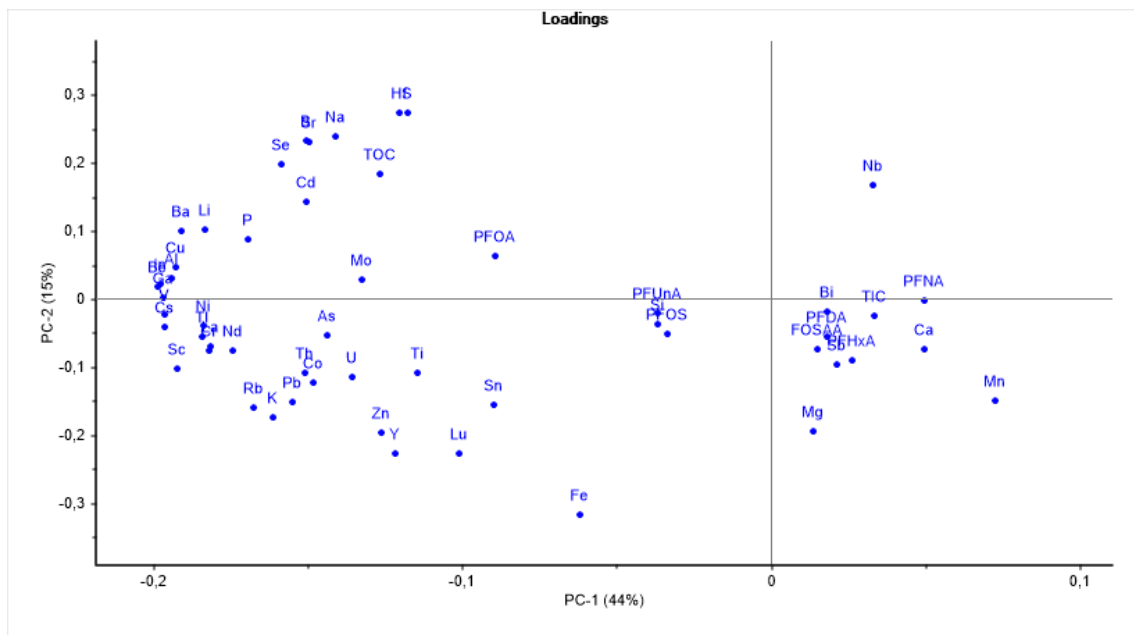


Figure 4.38: Loading plot for sediment and soil samples.
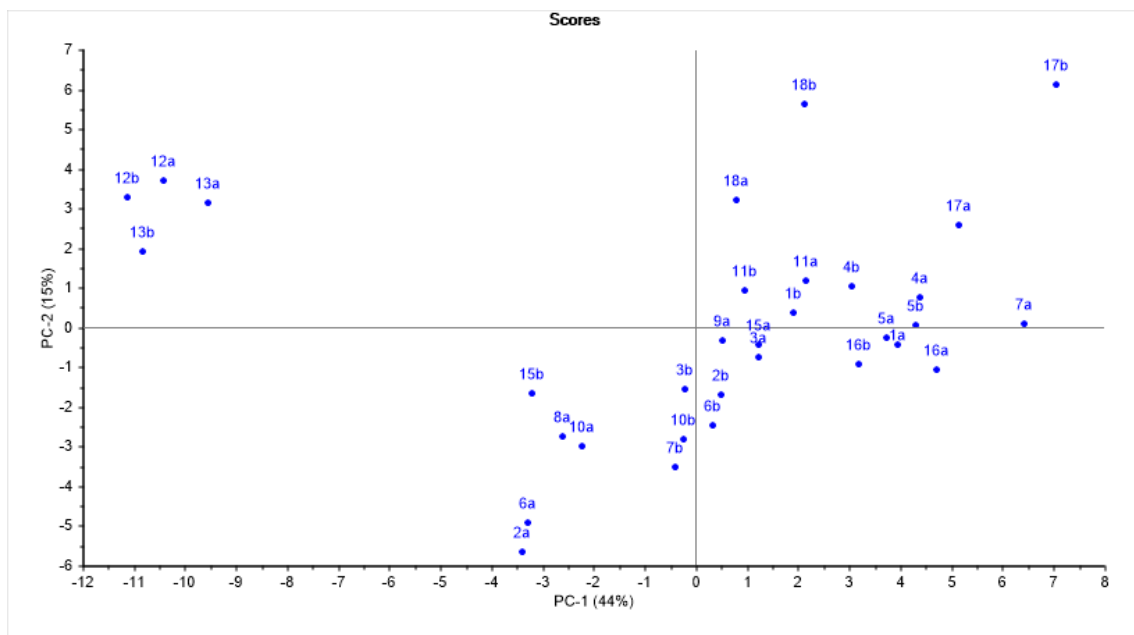
Figure 4.39: Score plot for sediment ans soil samples.

Upon assessing the loading plot, several PFAS are highly correlated and located close to the origin of the plot. They are slightly placed on both sides of PC-1, but the proximity to the origin implies that PFAS do not have a large influence on the plot. However, PFOA is placed further on the negative side PC-1 axis. Cr, Tl, Sc, Nd, and La, placed far on the negative PC-1 axis. These will have a larger influence on PC-1. TOC and TIC are observed to be on opposite sides of PC-1. TIC is placed on the PC-1 axis, relatively close to the origin. The TOC, however, is centered in the upper left quadrant, a placement that indicated the influence from several sources on the TOC levels in the samples.

In the score plot, the four sediment samples 12a, 12b, 13a and 13b stand out far to the upper left. The loading plot relates these samples to higher levels of Ba, Li, B, Se and Na, as well as higher TOC, and low levels of elements such as Ca.

The samples were separated into three locations on the basis of their location. L1 includes samples taken around Tvillingvatnet, L2 includes samples collected in the hill area, east of the road, and L3 includes samples collected close to Smithelva. These location groups are illustrated in Figure 4.40, and Figure 4.41 shows the score plot with this division. All samples marked L3 are placed to the right of the PC-2 axis, and generally high on the PC-2 axis. However, they have a wide spread in the plot and, according tot he loading plot, are not assosiated to any specific elements. L2 samples also have a wide spread, mostly due to the placement of samples 12a, 12b, 13a, and 13b, far from the rest. There is some difference in the L1 and L2 samples in the plot, with L2 samples generally higher on PC-1 and lower on PC-2.

Figure 4.40: Location grouping L1, L2 and L3 marked on map.
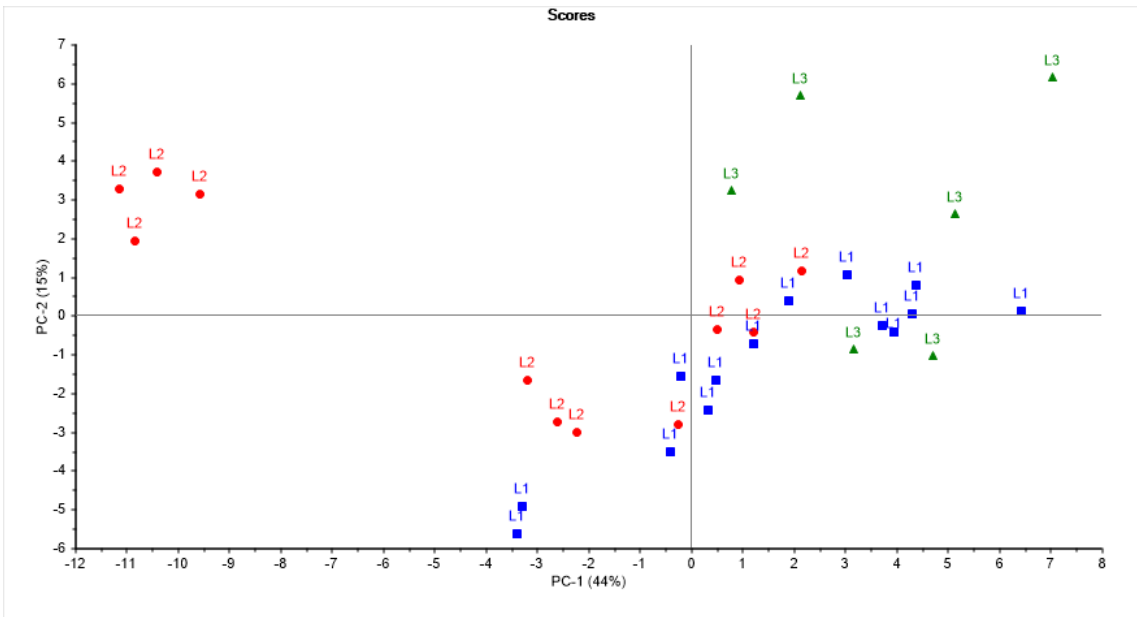


Figure 4.41: Scores plot including location categorization.

### 4.5.2 PCA of water samples

As with sediment samples 14a and 14b, water sample W14 was excluded from the PCA plot, as this sample is considerable different from the other water samples and had a significant influence on the PCA plot. Figures 4.42 and 4.43 present the loading and score plot for the water samples. PC-1 explains 48% of the variance and PC-2 explains 19%.
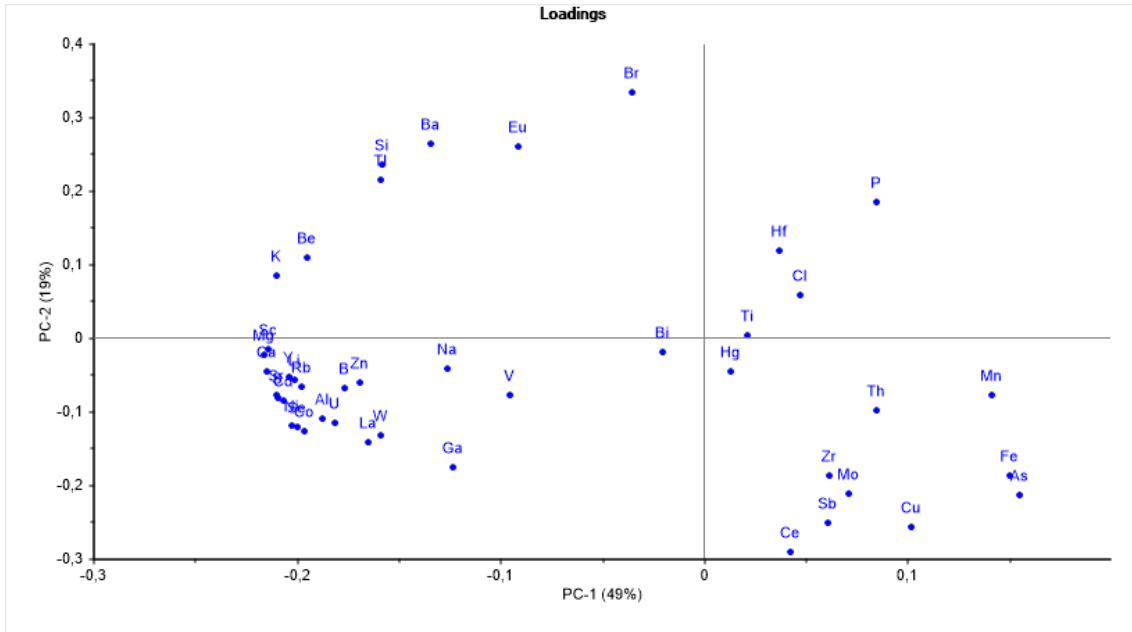


Figure 4.42: Loading plot for water samples.
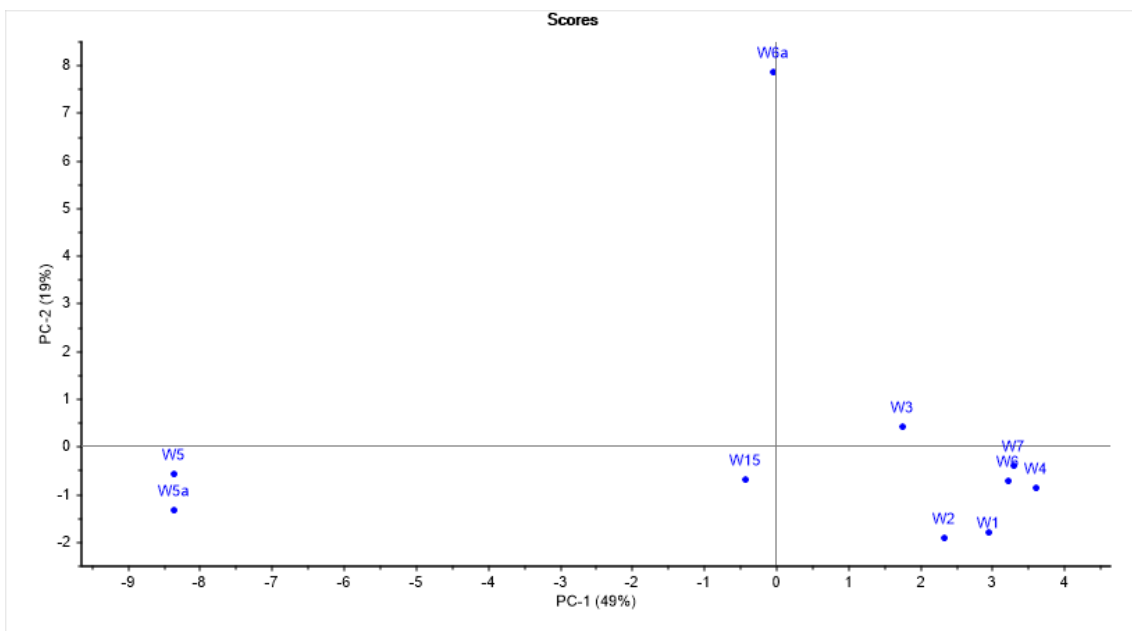


Figure 4.43: Score plot for water samples.

In the score plot, samples W5 and W5a are located far from the other samples, to the left of the plot. W5a is drain water from the hill area east of Tvillingvatnet. Sample 5 taken directly from Tvillingvatnet is heavily affected by this drain water. Therefore, these samples are highly related to the hill area closer to the industry area. The loading plot indicated higher concentrations of Mg, Ca and S, as well as Cd, Li, B and Al, which were also found for the soil samples collected in the hill. Sample W15 was also sampled from the area east of Tvillingvatnet, but is placed close to the origin of the score plot. This might indicate that the smaller water at location 15 is not as affected by the former industrial area. Sample W6a is also drain water and is also located far from the other samples in the score plot, including samples W5 and W5a, with W6a high on the PC-2 axis. Although they are both drain water, they seem to have very different content. The two drainage systems are therefore likely originating from different locations. It is more likely that sample W6a is drain water from the Zeppelin mountain. Satellite photos also reveal a trench dug alongside the mountain, leading towards Tvillingvatnet and location 6 [52], which strengthens this theory. Figure A.2 in Appendix A shows a photo of this trench. However, all samples related to the hill area east of Tvillingvatnet (including sample 5 due to the high influence by drain water) are separated from the samples collected in Tvillingvatnet. Figure 4.44 presents the score plot with the categorization H (hill area) and T (Tvillingvatnet).
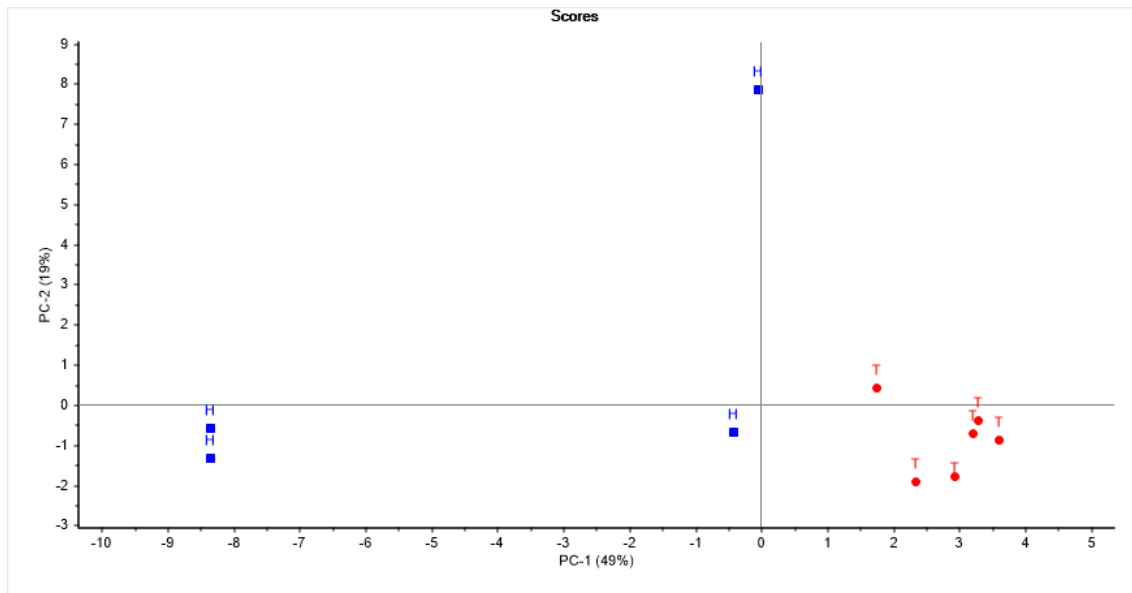


Figure 4.44: Score plot with hill area and Tvillingvatnet categorization.

### 4.5.3 PCA of water, soil, and sediment samples

PCA was also performed with all water, soil and sediment samples combined (excluding samples from location 14). Loading and score plots are presented in Figures 4.45 and 4.46. PC-1 and PC-2 explain 71% and 12% of the variance, respectively.
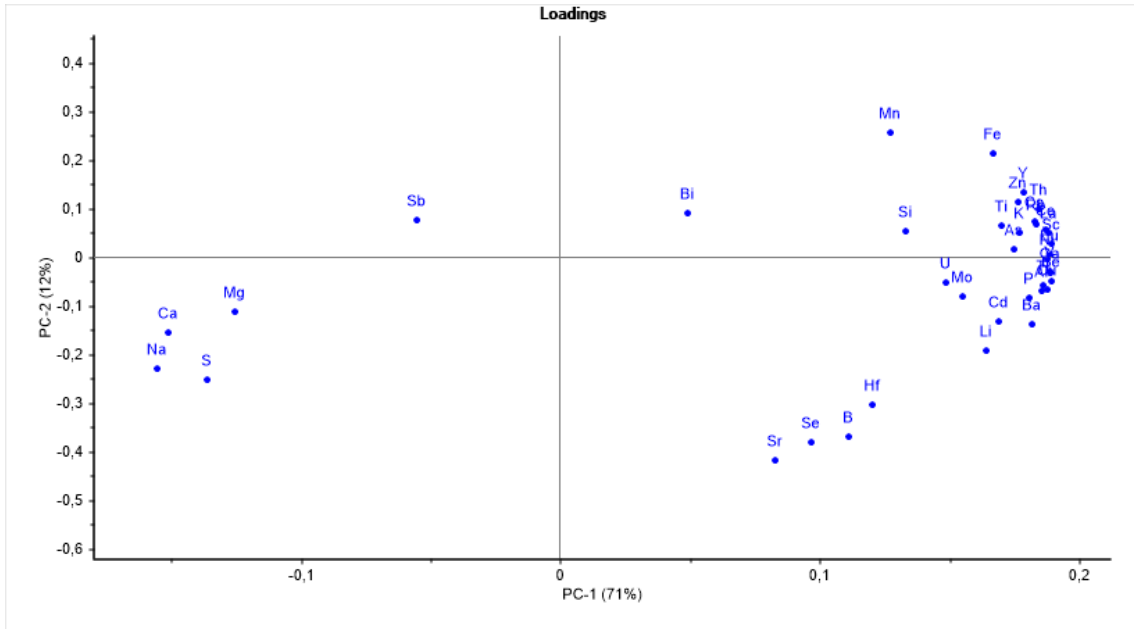


Figure 4.45: Loading plot for soil, sediment, and water samples.
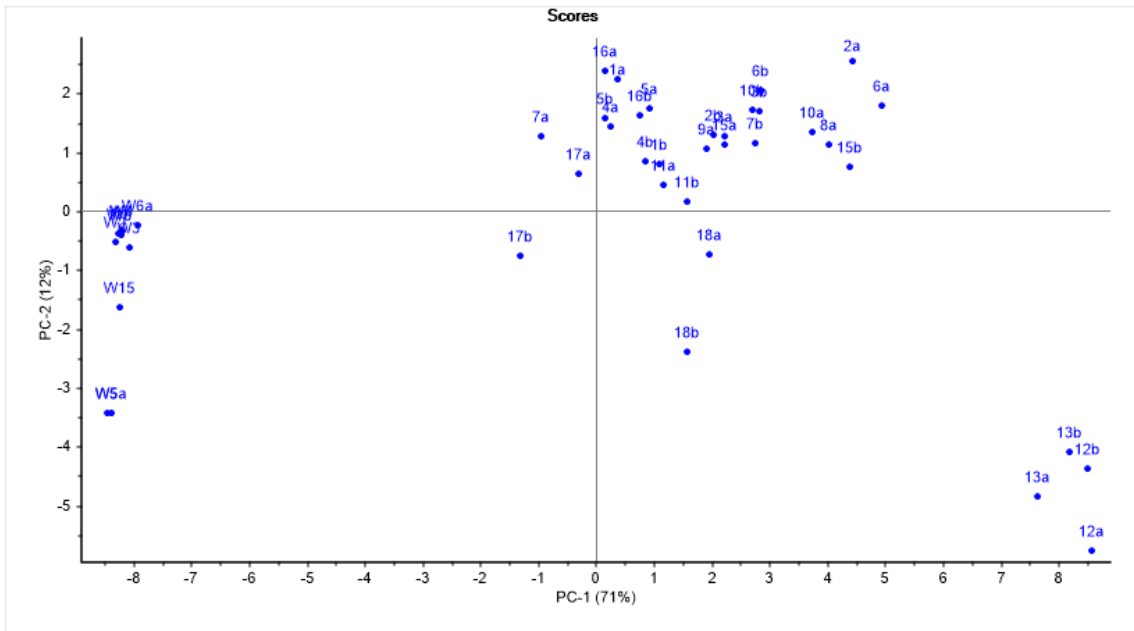


Figure 4.46: Score plot for soil, sediment, and water samples.

Several elements are correlated in the loading plot, high on the PC-1 axis, including Be, Al, Cu, As, Ni, and V. The only elements found on the negative side of the PC-1 axis are Na, Ca, S, Mg and Sb.

The water samples are generally placed far from the rest of the samples, far to the left of the plot. Sediment samples are located further right and to the origin of the plot. Samples 12a, 12b, 13a, and 13b, however, are also here standing out from the other samples, far down to the right of the score plot. Looking at the loading plot again, the water samples are related to elements Na, Ca, Mg and S, while sediment samples are more related to Bi, Si, Fe, and heavy metals.

# 5  Conclusion

The aim of this study was to quantify and assess the concentrations of multiple elements and PFAS in the drinking water reservoir Tvillingvatnet and the surrounding areas of Ny-Ålesund on Svalbard, and possibly relate these results to the former industry areas. Pollution of PFAS are of rising concern globally, and this study is contributing to the monitoring of these pollutants in the Arctic. The assessment of element concentrations in the area was also of interest as several elements, including heavy metals, have been associated with mining activity and AMD.

Concentrations of 10 PFAS were detected in 15 of the sediment and soil samples. As expected, due to the historically widespread use, the highest concentrations were found for PFOS. These concentrations were found in soil samples collected at locations 8, 9 and 10, in the hill area east of Tvillingvatnet. The second highest concentrations were found for PFUnA, also in soil samples at locations 9 and 10.

Levels of several elements were found to be higher in the hill area. Especially sampling location 14, the puddle, stood out. Both the water and sediment samples had considerably higher concentrations of Ni, Cd, Cu, and Zn at this location. The two drain water samples, W5a and W6a, were expected to have similar concentrations but large differences in the element concentrations indicated different sources. Further assessment of the geology of the area indicated that sample W6a originates from Zeppelin mountain. Sediment samples collected at locations 16, 17 and 18, closer to Smithelva, had generally lower concentrations of the selected elements.

So, some concentrations of PFAS and elements were found to be higher in the area close to former mining area, in the hill east of Tvillingvatnet. However, the lower concentrations of the relevant elements at locations 16, 17, and 18 indicates that the mining area does not contribute to contamination. In future studies it could be advised to sample from several locations within the former industry area, as well as runoff water from this area to more specifically find sources and gradients of elemental pollution. Furthermore, due to climate change, fluxes of organic and inorganic pollutants may change over time, so regular monitoring could be necessary.

# References

[1] K. Borgå, M.A. McKinney, H. Routti, K.J. Fernie, J. Giebichenstein, I. Hallanger, and D.C.G. Muir. The influence of global climate change on accumulation and toxicity of persistent organic pollutants and chemicals of emerging concern in arctic food webs. *Environ. Sci.: Processes Impacts*, 24:1544–1576, 2022. URL http://dx.doi.org/10.1039/D1EM00469G.

[2] S.O. Hauge. Sampling in and around the drinking water Tvillingvatnet, Svalbard, and initial analyses of the water chemical status. 2022.

[3] ITRC (Interstate Technology & Regulatory Council). 1 Introduction. *PFAS Technical and Regulatory Guidance Document and Fact Sheets*, 2021. URL https://pfas-1.itrcweb.org/1-introduction/.

[4] ITRC (Interstate Technology & Regulatory Council). 2 PFAS Chemistry and Naming Conventions, History and Use of PFAS, and Sources of PFAS Releases to the Environment. *PFAS Technical and Regulatory Guidance Document and Fact Sheets*, 2022. URL https://shorturl.at/uF258.

[5] D.A. Skoog, D.M. West, F.J. Holler, and S.R. Crouch. *Fundametals of Analytical Chemistry.* Brooks/Cole, 9. edition, 2014.

[6] P.B. Tchounwou, C.G. Yedjou, A.K. Patlolla, and D.J. Sutton. *Heavy Metal Toxicity and the Environment*, pages 133–164. Springer Basel, Basel, 2012. ISBN 978-3-7643-8340-4. URL https://doi.org/10.1007/978-3-7643-8340-4_6.

[7] H.B. Bradl. *Heavy metals in the Environment: Origin, Interaction and remediation*, volume 6. Academic Press, 2005.

[8] Arctic Monitoring & Assessment Programme (AMAP). Physical/Geographical Characteristics of the Arctic. *Arctic Pollution Issues: A State of the Arctic Environment Report*, pages 9–23, 1998. URL https://www.amap.no/documents/doc/amap-assessment-report-arctic-pollution-issues/68.

[9] Arctic Monitoring & Assessment Programme (AMAP). Introduction. *Arctic Pollution Issues: A State of the Arctic Environment Report*, pages 1–7, 1998. URL https://www.amap.no/documents/doc/amap-assessment-report-arctic-pollution-issues/68.

[10] Arctic Monitoring & Assessment Programme (AMAP). The Influence of Physical and Chemical Processes on Contaminant Transport into and within the Arctic. *Arctic Pollution Issues: A State of the Arctic Environment Report*, pages 26–104, 1998. URL https://www.amap.no/documents/doc/amap-assessment-report-arctic-pollution-issues/68.

[11] W.G. Landis, R.M. Sofield, and M. Yu. *Introduction to Environmental Toxicology.* CRC Press, 5. edition, 2018.

[12] S. Barr and N.P. Thuesen. Svalbard, Store norske leksikon. URL https://snl.no/Svalbard. Accessed 24.10.2022.

[13] L.K.J. Van Bets, M.A.J. Lamers, and J.P.M. van Tatenhove. Collective self-governance in a marine community: expedition cruise tourism at Svalbard. *Journal of Sustainable Tourism*, 25(11):1583–1599, 2017. URL https://doi.org/10.1080/09669582.2017.1291653.

[14] Kulturminneplan for Svalbard 2013-2023. *Sysselmesteren på Svalbard*, Rapporterie Nr.1, 2013. URL https://www.sysselmesteren.no/contentassets/bffbcd7fa7ae42ad8c6c22f047b360b3/kulturminneplan-2013---2023.pdf.

[15] S. Barr. Ny-Ålesund, Store norske leksikon. URL https://snl.no/Ny-lesund. Accessed 24.10.2022.

[16] R. Hanoa. *Kings Bay Kull Comp. A/S 1917-1992: Fra gruvedrift til forskningsservice på Svalbard*. Chr. Schibsteds Forlag A/S, 1993.

[17] Kommunal og arbeidsdepartementet. St. meld. nr 86 1962-1963 Om eksplosjonsulykken på Svalbard (Ny-Ålesund) 5. november 1962. URL https://www.stortinget.no/globalassets/pdf/stortingsarkivet/kings-bay/st.-meld.-nr.-86-1962-1963.pdf.

[18] R.C. Buck, J. Franklin, U. Berger, J.M. Conder, I.T. Cousins, P.D.J. Voogt, A.K.Allan, M. Kurunthachalam, S.A. van Leeuwen, and P.J.J. Stefan. Perfluoroalkyl and Polyfluoroalkyl Substances in the Environment: Terminology, Classification, and Origins. *Integrated Environmental Assessment and Management*, 7(4):513–541, 2011. URL https://doi.org/10.1002/ieam.258.

[19] J. Glüge, M. Scheringer, I.T. Cousins, J.C. DeWitt, G. Goldenman, D. Herzke, R. Lohmann, C.A. Ng., X. Trier, and Z. Wang. An overview of the uses of per- and polyfluoroalkyl substances (PFAS). *Enviornmental Science: Processes & Impacts*, 22:2345–2373, 2020. URL https://doi.org/10.1039/D0EM00291G.

[20] ITRC (Interstate Technology & Regulatory Council). 4 Physical and Chemical properties. *PFAS Technical and Regulatory Guidance Document and Fact Sheets*, 2021. URL https://pfas-1.itrcweb.org/4-physical-and-chemical-properties/#4_2.

[21] W.M. Meylan and P.H. Howard. Estimating octanol–air partition coefficients with octanol–water partition coefficients and Henry's law constants. *Chemosphere*, 61(5):640–644, 2005. ISSN 0045-6535. URL https://doi.org/10.1016/j.chemosphere.2005.03.029.

[22] M. Kim, L.Y. Li, J.R. Grace, and C. Yue. Selecting reliable physicochemical properties of perfluoroalkyl and polyfluoroalkyl substances (PFASs) based on molecular descriptors. *Environmental Pollution*, 196:462–472, 2015. ISSN 0269-7491. URL https://doi.org/10.1016/j.envpol.2014.11.008.

[23] Y. Wang, U. Munir, and Q. Huang. Occurrence of per- and polyfluoroalkyl substances (PFAS) in soil: Sources, fate, and remediation. *Soil & Environmental Health*, 1(1):100004, 2023. ISSN 2949-9194. URL https://doi.org/10.1016/j.seh.2023.100004.

[24] S. Kurwadkar, J. Dane, S.R. Kanel, M.N. Nadagouda, R.W. Cawdrey, B. Ambade, G.C. Struckhoff, and R. Wilkin. Per- and polyfluoroalkyl substances in water and wastewater: A critical review of their global occurrence and distribution. *Science of The Total Environment*, 809:151003, 2022. ISSN 0048-9697. URL https://doi.org/10.1016/j.scitotenv.2021.151003.

[25] C.J. Young, V.I. Furdui, J. Franklin, R.M. Koerner, D.C.G. Muir, and S.A. Mabury. Perfluorinated Acids in Arctic Snow: New Evidence for Atmospheric Formation. *Environmental Science & Technology*, 41(10):3455–3461, 2007. URL https://doi.org/10.1021/es0626234.

[26] L.W.Y. Yeung, C. Dassuncao, S. Mabury, E.M. Sunderland, X. Zhang, and R. Lohmann. Vertical Profiles, Sources, and Transport of PFASs in the Arctic Ocean. *Environmental Science & Technology*, 51(12):6735–6744, 2017. URL https://doi.org/10.1021/acs.est.7b00788.

[27] ITRC (Interstate Technology & Regulatory Council). 5 Environmental Fate and Transport Processes. *PFAS Technical and Regulatory Guidance Document and Fact Sheets*, 2022. URL https://pfas-1.itrcweb.org/5-environmental-fate-and-transport-processes/.

[28] R.W. Macdonald, T. Harner, and J. Fyfe. Recent climate change in the Arctic and its impact on contaminant pathways and interpretation of temporal trend data. *Science of the Total Enviornment*, 342(1-3):5–86, 2005. URL https://doi.org/10.1016/j.scitotenv.2004.12.059.

[29] J.S. Skaar, E.M. Ræder, J.L. Lyche, L. Ahrens, and R. Kallenborn. Elucidation of contamination sources for poly- and perfluoroalkyl substances (PFASs) on Svalbard (Norwegian Arctic). *Environmental Science and Pollution Research*, 26:7356–7363, 2019. URL https://doi.org/10.1007/s11356-018-2162-4.

[30] The Convention: Overview. URL http://www.pops.int/TheConvention/Overview/tabid/3351/Default.aspx. Accessed 19.10.2022.

[31] EFSA. Risk to human health related to the presence of perfluoroalkyl substances in food. *EFSA Journal*, 18(9), 2020. URL https://doi.org/10.2903/j.efsa.2020.6223.

[32] F.W. Fifield and P.J. Haines. *Environmental Analytical Chemistry*. Blackwell Science Ltd, 2. edition, 2000.

[33] A. Kłos, Z. Ziembik, M. Rajfur, A. Dołhańczuk-Śródka, Z. Bochenek, J.W. Bjerke, H. Tømmervik, B. Zagajewski, D. Ziółkowski, D. Jerz, M. Zielińska, P. Krems, and P. Godyń. The Origin of Heavy Metals and Radionuclides Accumulated in the Soil and Biota Samples Collected in Svalbard, Near Longyearbyen. *Ecological Chemistry and Engineering S*, 24(2): 223–238, 2017. URL https://doi.org/10.1515/eces-2017-0015.

[34] E.B. Holm, P.J. Brandvik, and E. Steinnes. Pollution in acid mine drainage from mine tailings in Svalbard, Norwegian Arctic. 107, 05 2003. URL http://dx.doi.org/10.1051/jp4:20030381.

[35] A. Hossen, A.I.H. Chowdhury, R.A. Mullick, and A. Hoque. Heavy metal pollution status and health risk assessment vicinity to Barapukuria coal mine area of Bangladesh. *Environmental Nanotechnology, Monitoring & Management*, 16(100469), 2021. ISSN 2215-1532. URL https://www.sciencedirect.com/science/article/pii/S2215153221000441.

[36] F. Li, X. Li, L. Hou, and A. Shao. Impact of the Coal Mining on the Spatial Distribution of Potentially Toxic Metals in Farmland Tillage Soil. *Scientific Reports*, 8(14925), 2018. URL https://doi.org/10.1038/s41598-018-33132-4.

[37] P. Gombert, O. Sracek, N. Koukouzas, G. Gzyl, S. Valladares, R. Fraczek, C. Klinger, A. Bauerek, J. Areces, S. Chamberlain, K. Paw, and L. Pierzchala. An Overview of Priority Pollutants in Selected Coal Mine Discharges in Europe. *Mine Water and the Environment*, 38, 2018. URL https://doi.org/10.1007/s10230-018-0547-8.

[38] H. Jensen. Resultater av kjemiske analyser av prøver av Svalbard kull og tilgrensende bergarter over, under og mellom kull fløtsene. *NGU*, 2000. URL https://www.ngu.no/filearchive/156/99_140.pdf.

[39] FHI. Metaller. URL https://www.fhi.no/nettpub/luftkvalitet/temakapitler/metaller---luftkvalitetskriterier/. Updated 13.02.2018.

[40] I. Bisutti, I. Hilke, and R. Raessler. Determination of total organic carbon – an overview of current methods. *Trends in Analytical Chemistry*, 23(10-11):716–726, 2004. URL https://doi.org/10.1016/j.trac.2004.09.003.

[41] C.P. Higgins and R.G. Luthy. Sorption of Perfluorinated Surfactants on Sediments. *Environmental Science & Technology*, 40(23):7251–7256, 2006. URL https://doi.org/10.1021/es061000n.

[42] B. Buszewski and M. Szultka. Past, Present, and Future of Solid Phase Extraction: A Review. *Critical Reviews in Analytical Chemistry*, 42(3):198–213, 2012. URL https://doi.org/10.1080/07373937.2011.645413.

[43] D.E. Raynie and D.W. Watson. Understanding and Improving Solid-Phase Extraction. *LCGC North America*, 32(12):908–915, 2014. URL https://www.chromatographyonline.com/view/understanding-and-improving-solid-phase-extraction-1.

[44] E. Lundanes, L. Reubsaet, and T. Greibrokk. *Chromatography: Basic Principles, Sample Preparations and Related Methods*. Wiley-VCH, 2014.

[45] C.F. Poole and S.K. Poole. *Chromatography Today*. Elsevier Science Publishers, 1991.

[46] A. Van Eeckhaut, K. Lanckmans, S. Sarre, I. Smolders, and Y. Michotte. Validation of bioanalytical LC–MS/MS assays: Evaluation of matrix effects. *Journal of Chromatography B*, 877(23):2198–2207, 2009. ISSN 1570-0232. URL https://doi.org/10.1016/j.jchromb.2009.01.003. METHOD VALIDATION, COMPARISON AND TRANSFER.

[47] E. Stokvis, H. Rosing, and J.H Beijnen. Stable isotopically labeled internal standards in quantitative bioanalysis using liquid chromatography/mass spectrometry: necessity or not? *Rapid Communications in Mass Spectrometry*, 19(3):401–407, 2005. URL https://doi.org/10.1002/rcm.1790.

[48] A. Shrivastava and V.B. Gupta. Methods for the determination of limit of detection and limit of quantitation of the analytical methods. *Chronicles of Young Scientists*, 2:21–25, 06 2011. URL https://doi.org/10.4103/2229-5186.79345.

[49] V. Barwick. *Guide to Quality in Analytical Chemistry: An Aid to Accreditation*. Eurachem/CITAC Guide, 3. edition, 2016. URL https://www.eurachem.org/images/stories/Guides/pdf/Eurachem_CITAC_QAC_2016_EN.pdf.

[50] Y. Dodge. *The Concise Encyclopedia of Statistics*, pages 55–57. Springer New York, New York, NY, 2008. ISBN 978-0-387-32833-1. URL https://doi.org/10.1007/978-0-387-32833-1_43.

[51] B.K. Alsberg. *Chemometrics*. 0.5 edition.

[52] TopoSvalbard. *Norsk Polarinstitutt*, 2022. URL https://toposvalbard.npolar.no/.

[53] Shimadzu TOC-L User's Manual. pages 61–62, 2017.

[54] Sysselmesteren. *Norsk Polarinstitutt*. URL https://www.sysselmesteren.no/contentassets/225d990d15ff47a58050a1aa4948ed7b/ny---alesund-hefte.

# Appendices

## A    Overview photos
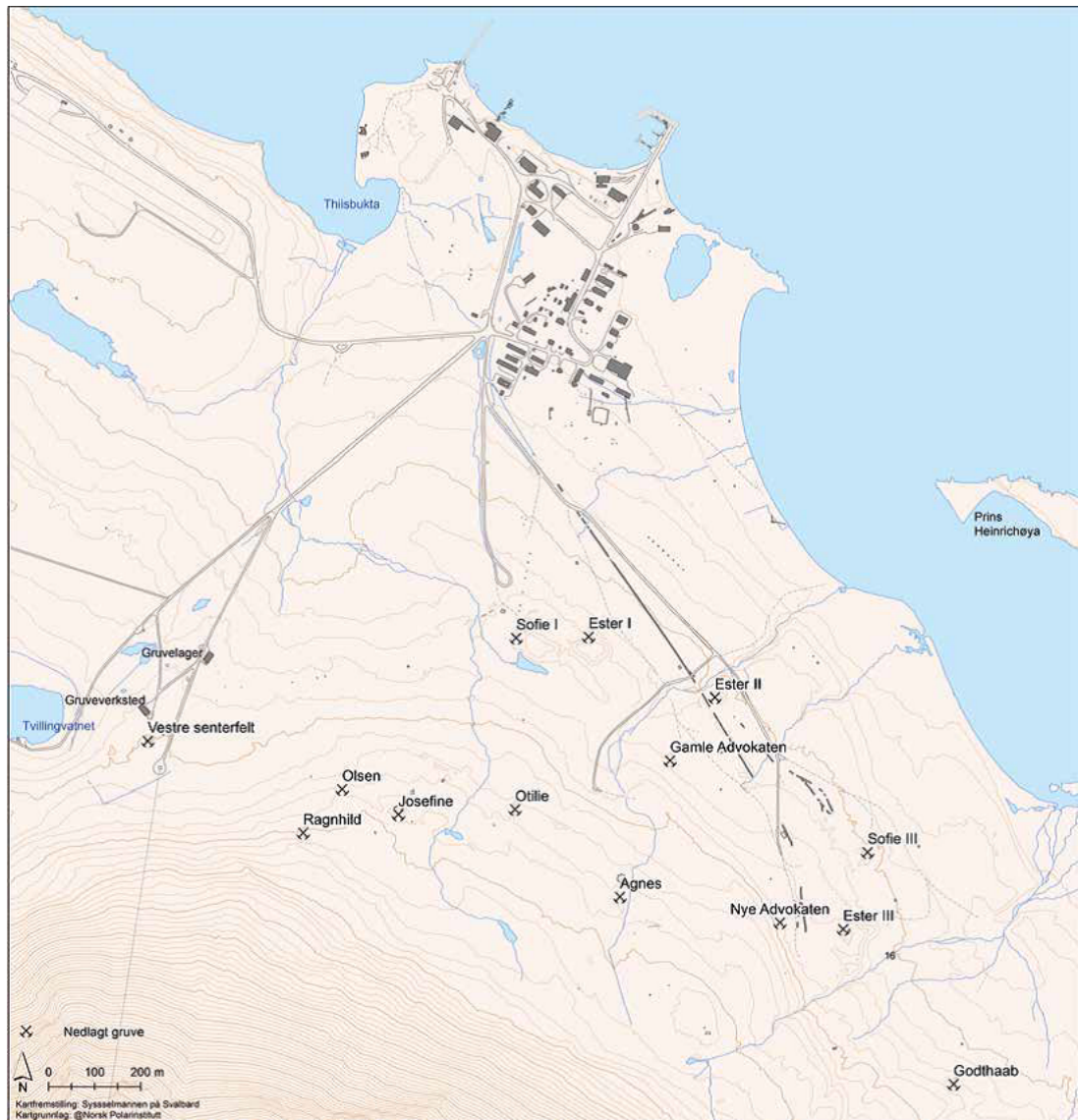


Figure A.1: Map given an overview over the mines that have been active in Ny-Ålesund[54].

Figure A.2: Trench alongside Zeppelin mountain, leading to Tvillingvatnet [52]. The trench is marked by white arrows.

# B    Photos from sampling



Figure B.1: Sampling from location 15.
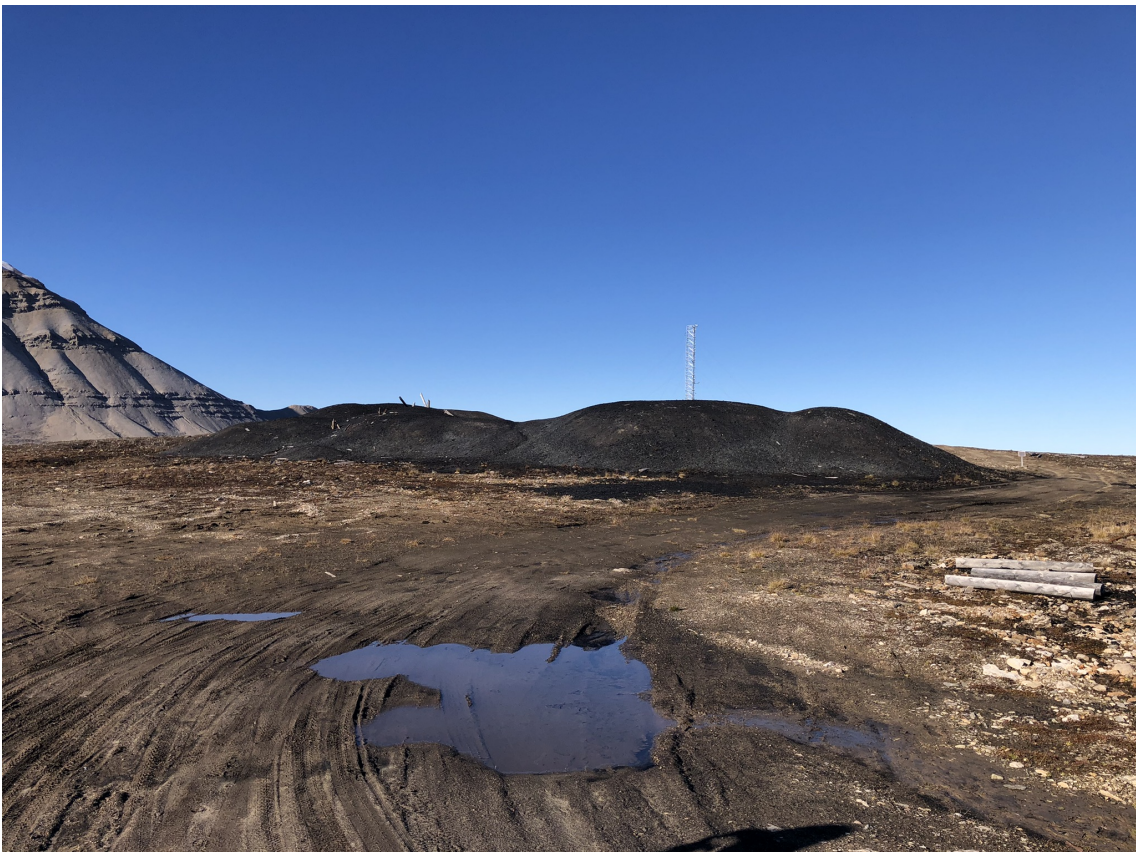


Figure B.2: Photo of Kolhaugen, north-west of Tvillingvatnet.

Figure B.3: pH and conductivity measured in Tvillingvatnet.

Figure B.4: Sample location 16.



Figure B.5: Sample location 17.

Figure B.6: Sample location 18.

# C Calibration curves PFAS
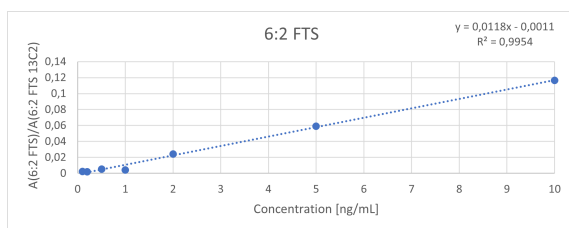


Figure C.1: Calibration curve for 6:2 FTS.



Figure C.2: Calibration curve for PFNA



Figure C.3: Calibration curve for PFHxA.



Figure C.4: Calibration curve for PFPeA.



Figure C.5: Calibration curve for 4:2 FTS.



Figure C.6: Calibration curve for 7H-PFHpA.



Figure C.7: Calibration curve for NaDONA.



Figure C.8: Calibration curve for PFHpS.



Figure C.9: Calibration curve for P37dMOA.
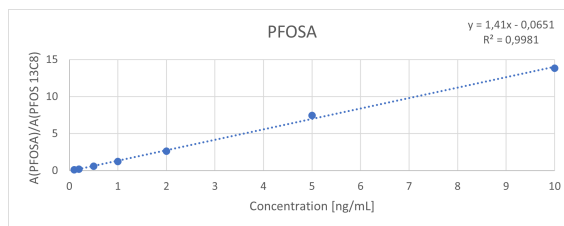


Figure C.10: Calibration curve for PFOSA.
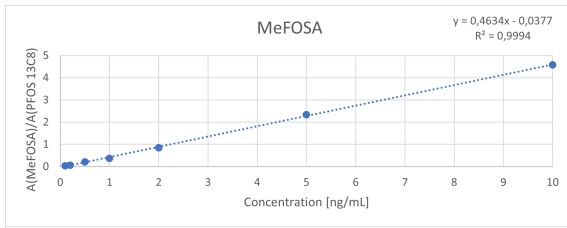
Figure C.11: Calibration curve for MeFOSA.
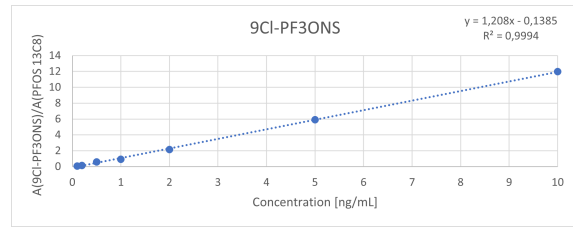


Figure C.16: Calibration curve for 9Cl-PF3ONS.
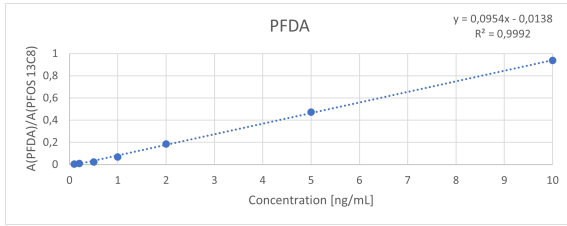


Figure C.12: Calibration curve for PFDA.
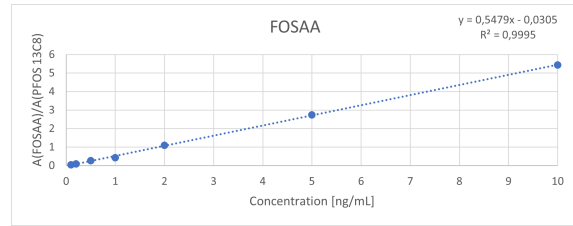


Figure C.17: Calibration curve for FOSAA.
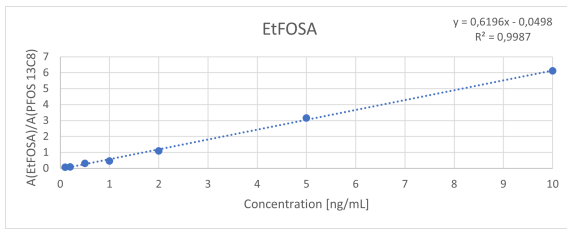


Figure C.13: Calibration curve for EtFOSA.
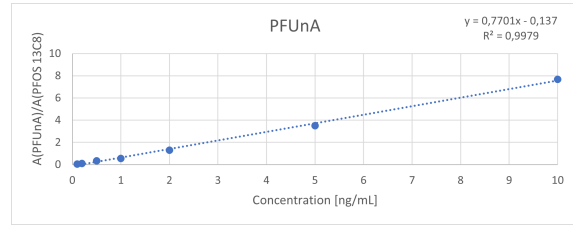


Figure C.18: Calibration curve for PFUnA.
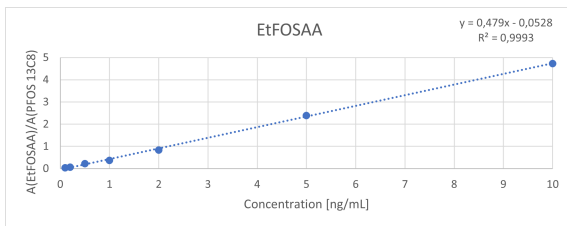


Figure C.14: Calibration curve for EtFOSAA.
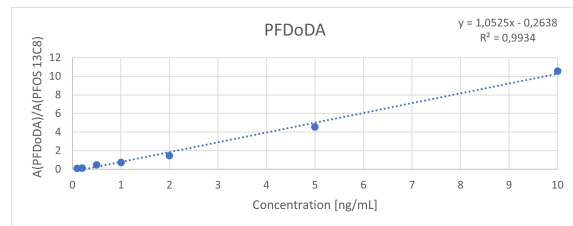


Figure C.19: Calibration curve for PFDoDA.
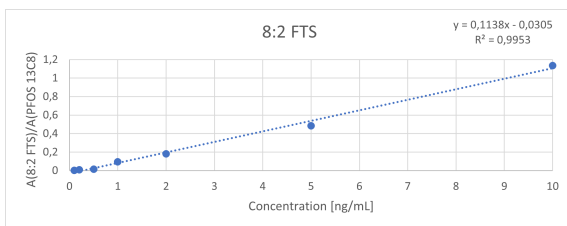


Figure C.15: Calibration curve for 8:2 FTS.
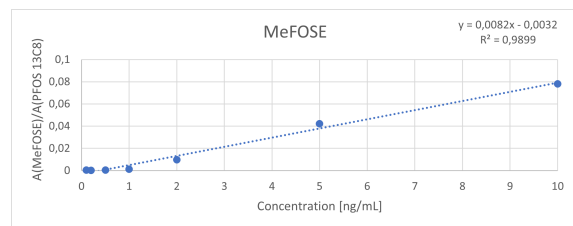


Figure C.20: Calibration curve for MeFOSE.
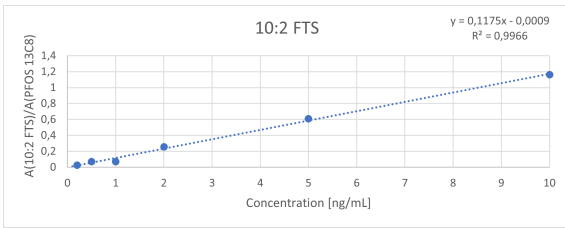
Figure C.21: Calibration curve for 10:2 FTS.
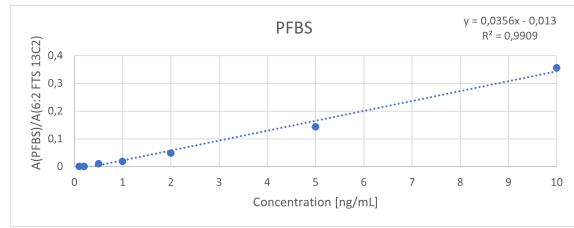


Figure C.26: Calibration curve for PFBS.
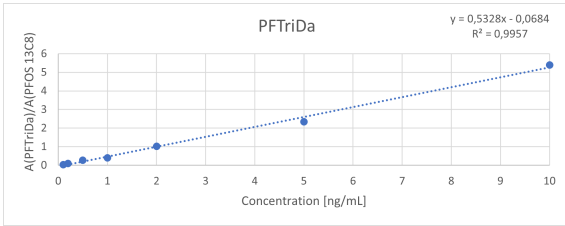


Figure C.22: Calibration curve for PFTriDa.
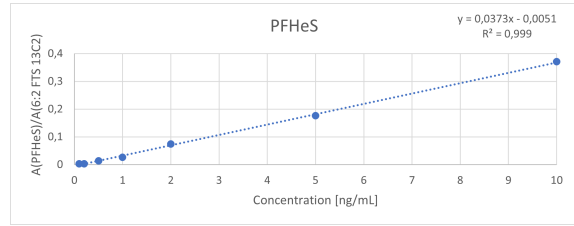


Figure C.27: Calibration curve for PFHeS.
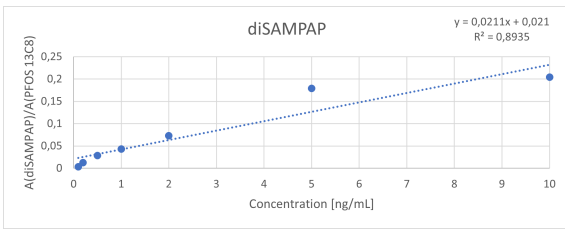


Figure C.23: Calibration curve for diSAMPAP.
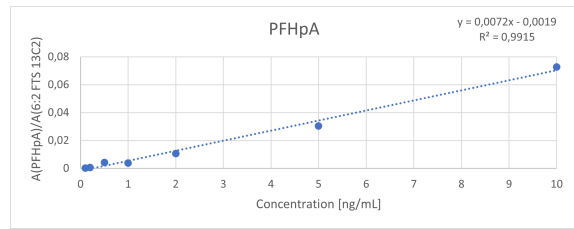


Figure C.28: Calibration curve for PFHpA.
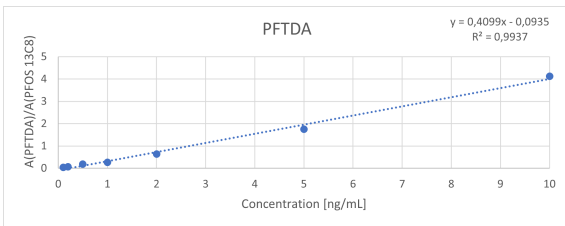


Figure C.24: Calibration curve for PFTDA.
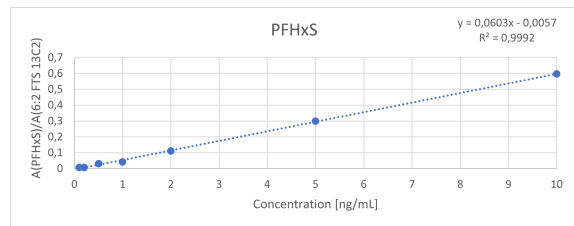


Figure C.29: Calibration curve for PFHxS
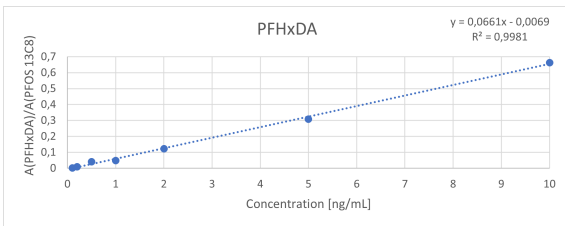


Figure C.25: Calibration curve for PFHxDA.
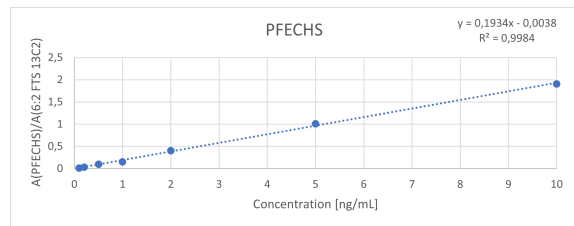


Figure C.30: Calibration curve for PFECHS.
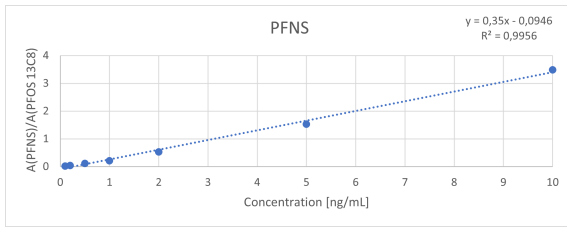
Figure C.31: Calibration curve for PFNS.
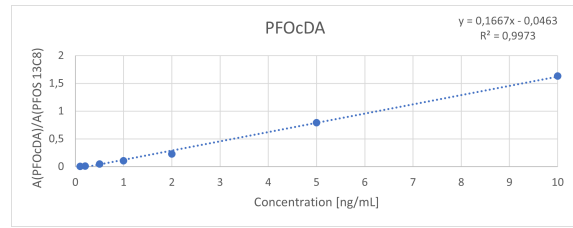


Figure C.33: Calibration curve for PFOcDA.
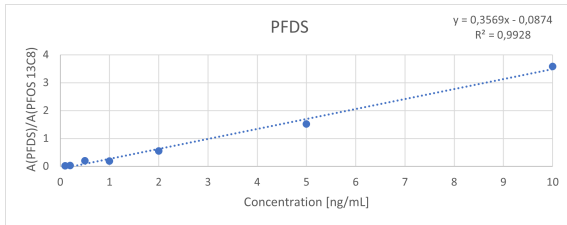


Figure C.32: Calibration curve for PFDS.

# D Element results from ICP-MS

## D.1 Sediment and soil
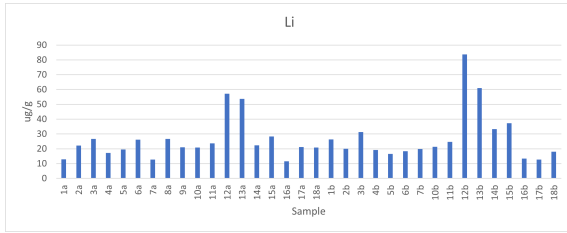


Figure D.1: Bar chart presenting concentrations of Li.



Figure D.2: Bar chart presenting concentrations of Be.



Figure D.3: Bar chart presenting concentrations of B.
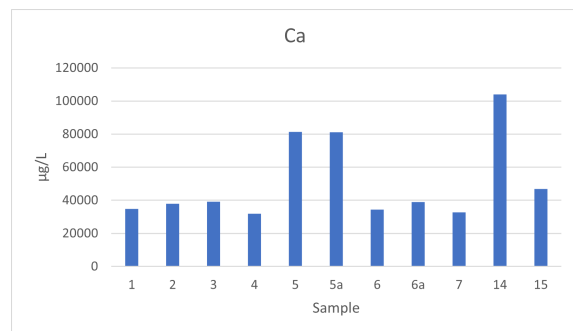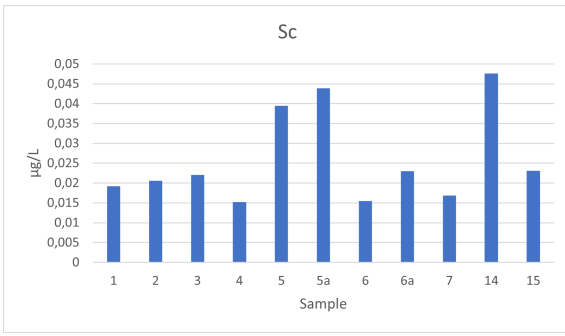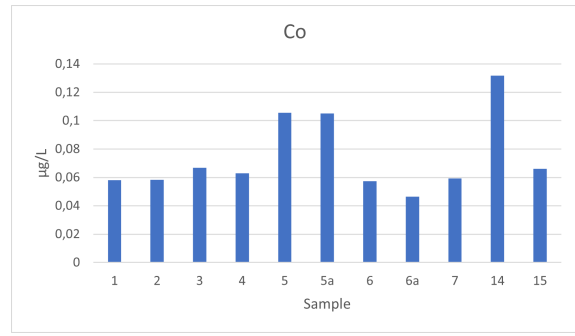


Figure D.4: Bar chart presenting concentrations of Na.
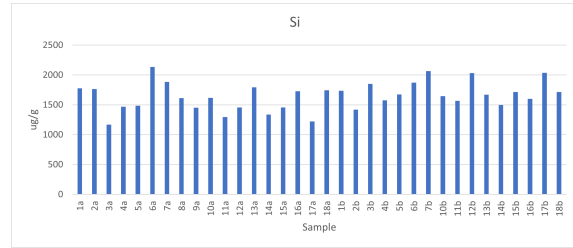


Figure D.5: Bar chart presenting concentrations of Si.
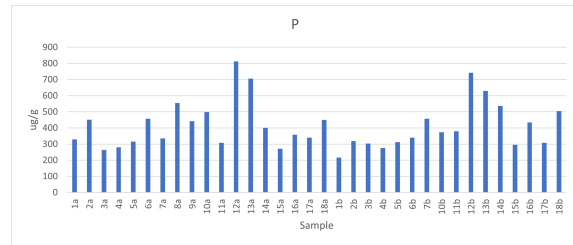


Figure D.6: Bar chart presenting concentrations of P
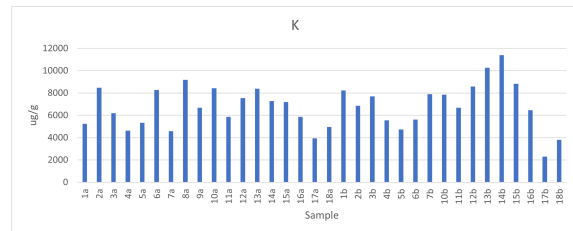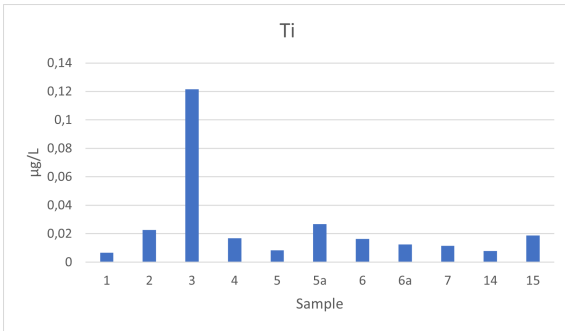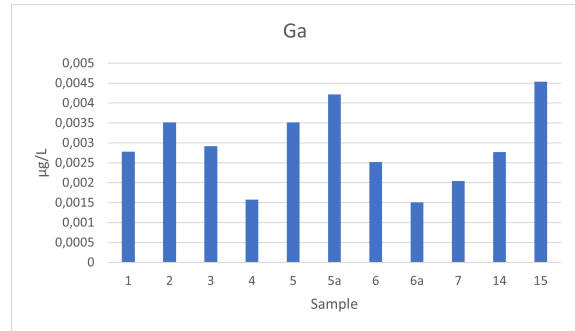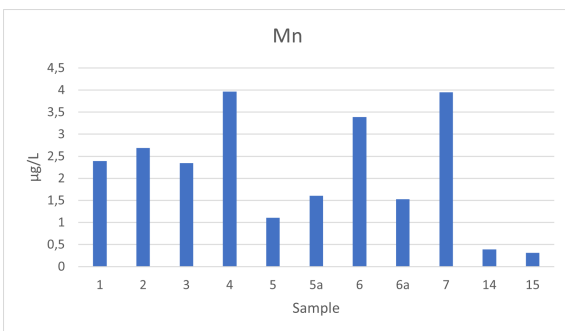


Figure D.7: Bar chart presenting concentrations of K.
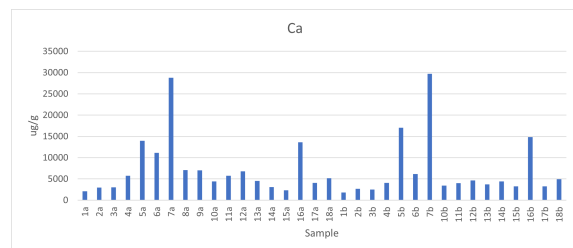


Figure D.8: Bar chart presenting concentrations of Ca.
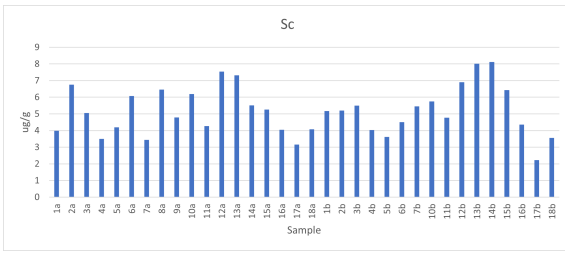
Figure D.9: Bar chart presenting concentrations of Sc
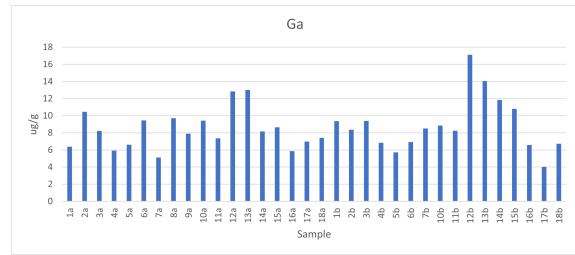


Figure D.13: Bar chart presenting concentrations of Ga.
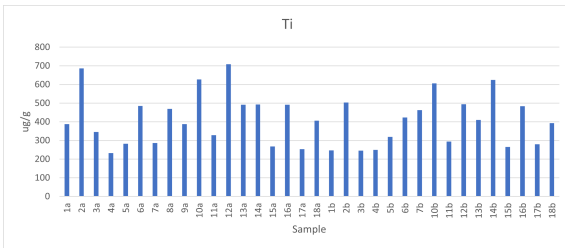


Figure D.10: Bar chart presenting concentrations of Ti.
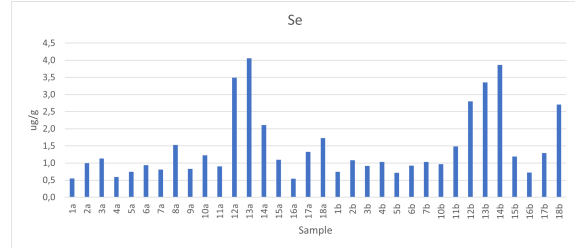


Figure D.14: Bar chart presenting concentrations of Se.
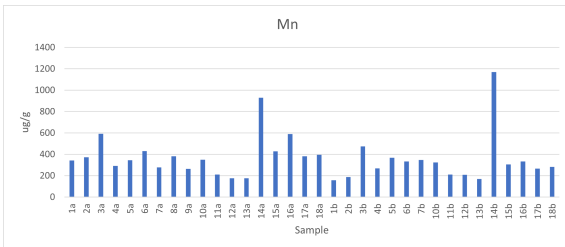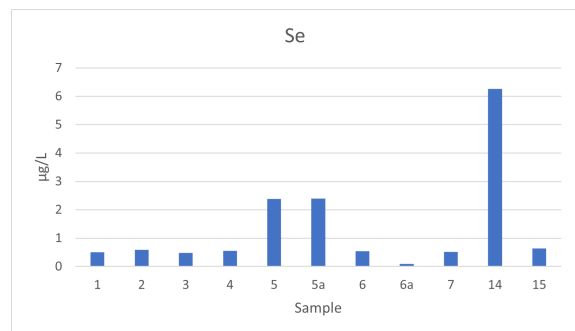


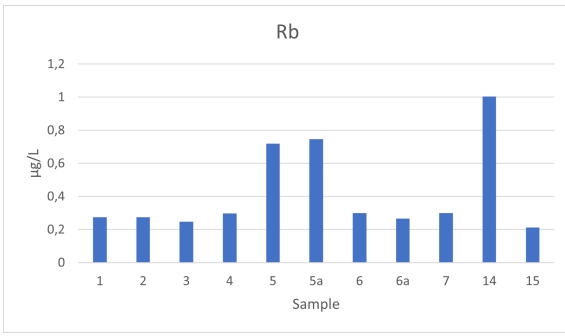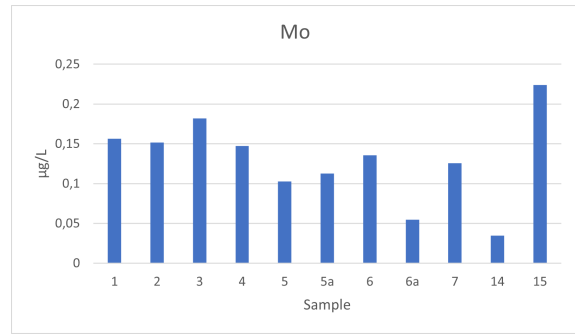Figure D.11: Bar chart presenting concentrations of Mn.
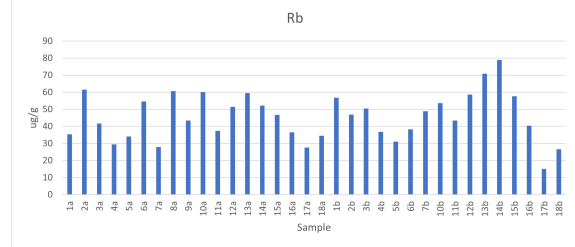


Figure D.15: Bar chart presenting concentrations of Rb.
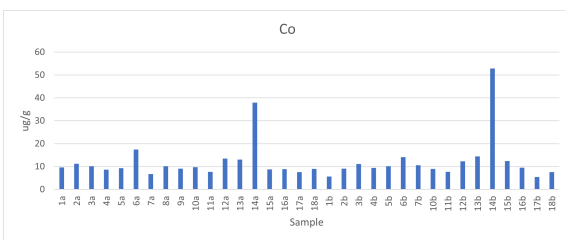


Figure D.12: Bar chart presenting concentrations of Co.
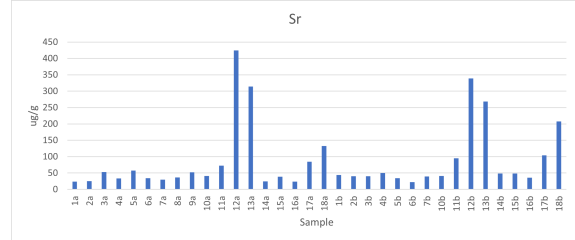


Figure D.16: Bar chart presenting concentrations of Sr.
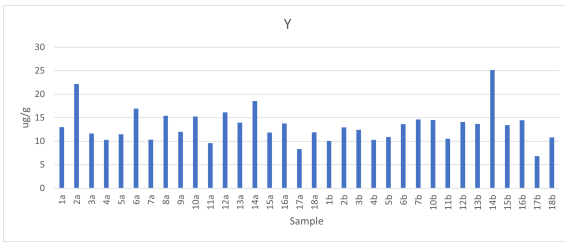
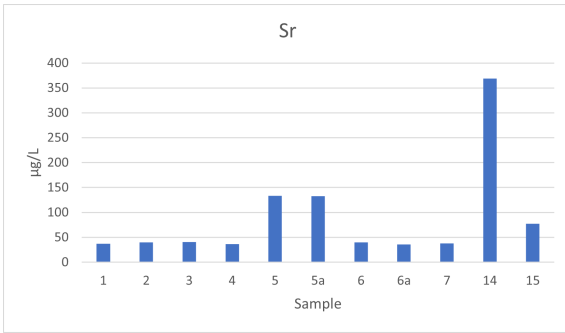Figure D.17: Bar chart presenting concentrations of Y
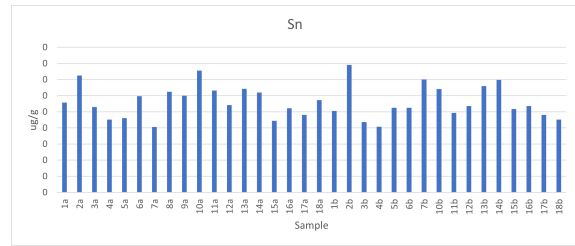


Figure D.21: Bar chart presenting concentrations of Sn.
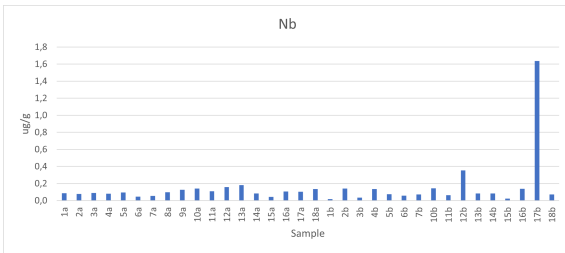


Figure D.18: Bar chart presenting concentrations of Nb.
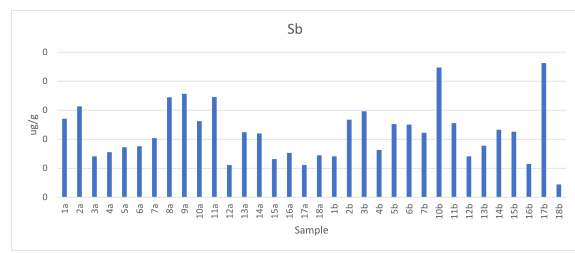


Figure D.22: Bar chart presenting concentrations of Sb.
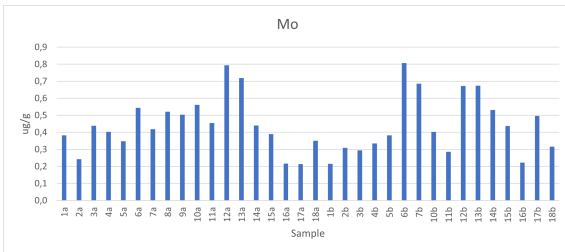


Figure D.19: Bar chart presenting concentrations of Mo.
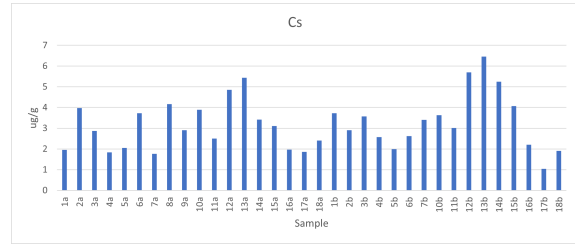


Figure D.23: Bar chart presenting concentrations of Cs.
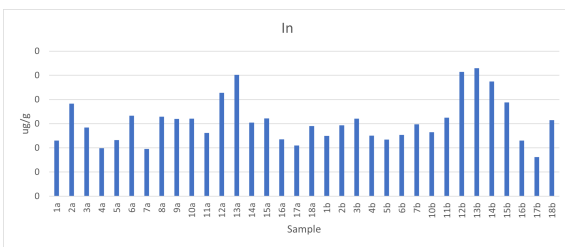


Figure D.20: Bar chart presenting concentrations of In.
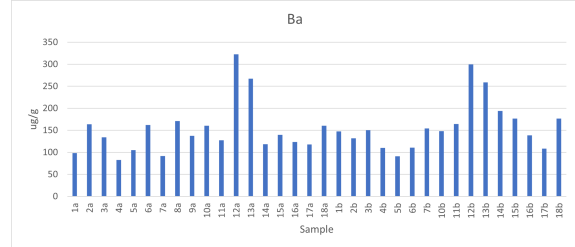


Figure D.24: Bar chart presenting concentrations of Ba.
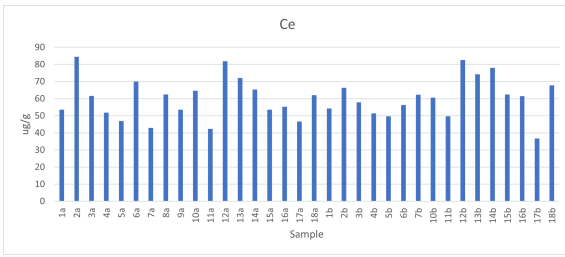
Figure D.25: Bar chart presenting concentrations of Ce.
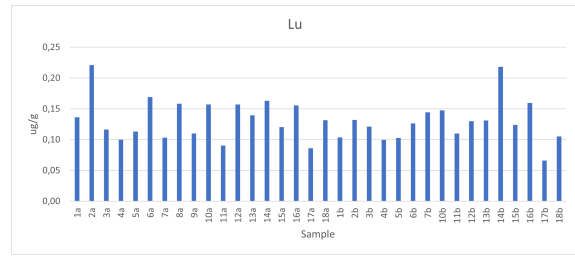


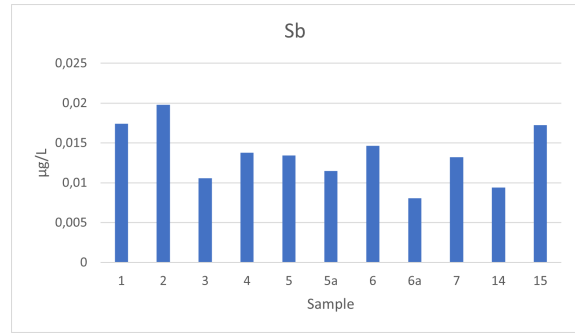Figure D.29: Bar chart presenting concentrations of Lu.
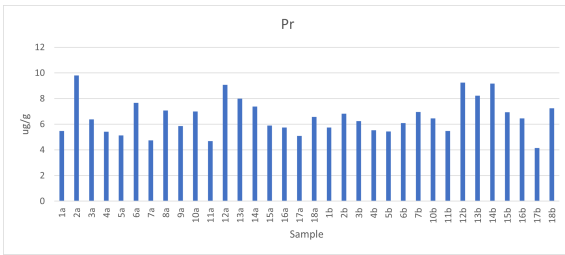


Figure D.26: Bar chart presenting concentrations of Pr.
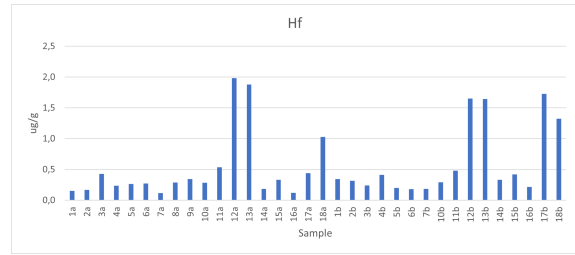


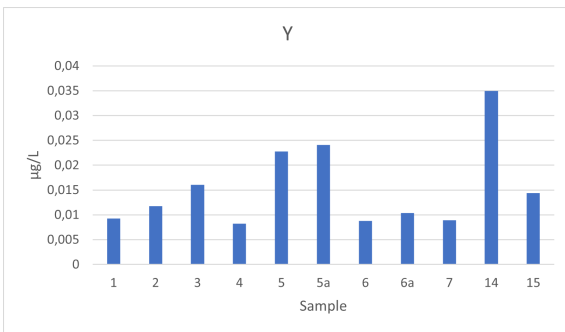Figure D.30: Bar chart presenting concentrations of Hf.
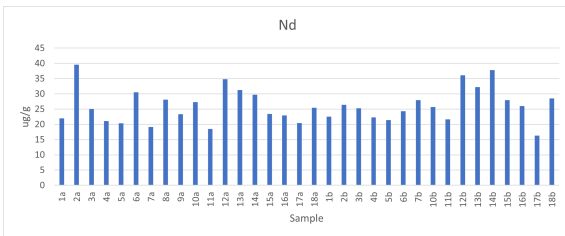


Figure D.27: Bar chart presenting concentrations of Nd.
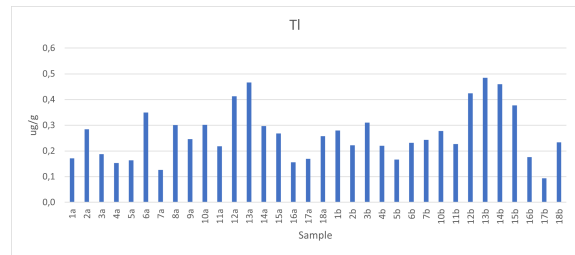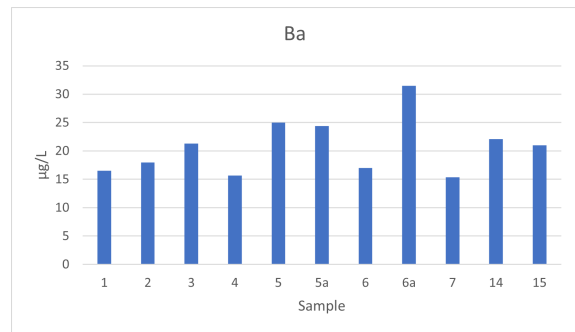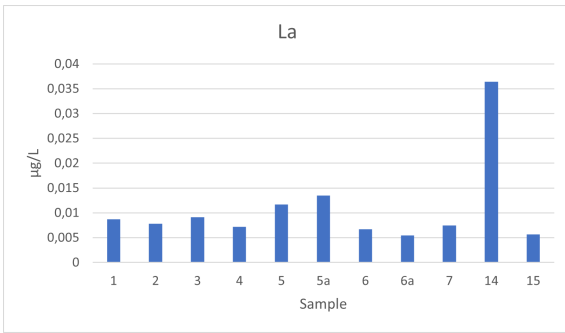


Figure D.31: Bar chart presenting concentrations of Tl.
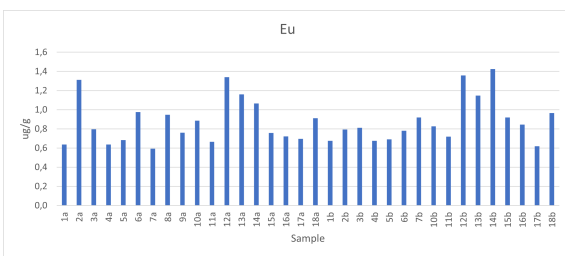


Figure D.28: Bar chart presenting concentrations of Eu.
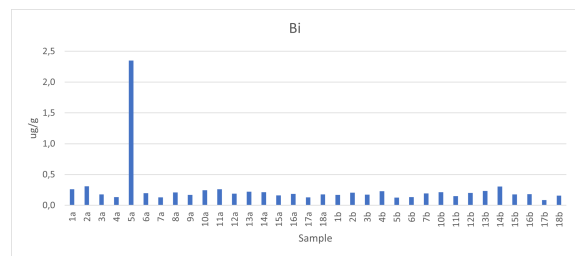


Figure D.32: Bar chart presenting concentrations of Bi.
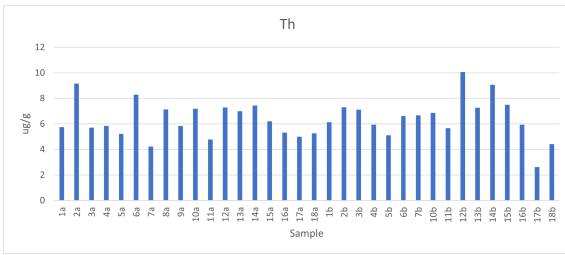
Figure D.33: Bar chart presenting concentrations of Th.
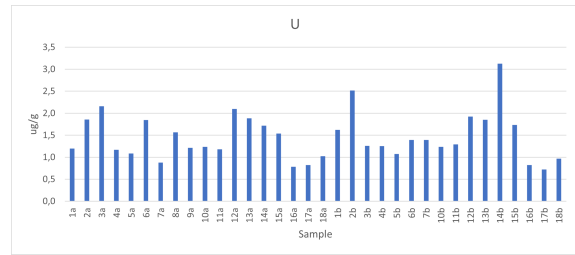


Figure D.34: Bar chart presenting concentrations of U.

## D.2 Water samples
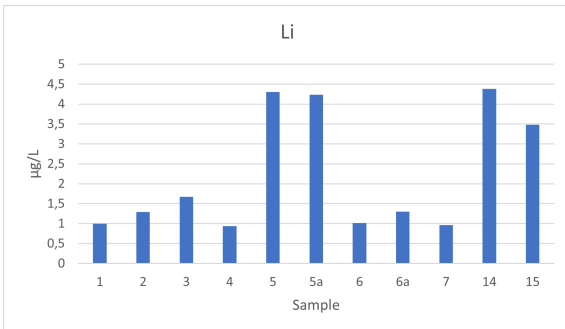


Figure D.35: Bar chart presenting concentrations of Li.
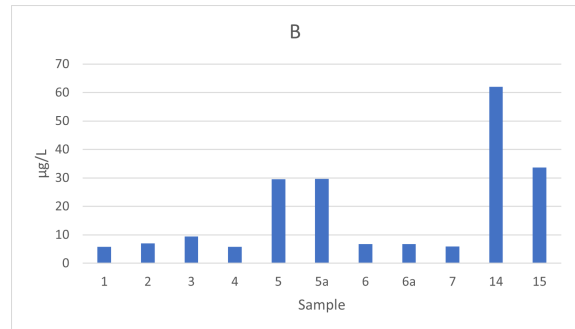


Figure D.37: Bar chart presenting concentrations of B.
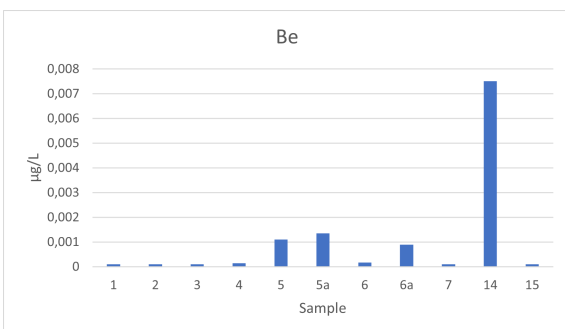


Figure D.36: Bar chart presenting concentrations of Be.
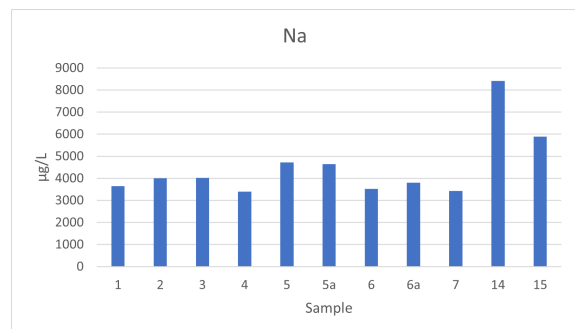


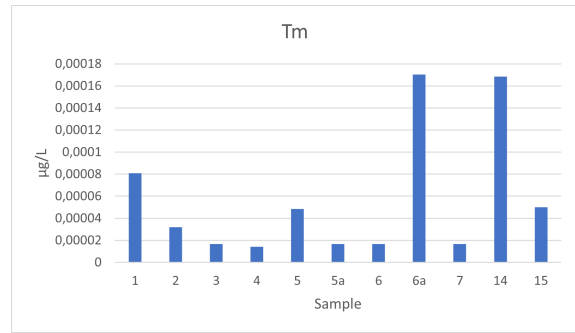Figure D.38: Bar chart presenting concentrations of Na.
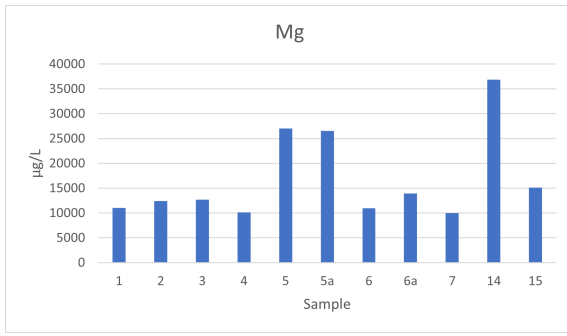
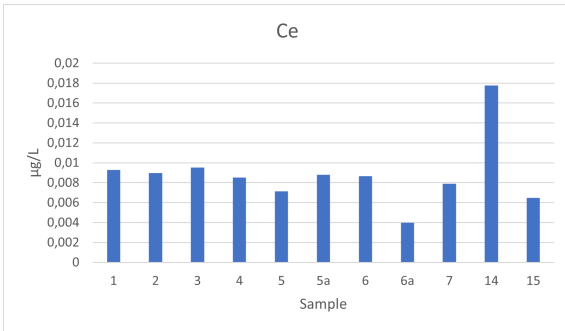Figure D.39: Bar chart presenting concentrations of Mg.
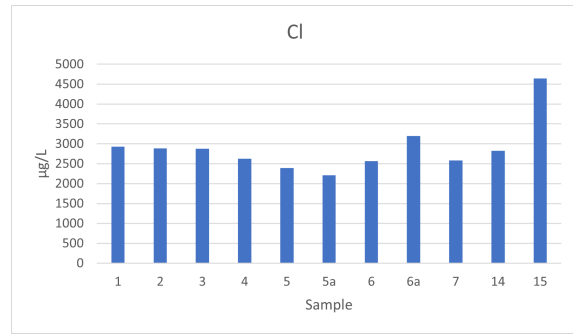


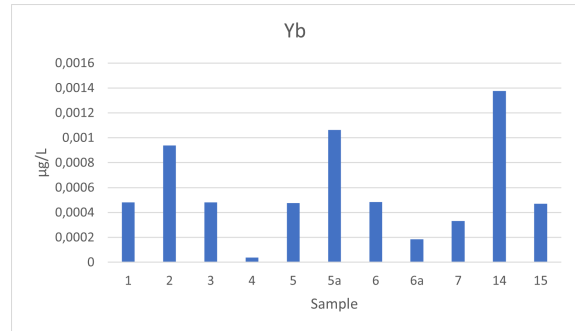Figure D.42: Bar chart presenting concentrations of Cl.
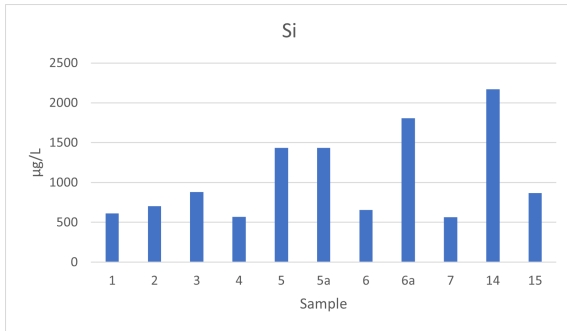


Figure D.40: Bar chart presenting concentrations of Si.
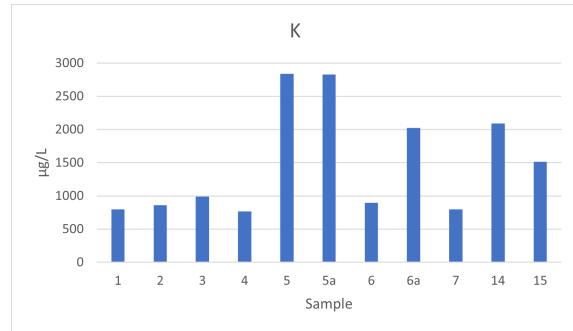


Figure D.43: Bar chart presenting concentrations of K.
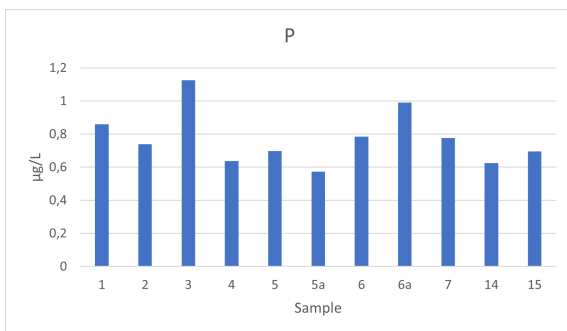


Figure D.41: Bar chart presenting concentrations of P.



Figure D.44: Bar chart presenting concentrations of Ca.

Figure D.45: Bar chart presenting concentrations of Sc.



Figure D.48: Bar chart presenting concentrations of Co.



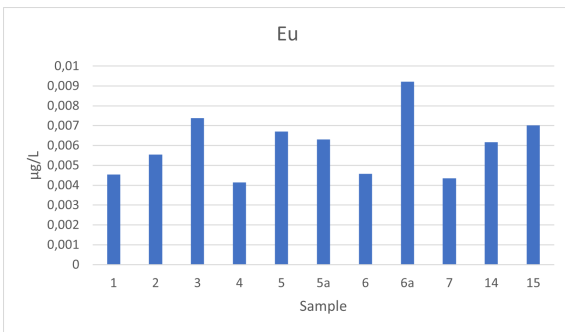Figure D.46: Bar chart presenting concentrations of Ti.



Figure D.49: Bar chart presenting concentrations of Ga.
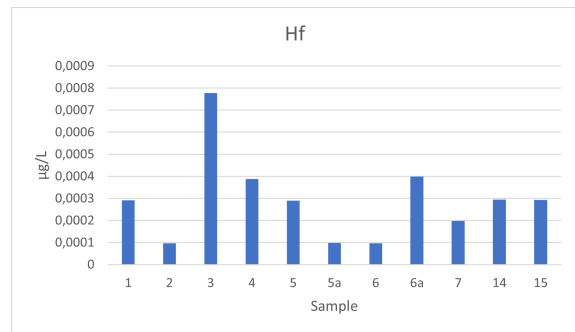


Figure D.47: Bar chart presenting concentrations of Mn.



Figure D.50: Bar chart presenting concentrations of Se.

Figure D.51: Bar chart presenting concentrations of Rb.



Figure D.54: Bar chart presenting concentrations of Mo.



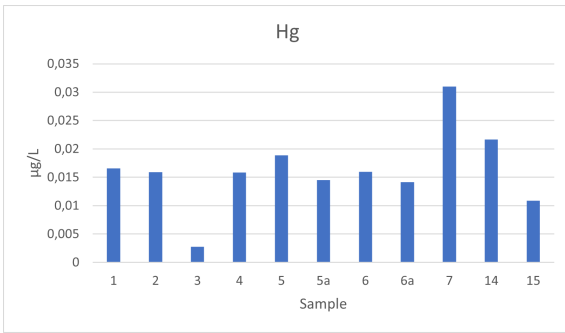Figure D.52: Bar chart presenting concentrations of Sr.



Figure D.55: Bar chart presenting concentrations of Sb.



Figure D.53: Bar chart presenting concentrations of Y.



Figure D.56: Bar chart presenting concentrations of Ba.

Figure D.57: Bar chart presenting concentrations of La.



Figure D.60: Bar chart presenting concentrations of Tm.



Figure D.58: Bar chart presenting concentrations of Ce.



Figure D.61: Bar chart presenting concentrations of Yb.



Figure D.59: Bar chart presenting concentrations of Eu.



Figure D.62: Bar chart presenting concentrations of Hf.

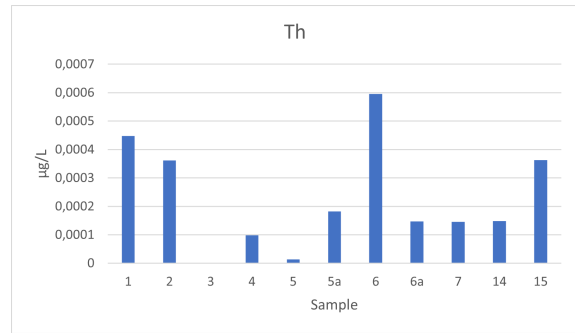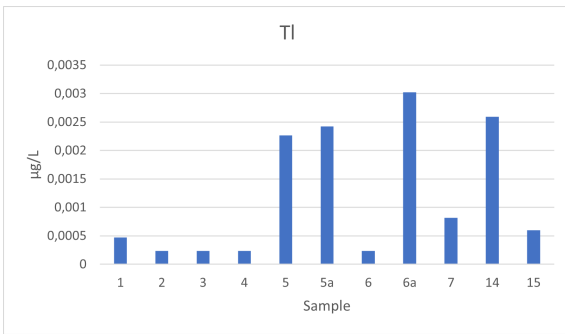Figure D.63: Bar chart presenting concentrations of Hg.



Figure D.66: Bar chart presenting concentrations of Th.



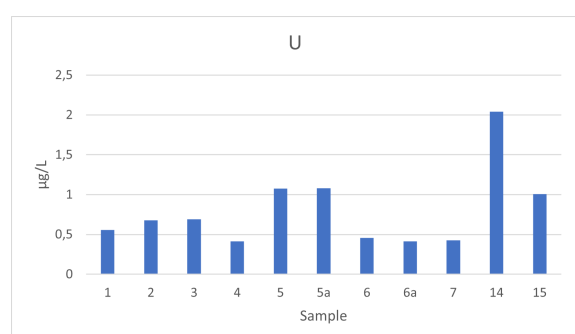Figure D.64: Bar chart presenting concentrations of Tl.



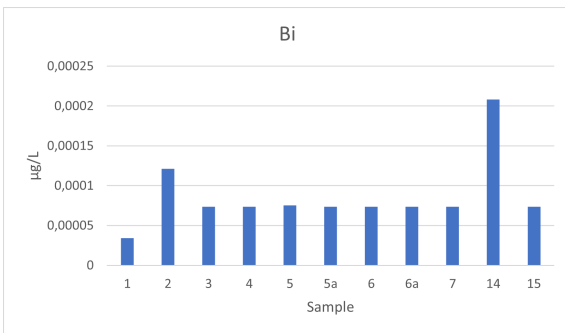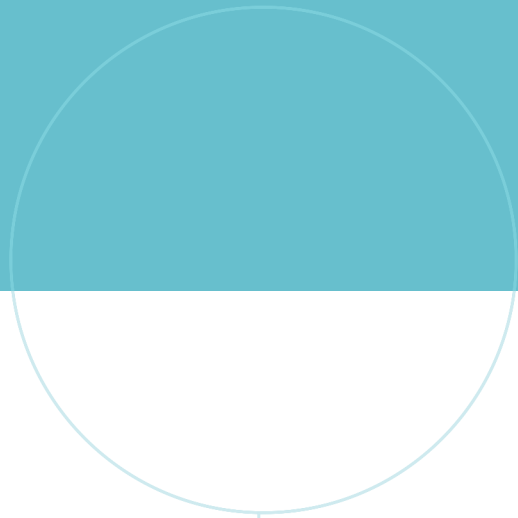Figure D.67: Bar chart presenting concentrations of U.



Figure D.65: Bar chart presenting concentrations of Bi.